CRANFIELD UNIVERSITY

Olivier Autin

MICROPOLLUTANT REMOVAL BY ADVANCED OXIDATION PROCESSES

SCHOOL OF APPLIED SCIENCES

PhD THESIS

CRANFIELD UNIVERSITY

CRANFIELD WATER SCIENCE INSTITUTE

SCHOOL OF APPLIED SCIENCES

PhD THESIS

Olivier Autin

MICROPOLLUTANT REMOVAL BY ADVANCED OXIDATION PROCESSES

October 2012

Supervisor: Prof. Bruce Jefferson

This thesis is submitted in partial fulfilment of the requirements for the degree of Doctor of Philosophy.

ABSTRACT

The use of pesticides in agriculture has been associated to high concentrations found in surface waters and ultimately to the tightening of drinking water regulations. Whilst traditional granular activated carbon filtration or ozone are effective barriers for the large majority of pesticides, new polar pesticides such as clopyralid or metaldehyde are not readily removed by such technologies. The use of advanced oxidation processes (AOPs) is suggested as an effective alternative for metaldehyde removal. Although metaldehyde's reactivity towards •OH appears in the last third of an extensive list of various pesticides' reactivity, it was still well removed by the two AOPs tested: UV/H_2O_2 and UV/TiO_2 in pure systems at similar rates of degradation under optimised doses of 100 mg.L^{-1} of TiO_2 and 8 mM of H_2O_2. The presence of scavengers in natural waters such as natural organic matter (NOM) and carbonate ions reduced the effectiveness of metaldehyde removal. Experiments were undertaken using model compounds in order to evaluate the influence of these scavengers by directly monitoring the competition for •OH between background organic matter and metaldehyde. It was found that the concentration of background scavengers rather than the concentration of micropollutant had the greatest impact on both AOPs. In addition, whilst the alkalinity did not significantly influence the UV/H_2O_2 process, it totally inhibited the UV/TiO_2 photocatalytic process due to the aggregation of TiO_2 particles and further investigations are critical in order to break these aggregates for UV/TiO_2 photocatalysis to become a competitive alternative to traditional treatments. Finally, a cost analysis showed that AOPs already appear as an economically viable technology for metaldehyde removal. Development of UV/LEDs will provide a lower energy option which will be economically competitive within the next 7-8 years.

ACKNOWLEDGMENTS

This research project would not have been possible without the advice, guidance and help of a range of people. Firstly, I would like to thank my supervisors, especially Bruce Jefferson for the constructive comments and guidance during my writing-up. The help and input of Simon Parsons and Peter Jarvis have also been greatly appreciated.

I would also like to thank all the people from the Cranfield Water Science Institute for their help in a way or another. Invaluable thanks to Marc Pidou for the opportunity he offered me to do my master placement at Cranfield University which has given me the passion for research. Thanks to Francesco Ometto, Jitka MacAdam and Richard Harnett for their support, especially in the last few weeks of writing-up.

Severn Trent Water is acknowledged for their financial support and special thanks to Julie Hart for providing useful information and support. Thanks to Felicity Roddick for welcoming me in her department at RMIT University which has been a fantastic experience.

Un grand merci à toute ma famille et amis, tout spécialement à mes parents pour leur aide, soutient, patience et persévérance durant toutes ces années.

Et enfin, un énorme merci à Aurelie pour m'avoir permis de garder une balance entre travail et à-côtés, m'avoir fait rire dans les mauvais moments et aidé dans les dernières heures d'écriture, j'en serai à jamais reconnaissant. Et puis, merci à toi qui durant les derniers mois du projet est passé d'un petit pois à une mangue (désolé à ce moment précis c'est ce que tu es !) et m'a donné les dernières forces nécessaires pour terminer et avec qui j'espère et j'en suis sur vais passer les plus beaux moments de ma nouvelle vie.

CONTENTS

LIST OF FIGURES

LIST OF TABLES

ABBREVIATIONS AND NOTATION

ζ – molar extinction coefficient

Φ – quantum yield

λ – irradiation wavelength

•OH – hydroxyl radical

AOP – advanced oxidation process

DBP – disinfection by-product

DOC – dissolved organic carbon

DWI – Drinking Water Inspectorate

EC – European Commission

EEo – electrical energy per order

GAC – granular activated carbon

GC – gas chromatography

k' – pseudo-first order rate constant

$k_{\bullet OH}$ – second order rate constant

LC – liquid chromatography

LED – light emitting diode

LGW – laboratory grade water

log K_{OC} – log (soil-water partition coefficient)

log K_{OW} – log (octanol-water partition coefficient)

LP – low pressure

LVRPA – local volumetric rate of photon absorption

MP – medium pressure

MS – mass spectrometry

MW – molecular weight

NOM – natural organic matter

NPOC – non-purgeable organic carbon

PAC – powdered activated carbon

RTE – radiation transfer equation

SF – scavenging factor

SPE – solid phase extraction

SR – scavenging rate

TOC – total organic carbon

UP - ultrapure

USEPA – United States Environmental Protection Agency

UV - ultraviolet

VRPA – volumetric rate of photon absorption

WHO – World Health Organisation

WLC – whole life cost

WTWs – water treatment works

CHAPTER 1 INTRODUCTION

CHAPTER1: INTRODUCTION

1.1 Background

The poor efficiency of pesticide application in agriculture, where only 10% of the amount applied reaches its target, leads to high levels of pesticides being reported in many surface waters (Gray, 2008). Whilst pesticides are effective at destroying their target pests or weeds, they can also be harmful and toxic to the environment and to humans (Kirkhorn et al., 2002). For that reason, the European Union developed the EC Drinking Water Directive 98/83/EC which has set a concentration limit of 0.1 $\mu g.L^{-1}$ for each individual pesticide as well as a maximum level of 0.5 $\mu g.L^{-1}$ for the total pesticide concentration (EC, 1998). As a result of this legislation, drinking water treatment works (WTWs) have installed new process operations that are capable of removing the pesticides to below the 0.1 $\mu g.L^{-1}$ standard. Since the early 1980s, a range of new processes have been developed and applied that are able to degrade pesticides to sub-$\mu g.L^{-1}$ concentrations. This includes processes such as activated carbon (Hyde, 1989) and ozonation (Meijers et al., 1993). Although these processes are effective at removing the majority of pesticides and other micropollutants, there is growing evidence to suggest that polar pesticides such as metaldehyde are not removed by this combination of treatment processes (Hall et al., 2011).

In 2009, the Drinking Water Inspectorate (DWI) Annual Reports for drinking water quality in England and Wales reported that metaldehyde was responsible for one third of the 1103 failures observed in these two countries. The regions most affected by metaldehyde are in areas where arable farming impacts on water catchments. This predominantly includes the central, eastern and south eastern regions of England (DWI, 2010). As a consequence, the UK water industry is exploring new ways of controlling metaldehyde levels for drinking water distribution. Severn Trent Water decided to support this project in order to investigate the

development of an alternative barrier for metaldehyde removal. Previous work at Cranfield University, in addition to the literature, showed that advanced oxidation processes (AOPs) were effective at degrading various types of organic compounds including pesticides (Chelme-Ayala et al., 2010). However, concerns over the impact of background water constituents on the viability of AOPs for micropollutants remains. For that reason, this study investigated the use of two advanced oxidation processes, UV/H_2O_2 and heterogeneous photocatalysis UV/TiO_2, for the removal of metaldehyde in surface water including reservoir water sampled from the Severn Trent Water area.

1.2 Objectives

The hypothesis of this thesis was that the efficacy of micropollutant removal is controlled by the presence of natural organic matter (NOM) and alkalinity in the water. Accordingly, a series of objectives were derived to establish the role of background constituents on the efficacy of AOPs for micropollutant removal:

(1) To identify the relationships between the physico-chemical properties of pesticides, background water quality and AOP design on the treatability of pesticides by AOPs.
(2) To compare the efficacy of two AOPs: UV/H_2O_2 and UV/TiO_2 for metaldehyde removal.
(3) To understand the role of alkalinity as well as NOM concentration and character on the efficacy of metaldehyde removal in AOPs.
(4) To evaluate the potential of UV light emitting diodes (LEDs) as a new source of UV light for low energy AOPs in water treatment.

1.3 Thesis structure

This thesis takes the form of a series of chapters formatted as papers for publication. All papers were written by the first author, Olivier Autin and have been edited by Prof Bruce

Jefferson. All experimental work was undertaken at Cranfield University by Olivier Autin with the exceptions of Chapter 6: preliminary work on the penetration and coverage of the UV light emitted by LEDs was carried out by Christophe Romelot as part of his internship and the comparison of traditional low pressure lamps and UV LEDs for the degradation of methylene blue was carried out by Lena Rust as part of her internship.

Chapter 2 focuses on the links between the physicochemical properties of both the micropollutants and NOM, and the treatability of micropollutants by AOPs, and is entitled: *Understanding the reactivity of pesticides towards •OH in drinking water treatment by advanced oxidation processes* by O. Autin, J. Hart, J. MacAdam, P. Jarvis, S.A. Parsons and B. Jefferson, submitted to *Critical Reviews in Environmental Science and Technology*. The chapter looks at the importance of the reactivity of pesticides, characterised by the second order hydroxyl radical rate constant $k_{\bullet OH}$, on their degradation by AOPs. It also looks at the influence of •OH scavengers (NOM and carbonate ions) on the efficiency of AOPs, and finally at other critical operational parameters that can affect the effectiveness of AOPs.

Chapter 3, entitled *Comparison of UV/H_2O_2 and UV/TiO_2 for the degradation of metaldehyde: Kinetics and the impact of background organics* by O. Autin, J. Hart, P. Jarvis, J. MacAdam, S.A. Parsons and B. Jefferson is published in the journal *Water Research*. It directly compares the influence of H_2O_2 and TiO_2 concentrations on the kinetics of degradation of metaldehyde. The comparison was made in both laboratory grade water where metaldehyde is the only organic compound in solution and in surface water where background organic matter competes with the micropollutant for •OH.

Chapter 4, *The impact of background organic matter and alkalinity on the degradation of the pesticide metaldehyde by two advanced oxidation processes: UV/H_2O_2 and UV/TiO_2* by O. Autin, J. Hart, J. MacAdam, P. Jarvis, S.A. Parsons and B. Jefferson has been accepted in the

journal *Water Research*. It examines the influence of water parameters on the degradation of metaldehyde by the two AOPs using model compounds to simulate NOM. The concentration of model compounds was measured to monitor the influence of NOM on the degradation competition between micropollutants and background organic matter.

Chapter 5 follows the previous chapter and also looks at the influence of water parameters on the degradation of metaldehyde but at pilot scale in an annular photoreactor. The chapter is *Comparison of UV/TiO_2 and UV/H_2O_2 processes in an annular photoreactor: influence of water quality on micropollutant removal, quantum yields and energy consumption* by O. Autin, P. Jarvis, S.A. Parsons and B. Jefferson accepted in *Applied Catalysis B*. It examines the impact of NOM and alkalinity on the efficacy of metaldehyde removal in pilot UV/H_2O_2 and UV/TiO_2 reactors. A radiation transfer model was utilised to understand the impact on reactor design with specific reference to channel width.

Chapter 6, *Evaluation of a UV-LEDs unit for the removal of micropollutants in water for low energy advanced oxidation processes* by O. Autin, C. Romelot, L. Rust, J. Hart, J. MacAdam, P. Jarvis, S.A. Parsons and B. Jefferson has been submitted to *Desalination*. It evaluates the potential of LEDs as an alternative to traditional low pressure (LP) lamps in order to reduce the high energy costs associated to light input power. To do so, two micropollutants methylene blue and metaldehyde were irradiated by both traditional LP lamps and LEDs. The economics of the two processes were calculated such that the chapter identifies trends on the future of UV LEDs in advanced oxidation processes.

Chapter 7 entitled *Implication of the work* is an overall discussion which presents the objectives of this study as questions, answered to highlight the key findings of the work.

Finally, Chapter 8, *Conclusions and future work* lists the key results and suggests recommendations for future investigations on AOPs for its development in water treatment.

Table 1-1.1 - Thesis structure

Chapter	Objectives addressed	Focus	Journal	Status
2	1, 3	Literature pesticides treatment by AOPs	*Critical reviews in Environmental Science and Technology*	Submitted
3	1, 2	Comparison UV/H_2O_2 and UV/TiO_2, kinetics	*Water Research*	Published
4	1, 2, 3	Influence NOM and alkalinity	*Water Research*	Accepted
5	1, 2, 3	Pilot study, modelling	*Applied Catalysis B*	Accepted
6	2, 4	Comparison LP lamps vs. LEDs, economics	*Desalination*	Submitted
7	1, 2, 3, 4	Implication of the work		

1.4 References

Chelme-Ayala, P., El-Din, M.G., Smith, D.W., 2010. Degradation of bromoxynil and trifluralin in natural water by direct photolysis and UV plus H_2O_2 advanced oxidation process. Water Res. 44(7), 2221-2228.

Drinking Water Inspectorate, Available at: http://www.dwi.gov.uk, 2010, (accessed May 2011).

EC, 1998. Council Directive 98/83/EC of 3 November 1998 on the quality of water intended for human consumption, Off. J. Eur. Commun. L330 (32).

Gray, N. F., 2008. Drinking Water Quality: Problems and solutions, Chapter 6: Pesticides and organic micro-pollutants, second edition. Cambridge University Press, Cambridge, 137-168.

Hall, T., Holden, B., Haley, J., 2011. Treatment for metaldehyde and other problem pesticides. 4th Developments in Water Treatment and Supply Conference, Cheltenham, June 7-8 2011.

Hyde, R. A., 1989. Application of Granular Activated Carbon in the Water Industry. J. Inst. Water Env. Man. 3(2), 174-179.

Kirkhorn, S. R., Schenker, M. B., 2002. Current health effects of agricultural work: Respiratory disease, cancer, reproductive effects, musculoskeletal injuries, and pesticide-related illnesses. J. Agric. Saf. Health 8(2), 199-214.

Meijers, R. T., Van der Veer, A. J., Kruithof, J. C., 1993. Degradation of pesticides by ozonation and advanced oxidation. Water Supply 11(3-4), 309-320.

CHAPTER 2 UNDERSTANDING THE REACTIVITY OF PESTICIDES TOWARDS •OH IN DRINKING WATER TREATMENT BY ADVANCED OXIDATION PROCESSES

CHAPTER 2: UNDERSTANDING THE REACTIVITY OF PESTICIDES TOWARDS •OH IN DRINKING WATER TREATMENT BY ADVANCED OXIDATION PROCESSES

Olivier Autin [a], *Julie Hart* [b], *Peter Jarvis* [a], *Jitka MacAdam* [a], *Simon A. Parsons* [a], *Bruce Jefferson* [a]

[a] Cranfield Water Science Institute, Department of Environmental Science and Technology, Cranfield University, Bedfordshire, MK43 0AL, UK.

[b] Severn Trent Water LTD., Severn Trent Centre, PO Box 5309, Coventry, West Midlands, CV3 9FH, UK.

2.1 Abstract

This review highlights the important parameters that need to be considered in the evaluation of AOPs potential for the removal of specific micropollutants. It showed that although the reactivity towards •OH was critical in the evaluation of the AOPs effectiveness, its accurate determination is still very difficult to achieve and poor reproducibility from study to study was observed. Along with reactivity of micropollutant, the quality of the water is another key parameter often discarded in research studies. Background organic material can have a significant inhibition effect on the degradation of micropollutants, and whilst micropollutants with high reactivity can be affected by less than 25%, those with low reactivities can be inhibited by more than 90%.

Keywords: Advanced oxidation processes, pesticides, reactivity, scavenging, natural organic matter, alkalinity.

2.2 Introduction

Pesticides are defined as any substance or mixture of substances intended for controlling or destroying pests (Environment Agency, 2012). Pesticides have been used on an industrial scale since the 1930s following the discovery and manufacture of the first synthetic organic pesticides for control of insects, weeds, fungus, molluscs and other unwanted organisms. By the 1950s, pesticides such as dichlorodiphenyltrichloroethane (DDT) were widely applied due to being highly effective contact poisons (Heberer and Dunnbier, 1999). Whilst chemicals such as DDT are no longer used, there are now thousands of chemicals available for pesticide application. Agriculture and horticulture are the industries which are the major users of pesticide, accounting for nearly 80% of the total pesticide use (Environment Agency, 2012). It has been estimated that of the chemical applied, only 10% of the application reaches their target weeds or pests (Gray, 2008). A significant proportion of the pesticide may remain in the soil which in turn drains into surface waters after periods of rainfall. Surface and groundwater pollution by pesticides has been shown to affect aquatic life and traces of pesticide have been found in fishes, molluscs and birds (Miglioranza et al., 2002; Kasozi et al., 2006).

As pesticides may represent a significant health concern for humans, there has been increased awareness regarding the occurrence of pesticides in the environment and safe exposure limits for consumption of pesticides by humans. To address this, the World Health Organisation (WHO) has produced guidelines for exposure limits for individual pesticides in drinking water (WHO, 2004). In the European Union a more stringent approach has been adopted, where a fixed limit of 0.1 $\mu g.L^{-1}$ has been set for all individual pesticides. In addition, the allowable total pesticide concentration (i.e. the sum of all individual pesticides) is set at 0.5 $\mu g.L^{-1}$ (EC Drinking Water Directive 98/83/EC).

Currently, more than 1600 pesticides are available for use across the world (Pimentel and Lehman, 1993) and each year more than 2.3 million tons of active pesticide ingredient is applied worldwide (Kiely et al., 2004). Although herbicides are the largest group of pesticides in terms of the number of compounds and total weight used, insecticides have historically posed the major environmental and health hazards (Gray, 2008). The progression of pesticide development has moved from highly toxic and persistent chemicals in the 1970s to today's pesticides that degrade relatively quickly in the environment and are less toxic to non-target organisms (Gray, 2008).

Since EC legislation was tightened, drinking water treatment works (DWTWs) have adapted and installed new operations capable of reducing the level of pesticides to below the target level of 0.1 $\mu g.L^{-1}$. Rudimentary water treatment flow sheets consisting of coagulation-flocculation, sedimentation, conventional filtration and chlorination only partially eliminate pesticides from finished drinking water (US EPA, 2001). During coagulation, some removal of pesticides (particularly hydrophobic chemicals) is observed from their adsorption onto flocs and natural organic material present in the water (Thuy et al., 2008). However, no more than 40% removal has been observed during coagulation for a wide range of pesticides (Table 2-1). Chlorination is also able to partially remove pesticides but concerns about the formation of disinfection by-products (DBPs) from the reaction of chlorine with both natural organic matter and pesticides have arisen because these DBPs may present a potential health risk (Goslan et al., 2009). As a result of the poor removal of pesticides by these treatment stages, a range of new processes have been developed and installed since the 1980s to reduce pesticide concentrations in drinking water to sub-$\mu g.L^{-1}$ levels. The most widely used processes for this application has been either activated carbon or ozonation or a combination of the two (Hyde, 1989; Pirbazari et al., 1991; Foster et al., 1991; Meijers et al., 1993; Hu et al., 1998; Hossain et al., 2006). Ozonation has proven to be effective in the removal of many

micropollutants and is still widely used for this purpose, however a number of pesticide chemicals are resistant to oxidation by ozone. For example, the triazine pesticides are difficult to remove due to the stability of the triazinic ring in the molecule (Ormad et al., 2008). Pesticides such as clopyralid resist degradation due to the electron-withdrawing properties of the N and two Cl atoms in the molecule which act to stabilise the molecule (Tizaoui et al., 2011). Metaldehyde is hard to remove as it is not aromatic in nature and does not have any double bonds or heteroatoms in its structure: features which are known to be selectively attacked by ozone (von Gunten, 2003) (Table 2-1). A review by Ikehata and El-Din (2005) concluded that complete destruction of pesticides by ozonation would not be possible. Activated carbon, the other technology of choice for pesticide removal, has also proven relatively ineffective for removal of polar pesticides such as metaldehyde and clopyralid. These compounds exhibit low log k_{ow} values and therefore have a relative higher hydrophilicity than other pesticides which are generally well removed by activated carbon (Table 2-1). The water industry is therefore looking for new technologies that would be less selective and be able to remove all types of pesticides. Membrane filtration processes and advanced oxidation processes (AOPs) have received particular attention. Whilst nanofiltration is able to remove high levels of pesticides and often produce compliant treated waters, the pollutants are concentrated in the rejection phase and additional treatments are required for these highly concentrated slurries of pesticides (Ikehata and El-Din, 2005).

Over the last decade, AOPs have been widely studied and processes have been developed in order to degrade what are generally very low concentrations of pesticides. This includes Fenton's reagent processes (Huston and Pignatello, 1999; Ijpelaar et al., 2000; Catalkaya et al., 2008; Macadam and Parsons, 2009); UV/H_2O_2 (Kruithof et al., 2002; Chelme-Ayala et al., 2010a); H_2O_2/O_3 (Tanghe et al., 1992; Ormad et al., 1997); and UV/photocatalysis (Herrmann et al., 1998; Tizaoui et al., 2011). AOPs are principally based on the production of

the highly reactive and quasi-unselective hydroxyl radical (•OH) in water. This radical has been shown to be able to oxidise a broad range of organic micropollutants very quickly, with first order rate constants in the range 10^8-10^{10} $M^{-1}.s^{-1}$ (Haag and Yao, 1992). A large number of complex reactions are involved in AOPs and the rate of oxidation will generally vary with the •OH, pollutant concentrations and, in the case of UV/TiO_2, oxygen which by trapping electrons reduces the recombination rate of electron-hole pairs. Of the existing AOPs, UV/H_2O_2 is one of the most widely applied due to the high yield of •OH radicals from this process (Parsons, 2004). UV/titanium dioxide (UV/TiO_2) photocatalysis is an AOP of great interest as it offers the potential for what is effectively a chemical free treatment due to the continuous recycling of the catalyst material. For these reasons, this review focuses specifically on these two AOPs for application for micropollutant removal. Many studies have looked at the degradation of a wide range of pesticides and micropollutants and this review aims to understand how the structure and properties of micropollutants impact on their reactivity towards •OH. Fundamental to the removal of contaminants at such low concentrations is understanding the matrix within which the target pollutant is found and knowing how other competing molecules may interfere with this removal. The review will therefore also look at the type and quality of water used in past work and determine how critical specific water quality parameters are on the accurate evaluation of the kinetics of degradation by UV/H_2O_2 and UV/TiO_2. Finally, the influence of operational conditions on the rates of degradation will be discussed for the two processes.

Table 2-1 - Removal of pesticides by traditional water treatment processes

Chemical family	Pesticide	Log k_{OW}	Water characteristics	Removal by coagulation	Removal by chlorination	Removal by ozonation	Removal by activated carbon	Removal by nanofiltration	References
Aniline	Alachlor	3.05	[TOC]=3 mg.L^{-1} [P]=50 µg.L^{-1}	[Alum]=30 mg.L^{-1} **4%** [$FeCl_3$]=20 mg.L^{-1} **4%**	[HOCl]=6 mg.L^{-1} pH7: **0%**	[O_3]=3 mg.L^{-1} **63%**			Hladik et al., 2005
			River water [P]=0.5 µg.L^{-1}		[HOCl]=18 mg.L^{-1} **30%**	[O_3]= 4.3 mg.L^{-1} **70%**	Powdered (10 mg.L^{-1}) **75%**		Ormad et al., 2008
	Metolachlor	3.03	[TOC]=3 mg.L^{-1} [P]=50 µg.L^{-1}	[Alum]=30 mg.L^{-1} **5%** [$FeCl_3$]=20 mg.L^{-1} **6%**	[HOCl]=6 mg.L^{-1} pH7: **0%**	[O_3]=3 mg.L^{-1} **60%**			Hladik et al., 2005
			River water [P]=0.524 µg.L^{-1}		[HOCl]=18 mg.L^{-1} **25%**	[O_3]= 4.3 mg.L^{-1} **70%**	Powdered (10 mg.L^{-1}) **75%**		Ormad et al., 2008
	Acetochlor	3.05	[TOC]=3 mg.L^{-1} [P]=50 µg.L^{-1}	[Alum]=30 mg.L^{-1} **4%** [$FeCl_3$]=20 mg.L^{-1} **6%**	[HOCl]=6 mg.L^{-1} pH7: **0%**	[O_3]=3 mg.L^{-1} **61%**			Hladik et al., 2005
	Heptachlor	5.71	River water [P]=0.5 µg.L^{-1}		[HOCl]=18 mg.L^{-1} **70%**	[O_3]= 4.3 mg.L^{-1} **90%**	Powdered (10 mg.L^{-1}) **95%**		Ormad et al., 2008
Triazine	Atrazine	2.63	Ground water [P]=300 µg.L^{-1}					NF70: **96.8%** NF45: **92.4%** UTC20: **87.5%** NTR7450: **26.2%**	Van der Bruggen et al., 1998
			River water [DOC]=6.7 mg.L^{-1} pH=7.2 [P]=10 µg.L^{-1}	[$Al_2(SO_4)_3$]= 100 mg.L^{-1} **29%**					Thuy et al., 2008

Table 2-1 (Continued)

Chemical family	Pesticide	Log k_{OW}	Water characteristics	Removal by coagulation	Removal by chlorination	Removal by ozonation	Removal by activated carbon	Removal by nanofiltration	References
			River water [P]=0.551 μg.L^{-1}		[HOCl]=18 mg.L^{-1} **20%**	[O_3]= 4.3 mg.L^{-1} **50%**	Powdered (10 mg.L^{-1}) **55%**		Ormad et al., 2008
			Distilled water [P]=10 μg.L^{-1}					NF270: **83.6%**	Caus et al., 2009
			River water [P]=5 μg.L^{-1} DOC=5-7 mg.L^{-1} Alk=203-210 mg.L^{-1} as $CaCO_3$	[$Al_2(SO_4)_3$]=0-107 mg.L^{-1}: **0%**	[Cl_2]=2 mg.L^{-1} pH=6.1 30 min contact time: **0%**	[O_3]=5 mg.L^{-1} pH6 **61%**	WPH Powdered (5 mg.L^{-1}) 4h contact time **69%**		Jiang and Adams, 2006
	Simazine	2.28	Ground water [P]=300 μg.L^{-1}					NF70: **96.4%** NF45: **82.6%** UTC20: **78.0%** NTR7450: **17.4%**	Van der Bruggen et al., 1998
			River water [P]=0.554 μg.L^{-1}		[HOCl]=18 mg.L^{-1} **50%**	[O_3]= 4.3 mg.L^{-1} **65%**	Powdered (10 mg.L^{-1}) **55%**		Ormad et al., 2008
	Propazine	2.99	River water [P]=0.5 μg.L^{-1}		[HOCl]=18 mg.L^{-1} **30%**	[O_3]= 4.3 mg.L^{-1} **50%**	Powdered (10 mg.L^{-1}) **55%**		Ormad et al., 2008
			Distilled water [P]=10 μg.L^{-1}					NF270: **89.5%**	Caus et al., 2009
Chloro-phenoxy-carboxylic acid	MCPA		Surface water [P]=0.05-0.5 μg.L^{-1}			[O_3]= 7.5 mg.L^{-1} **84%**			Hall et al., 2011

Table 2-1 (Continued)

Chemical family	Pesticide	Log k_{OW}	Water characteristics	Removal by coagulation	Removal by chlorination	Removal by ozonation	Removal by activated carbon	Removal by nanofiltration	References
Urea	Diuron	2.68	Ground water [P]=300 µg.L^{-1}					NF70: **91.6%** NF45: **50.6%** UTC20: **47.9%** NTR7450: **6.4%**	Van der Bruggen et al., 1998
			River water [P]=0.5 µg.L^{-1}		[HOCl]=18 mg.L^{-1} **100%**	[O_3]= 4.3 mg.L^{-1} **75%**	Powdered (10 mg.L^{-1}) **55%**		Ormad et al., 2008
	Isoproturon	2.89	Ground water [P]=300 µg.L^{-1}					NF70: **95.7%** NF45: **76.5%** UTC20: **71.1%** NTR7450: **23.1%**	Van der Bruggen et al., 1998
			River water [P]=0.5 µg.L^{-1}		[HOCl]=18 mg.L^{-1} **100%**	[O_3]= 4.3 mg.L^{-1} **70%**	Powdered (10 mg.L^{-1}) **60%**		Ormad et al., 2008
Organo-phosphate	Chlorpyrifos	5.00	River water [P]=0.52 µg.L^{-1}		[HOCl]=18 mg.L^{-1} **100%**	[O_3]= 4.3 mg.L^{-1} **80%**	Powdered (10 mg.L^{-1}) **90%**		Ormad et al., 2008
Organo-chlorine	Aldrin	6.23	River water [P]=0.5 µg.L^{-1}		[HOCl]=18 mg.L^{-1} **100%**	[O_3]= 4.3 mg.L^{-1} **85%**	Powdered (10 mg.L^{-1}) **100%**		Ormad et al., 2008
			Distilled water [P]=10 µg.L^{-1}					NF270: **94.3%**	Caus et al., 2009
	Dieldrin	4.48	River water [P]=0.5 µg.L^{-1}		[HOCl]=18 mg.L^{-1} **30%**	[O_3]= 4.3 mg.L^{-1} **90%**	Powdered (10 mg.L^{-1}) **85%**		Ormad et al., 2008

Table 2-1 (Continued)

Chemical family	Pesticide	Log k_{OW}	Water characteristics	Removal by coagulation	Removal by chlorination	Removal by ozonation	Removal by activated carbon	Removal by nanofiltration	References
			River water [DOC]=6.7 $mg.L^{-1}$ pH=7.2 [P]=10 $\mu g.L^{-1}$	$[Al_2(SO_4)_3]$= 100 $mg.L^{-1}$ **38%**					Thuy et al., 2008
			Distilled water [P]=10 $\mu g.L^{-1}$					NF270: **97.3%**	Caus et al., 2009
	Endrin	4.48	River water [P]=0.5 $\mu g.L^{-1}$		[HOCl]=18 $mg.L^{-1}$ **15%**	$[O_3]$= 4.3 $mg.L^{-1}$ **80%**	Powdered (10 $mg.L^{-1}$) **85%**		Ormad et al., 2008
			River water [DOC]=6.7 $mg.L^{-1}$ pH=7.2 [P]=10 $\mu g.L^{-1}$	$[Al_2(SO_4)_3]$= 100 $mg.L^{-1}$ **33%**					Thuy et al., 2008
Pyridine	Clopyralid	1.06	Surface water [P]=0.05-0.5 $\mu g.L^{-1}$			$[O_3]$= 7.5 $mg.L^{-1}$ **14%**	Powdered (15 $mg.L^{-1}$) **0%**		Hall et al., 2011
Diazine	Bentazone	0.35	River water [DOC]=6.7 $mg.L^{-1}$ pH=7.2 [P]= 10$\mu g.L^{-1}$	$[Al_2(SO_4)_3]$= 100 $mg.L^{-1}$ **16%**					Thuy et al., 2008
			Distilled water [P]=10 $\mu g.L^{-1}$					NF270: **97.9%**	Caus et al., 2009
Aldehyde	Metaldehyde	0.12	Surface water [P]=0.05-0.2 $\mu g.L^{-1}$			$[O_3]$= 4 $mg.L^{-1}$ **4%**	GAC **20-35%**		Hall et al., 2011

2.3 Basic principles of UV/H_2O_2

The irradiation of hydrogen peroxide with UV light in the range 200-280 nm leads to the formation of hydroxyl radicals (Shemer and Linden, 2006) with a yield of two radicals formed per photon absorbed as follows:

$$H_2O_2 + h\nu \rightarrow 2\ \bullet OH \quad (2\text{-}1)$$

The quantum yield of the photolysis of H_2O_2 by 253.7 nm light is 1.0 at 25ºC and is independent of both the concentration and light intensity over the range $2x10^{-5}$ to $1x10^{-1}$ M H_2O_2 and $3.5x10^{-2}$ to 39 $mW.cm^{-3}$ respectively (Parsons, 2004). The initial hydrogen peroxide concentration is linked to the rate of degradation, where an increase in concentration leads to the production of more hydroxyl radicals which can therefore react with the target molecule. The maximum absorbance of hydrogen peroxide occurs at about 220 nm, but most UV/H_2O_2 systems use low pressure Hg lamps with a peak emission at 254 nm for economic reasons (Parsons, 2004). However, the molar extinction coefficient (ξ), which expresses the light absorption capacity of a compound from the Beer-Lambert law, of H_2O_2 is very low, ξ = 19.6 $M^{-1}.cm^{-1}$ at 254 nm (Parsons, 2004). This means that a sufficiently high concentration of H_2O_2 is required in order to form •OH. Nevertheless, the rate of degradation has a limit, and for very high hydrogen peroxide concentrations, H_2O_2 molecules themselves will act as scavengers of radicals, reducing the effectiveness of the process:

$$HO\bullet + H_2O_2 \rightarrow HO_2\bullet + H_2O \quad (2\text{-}2)$$

$$HO_2\bullet + H_2O_2 \rightarrow HO\bullet + H_2O + O_2 \quad (2\text{-}3)$$

$$HO_2\bullet + HO_2\bullet \rightarrow H_2O_2 + O_2 \quad (2\text{-}4)$$

During UV/H_2O_2 treatment, both direct photolysis (direct breakage of the chemical bonds by absorption of photons by the molecule) and indirect photolysis (breakage of molecules via the free radicals •OH) are responsible for the degradation of micropollutants. As two distinct mechanisms drive the process, the rate of degradation of organic compounds is the combined rate of degradation via direct and indirect photolysis. The degradation kinetics by direct photolysis is defined by:

$$-\frac{d[P]}{dt} = \Phi(\lambda)K_s[P] = k'_d\,[P] \tag{2-5}$$

with

$$K_s(\lambda) = \frac{E^0{}_p(\lambda)\varepsilon(\lambda)[1-10^{-a(\lambda)z}]}{a(\lambda)z} \tag{2-6}$$

where [P] is the molar concentration of the pollutant P, Φ is the quantum yield, K_s represents the specific rate of light absorption by the compound, k'_d is the time-based pseudo-first order rate constant of degradation of P by direct photolysis, E^0_p is the incident photon irradiance, ε is the decadic molar absorption coefficient, a is the absorbance of the solution and z is the solution depth.

The degradation kinetics from indirect photolysis is given by:

$$-\frac{d[P]}{dt} = k_{\bullet OH,P}[\bullet OH][P] = k'_i\,[P] \tag{2-7}$$

where $k_{\bullet OH,P}$ is the second-order rate constant of the hydroxyl radical with the pollutant P, [•OH] is the concentration of hydroxyl radicals in solution and k'_i is the time-based pseudo-first order rate constant of degradation of P by indirect photolysis.

The total rate of degradation by UV/H_2O_2 (direct and indirect photolysis) is:

$$-\frac{d[P]}{dt} = \Phi(\lambda)K_s(\lambda)[P] + k_{\bullet OH,P}[\bullet OH][P] \quad (2\text{-}8)$$

The concentration of •OH is considered constant over the range of reaction and therefore, an overall pseudo-first order rate constant can be used:

$$-\frac{d[P]}{dt} = (k'_d + k'_i)[P] = k'[P] \quad (2\text{-}9)$$

Where k' is the overall pseudo first order rate constant, and is expressed in unit of time^{-1}, or cm^2.mJ^{-1} if the UV fluence is used.

The integration of the equation gives:

$$\ln\frac{[P]_0}{[P]} = k't \quad (2\text{-}10)$$

2.4 Basic principles of heterogeneous photocatalysis

The ideal photocatalyst for destruction of organic compounds should principally be highly photoactive and have a band gap energy large enough to catalyse a wide range of chemicals (Beydoun et al., 1999). It should also be non-toxic, insoluble, inexpensive and consequently applicable for all scales of water treatment (Parsons, 2004). Although many semiconductors have high enough band gap energies to be very strong oxidants, few are able to meet all of the criteria required for practical use as some of them are known to be toxic and many are subject to photo-corrosion. Titanium dioxide (TiO_2) has received the most attention as an appropriate photocatalyst because it is biologically and chemically inert, resistant to chemical degradation and is inexpensive (Al-Ekabi et al., 1992; Howe, 1998). TiO_2 absorbs light at all wavelengths below 380 nm, and thus light sources from low and medium pressure Hg lamps are suitable to

activate TiO_2. Solar radiation can also activate TiO_2, although only 3-5% of this light is absorbed by TiO_2 (Herrmann, 2005).

Commercial TiO_2 powders are generally used as the catalyst in applied research studies. Degussa P25 and Hombikat UV100 are the most commonly used manufactured TiO_2 materials (Konstantinou et al., 2001; Chu and Wong, 2004; Doll and Frimmel, 2005). However, extensive work is also devoted to the synthesis of TiO_2 in order to 1) improve its photocatalytic activity by reducing the crystal size and minimise bulk defects (Yeung et al., 2002), and 2) make its activation possible by visible light. These effects are achieved by metal-doping, dye sensitization or from the controlled sol-gel manufacture of TiO_2 nanoparticles (Helaili et al., 2009). When the TiO_2 particle is irradiated by a photon that has an energy greater than the band gap energy, an electron passes from the valence band to the conductance band of the semiconductor, creating a hole in the valence band. The process of the creation of an electron-hole pair can be represented by the following equation:

$$TiO_2 + h\nu\ (E_{photons} > 3.2\ eV) \rightarrow TiO_2\ (e^-_{CB}) + TiO_2\ (h^+_{VB}) \qquad (2\text{-}11)$$

The excited electron and hole move to the surface of the TiO_2 and may react with adsorbed substances that can accept or give electrons (Akpan and Hameed, 2009). The normal fate, however, of the electron-hole pair is recombination, either at the surface or in the bulk material. The rate of recombination can be enhanced by the presence of impurities in the crystalline structure of the TiO_2. These properties can be artificially altered during the manufacture of the material to produce a more effective catalyst. If electrons and holes are able to make their way to the surface of TiO_2 particles, the holes can oxidise HO^- ions and H_2O molecules either adsorbed,

or very close to, the TiO_2 surface, but the holes may also react directly with the pollutants. These reactions are summarised by:

$$h^+ + H_2O \rightarrow HO\bullet + H^+ \quad (2\text{-}12)$$

$$h^+ + HO^- \rightarrow HO\bullet \quad (2\text{-}13)$$

$$h^+ + Ti^{IV}\text{-}OH \rightarrow Ti\text{-}OH\bullet \quad (2\text{-}14)$$

$$h^+ + \text{pollutant} \rightarrow \text{pollutant}_{oxidized} \quad (2\text{-}15)$$

To balance the reaction of the electron hole, the excited electron must also react with a scavenger because if the electron does not react quickly enough with a scavenger, it will recombine with the hole and the catalyst will lose its activity. When in water the electron acceptor is invariably dissolved oxygen reduced to the superoxide radical anion:

$$e^- + O2 \rightarrow O_2^-\bullet \quad (2\text{-}16)$$

$$O_2^-\bullet + H^+ \rightarrow HO_2\bullet \quad (2\text{-}17)$$

If enough energy is put into the system, the final products are usually the mineral forms of the compound, typically carbon dioxide, water and mineral acid if a heteroatom is present in the pollutant (Parsons, 2004).

The •OH radical plays an important role in the oxidation of pesticides by UV/TiO_2. However, other species can be formed when TiO_2 is irradiated and these can have a role in the degradation mechanism of the contaminant (unlike during UV/H_2O_2 where •OH radicals are the only species formed). This includes the formation of superoxide radicals $O_2^-\bullet$, hydroperoxyl radicals $HO_2\bullet$ or electron holes h^+. The rate of degradation of pesticides by UV/TiO_2 is generally obtained using

the Langmuir-Hinshelwood model. This model separates the observed kinetics of the contaminant removal into reaction and adsorption components (Zheng et al., 2010). A simple representation of the Langmuir-Hinshelwood model is described as follows:

$$r = -\frac{d[P]}{dt} = \frac{k_r K[P]}{1 + K[P]} \tag{2-18}$$

where r is the rate of degradation of the pollutant *P*, P_0 is the initial concentration of the compound P, k_r is the reaction rate constant and K is the adsorption coefficient of P.

The integration of the equation leads to:

$$\ln \frac{[P]_0}{[P]} + K([P]_0 - [P]) = k_r K t \tag{2-19}$$

This equation is the sum of zero-order and first-order rate equations. The contribution of each to the overall reaction depends on the initial concentration of the pollutant. In drinking water treatment, the pollutants being removed are usually at very low concentrations, so P_0 is generally very small and the equation can be reduced to:

$$\ln \frac{[P]_0}{[P]} = k_r K t = k' t \tag{2-20}$$

where k' is apparent pseudo-first-order rate constant.

A plot of ln $[P]_0/[P]$ vs. t should result in a straight line in which the slope represents the apparent first-order rate constant k'.

However, although the Langmuir-Hinshelwood is the most widely used model to describe kinetics in UV/TiO_2 systems its application has been questioned by different workers (Minero et

al., 1999; Valencia et al., 2011). This is because the Langmuir-Hinshelwood model is based on the degree of adsorption (K) of the pollutant onto the TiO_2 surface, and therefore does not explain the photocatalytic degradation when the contaminant is not adsorbed on the surface of the catalyst. New models are therefore being developed which take into consideration all of the key steps involved in heterogeneous photocatalysis (Montoya et al., 2009; Valencia et al., 2011).

2.5 Significance of first and second order rate constants

In AOP chemistry, the determination of both the first and second order rate constants are of great importance. By assuming that •OH oxidation is the dominant pathway for micropollutant degradation for both UV/H_2O_2 and UV/TiO_2, the kinetics of degradation become:

$$\frac{dC}{dt} = k_{\bullet OH} \times [\bullet OH] \times C = k' \times C \qquad (2\text{-}21)$$

$k_{\bullet OH}$ is an intrinsic property of a micropollutant which evaluates its reactivity towards •OH. The higher the $k_{\bullet OH}$, the more likely the compound is to be removed by AOPs. The first order rate constant k' is the product of $k_{\bullet OH}$ and [•OH] (the [•OH] is assumed constant during treatment as reactions occur very fast (Rosenfeldt and Linden, 2007)). Unlike $k_{\bullet OH}$, k' is specific to each system and will be dependent on the effectiveness of the system to be able to produce •OH. The $k_{\bullet OH}$ therefore permits the comparison of the relative reactivity of a target micropollutant to other common micropollutants whilst k' enables, for a given compound, comparison of the effectiveness of different systems at creating •OH.

2.6 Second-order rate constant $k_{\bullet OH}$

2.6.1 Background

Hydroxyl radicals (•OH) are the main oxidising species formed in AOPs and therefore the estimation of the reactivity of micropollutants towards •OH, expressed by the second-order rate constant $k_{\bullet OH}$, is very useful to evaluate the potential of AOPs for the removal of a specific micropollutant. The reaction between •OH and micropollutants is fast and the values of $k_{\bullet OH}$ are generally in the range 10^8 to 10^{10} $M^{-1}.s^{-1}$ (Haag and Yao, 1992). Second-order rate constants can be determined either experimentally or theoretically. The experimental methods used for obtaining rate constants include pulse radiolysis, laser flash photolysis and competition kinetics (Table 2-2).

Pulse radiolysis is a technique that utilises a high energy source, such as an electron accelerator which can produce voltages ranging from 2 to 30 MeV (Dorfman and Adams, 1973) to form transients detected on very short time scales by spectroscopic analysis (Mezyk et al., 2001; Peller and Kamat, 2005). During pulse radiolysis, the •OH are formed in N_2O-saturated water from the following reactions:

$$H_2O \rightsquigarrow e^-_{aq} + \bullet H + \bullet OH + H_2 + H_2O_2 + H_3O^+ \quad (2\text{-}22)$$

$$N_2O + e^-_{aq} + H_2O \rightarrow N_2 + OH^- + \bullet OH \quad (2\text{-}23)$$

Whilst radiolytic systems provide the most controlled conditions for the study of •OH reactions (Peller and Kamat, 1992), their high cost and the lack of universal availability of the equipment make their use very limited (Shemer and Linden, 2006).

Table 2-2 - Different methods used for the determination of $k_{\bullet OH}$. Information from Dorfman and Adam (1973); Scaiano (1982); Kerst et al. (1997).

	Pulse radiolysis	Laser flash photolysis	Competition kinetics
Principle	Radiation chemical method in which water is decomposed by ionising radiation	Photo-chemical method in which •OH are formed by absorption of UV light	Photo-chemical method in which •OH are formed by absorption of UV light
Excitation source	Electron pulse	UV light pulse laser (3 orders of magnitude faster than conventional flash photolysis)	UV irradiation
Duration	50 ns - 1µs	10 ns - 1µs	s - h
Chemical reaction	$H_2O \rightsquigarrow$ •OH, e^- (+ •H, H_2, H_2O_2, H_3O^+, OH^-)	$O_3 + h\upsilon \rightarrow O + O_2$ $O + H_2O \rightarrow 2\bullet OH$	$H_2O_2 + h\upsilon \rightarrow H_2O_2$
Typical source	Microwave linear accelerator with energy ranging from 2 to 30 MeV	Laser with energy in the range 1-100 mJ/pulse required	Low pressure UV lamp emitting at 254 nm
Mode of determination of $k_{\bullet OH}$	Optical absorption of the reactive intermediate or product formed	Determination of the kinetic laws of the system from the time evolution of the system	Competition kinetics between the target compound and a model compound for which $k_{\bullet OH}$ is well known
Limitations	High cost and lack of universal availability	High concentrations of •OH precursors required which can interfere in the reaction	- Absorption of light by the solute must be low in comparison to that of H_2O_2 (19.6 $M^{-1}.cm^{-1}$) - Model compound must be perfectly defined and must not react with O_3 or UV light at 254 nm - Analytical methods must be perfectly accurate for both the model and target compounds as the ratio is used

In laser flash photolysis, a short pulse of light typically from a frequency quadrupled photolysis laser irradiating at 266 nm is used to interact with a sample placed in the optical path of a spectrometer resulting in a transient absorption or emission process (Ravishankara et al., 1979). The •OH are produced by photolysis of O_3 followed by the reaction between O and H_2O to form 2 •OH (Ravishankara et al., 1979). The use of a laser for sample excitation gives the technique

nanosecond time resolution, single wavelength excitation and a high reproducibility (Orzel et al., 2010).

A simpler method for the determination of $k_{\bullet OH}$ is from competition kinetics, where radicals are produced by photochemical oxidation from processes such as UV/H_2O_2 or $UV/O_3/H_2O_2$ (Wu et al., 2007; De Laat et al., 1996). In all cases, the micropollutant competes for •OH with a reference compound whose $k_{\bullet OH}$ is well known. Para-chlorobenzoic acid (pCBA) is often used as reference compound as it does not undergo direct photolysis and reacts slowly with O_3 (Acero et al., 2003). Other compounds, such as nitrobenzene or acetophenone, have also been used (Armbrust, 2000; Shemer and Linden, 2006). The competition kinetics method relies on the assumption that the reaction with •OH is the only significant pathway for the degradation of both the micropollutant and the reference compound (Shemer and Linden, 2006). The reaction of the two organic compounds referred to as the reference (R) and the target micropollutant (T), with •OH can be described by the following kinetic equations:

$$\text{Micropollutant} + \bullet OH \rightarrow \text{Products} \quad (2\text{-}24)$$

$$r_T = k_{\bullet OH,T} \times [T] \times [\bullet OH] = k'_T \times [T] \quad (2\text{-}25)$$

$$\text{Reference compound} + \bullet OH \rightarrow \text{Products} \quad (2\text{-}26)$$

$$r_R = k_{\bullet OH,R} \times [R] \times [\bullet OH] = k'_R \times [R] \quad (2\text{-}27)$$

Where r_T and r_R are the reaction rates (in $M.s^{-1}$), [-] denotes the molar concentration (in M), $k_{\bullet OH}$ represents the second-order rate constant (in $M^{-1}.s^{-1}$) and k' is the pseudo-first-order rate constant (in s^{-1}).

The oxidation of both compounds follows the pseudo-first-order kinetic model and therefore:

$$\ln (C/C_0) = - k' \times t \quad (2\text{-}28)$$

The slope of the line gives the pseudo-first-order rate constant and subsequently the second-order rate constant between the micropollutant and •OH is obtained by substituting (2-25) and (2-27) such that:

$$\frac{k'_T}{k_{\bullet OH,T}} = \frac{k'_R}{k_{\bullet OH,R}} \quad (2\text{-}29)$$

$$k_{\bullet OH,T} = k_{\bullet OH,R} \times \frac{k'_T}{k'_R} \quad (2\text{-}30)$$

•OH rate constants can alternatively be predicted theoretically using mathematical algorithms. Most of the studies looked at $k_{\bullet OH}$ in gaseous phase but recently, a group contribution method (GCM) has been developed to predict $k_{\bullet OH}$ in the aqueous phase (Minakata et al., 2009). This method hypothesises that the observed experimental rate constant for an organic compound is the combined rate of all elementary reactions involving •OH: H-atom abstraction, •OH addition to alkenes, •OH addition to aromatic compounds and •OH interaction with sulphur-, nitrogen-, or phosphorus-atom-containing compounds (Minakata et al., 2009). The calculation requires knowledge of the molecule geometry and by entering the appropriate information in the model an estimated value of $k_{\bullet OH}$ is generated (Minakata et al., 2009).

2.6.2 Comparison of experimental and theoretical $k_{\bullet OH}$ for pesticides

Comparison of the predicted rate constants with experimental values reported in the literature reveals that prediction of rate constants for pesticides does not strongly match the experimental values (Figure 2-1). According to Minakata et al. (2009), theoretical values which differ from the

experimental values by up to a factor of two can be considered as an acceptable accuracy for model predictions. In this evaluation only 44% of the rate constants were in this range (out of a total of 61 rate constants) whilst 56% were greater than two times higher than the experimental values showing that the model overestimates experimental values. The modelled rate constants were shown to agree most closely with the experimentally determined values for low molecular weight compounds with relatively simple structure (linear and long chains) that exhibit relatively low $k_{\bullet OH}$. The results indicated a much wider discrepancy between modelled and observed data for higher molecular weight compounds, comprising a broad range of molecular structures. This difference is principally explained by interference between the different groups present in the larger molecule which block or slow down the predicted •OH attacks to happen at specific sites.

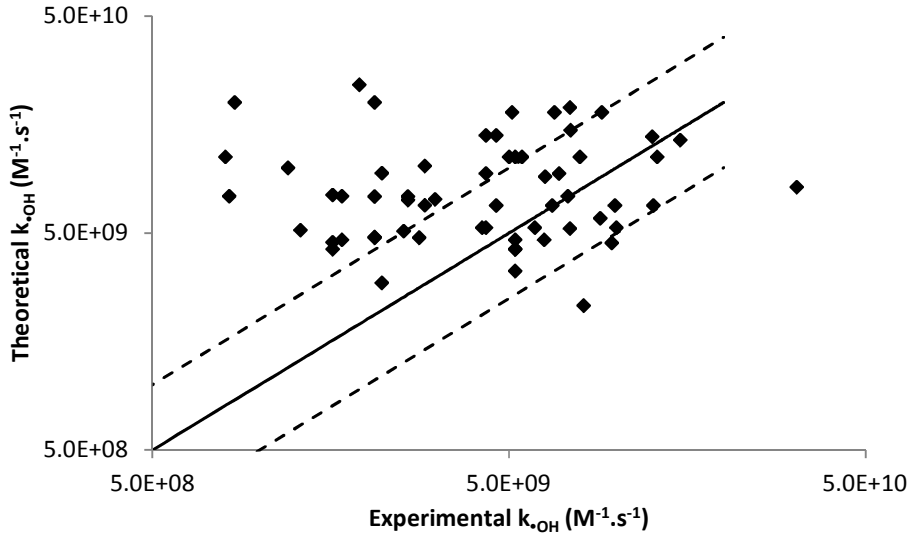

Figure 2-1 - Theoretical vs. experimental second-order rate constants for a range of pesticides. The solid line represents y=x and the dash lines represent the 0.5-2 range in which the modelling is considered acceptable.

There was no relationship between the accuracy of the theoretical and experimental rate constants based on the process used in the experiment with 50%, 52% and 56% of the values out of range for Photo-Fenton, UV/H_2O_2 and UV/O_3/H_2O_2 respectively. For laser flash photolysis,

71% of the obtained values were out of range, although most of the values were only just outside. The closest agreement between experimental and theoretical rate constants were obtained from results using the pulse radiolysis technique which had 100% of the values within the acceptable range however this data set only contained four data points.

For the calibration of the model developed by Minakata et al. (2009) nearly 70% of over 850 experimental values have been obtained by pulse radiolysis. As shown above, this method is the most accurate method available for determining $k_{\bullet OH}$ and correlates well with theoretical values for a wide number of organic compounds and more specifically for pesticides. Hence, it suggests that the model is accurate with experimental values when the rate constants are obtained from the pulse radiolysis method but not from those determined by the other techniques. The experimental $k_{\bullet OH}$ values for a given compound can vary significantly between different studies using different techniques. In fact, the $k_{\bullet OH}$ for isoproturon has been determined in four different studies with values of 8.00×10^8 $M^{-1}.s^{-1}$ by UV/H_2O_2, 5.20×10^9 $M^{-1}.s^{-1}$ by $UV/O_3/H_2O_2$, 7.90×10^9 $M^{-1}.s^{-1}$ by $UV/O_3/H_2O_2$ and 1.30×10^{10} $M^{-1}.s^{-1}$ by laser flash photolysis (De Laat et al., 1992; Lopez et al., 2005; Benitez et al., 2007; Sanches et al., 2010). This shows how experimental determination can be difficult and how the •OH production methods can be critical. As the model seems to better replicate $k_{\bullet OH}$ determined by pulse radiolysis than the other experimental techniques, the model appears a more reliable tool than the traditional competition kinetics by photochemical oxidation for the determination of $k_{\bullet OH}$.

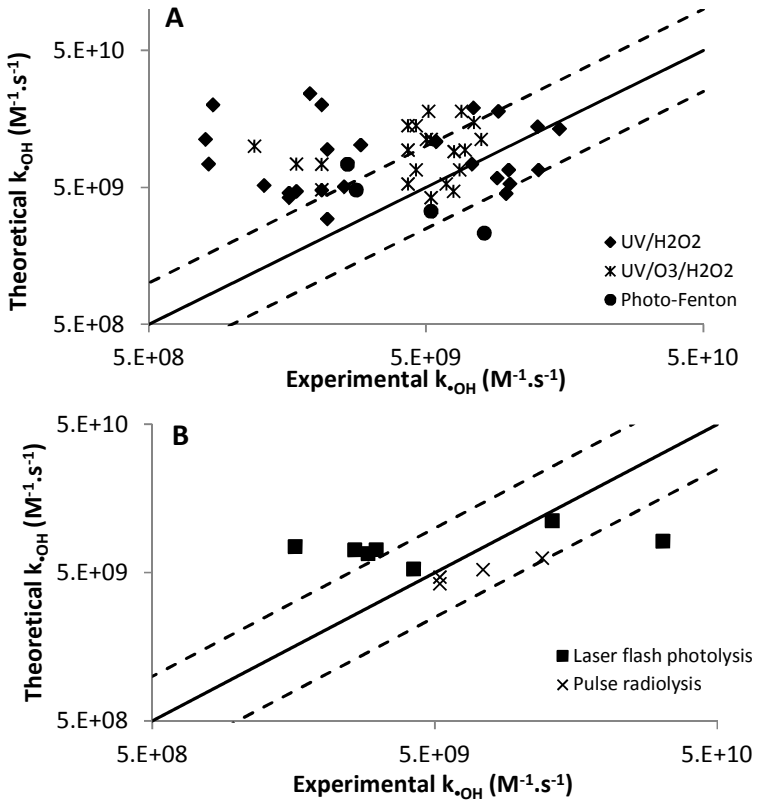

Figure 2-2 - Experimental vs. Theoretical second-order rate constants, with experimental values determined by A) Competition kinetics using UV/H_2O_2, UV/O_3/H_2O_2 and Photo-Fenton as source of •OH, B) Laser flash photolysis of Ar-saturated and pulse radiolysis. The solid line represents y=x and the dash lines represent the 0.5-2 range in which the modelling is considered acceptable.

2.7 Correlations between structure and properties of pesticides and their reactivities towards •OH

The second order rate constants $k_{\bullet OH}$ were determined theoretically using the model developed by Minakata et al. (2009) for over 50 common pesticides and were compared to their physico-chemical properties and their structure (Table 2-4). The correlation coefficients (r^2) between $k_{\bullet OH}$ and the physico-chemical properties were between 0.0084 and 0.3265 (Table 2-3). The lack of any strong correlation is supportive of the view that •OH reactions are non-selective. The best correlations with $k_{\bullet OH}$ were the molar volume (r^2 = 0.33) and polarisability of the pesticide molecules (r^2 = 0.31). These results suggest that it is the molecular structure and particularly the

arrangement of the atoms in the molecule that is more important than the molecular weight of the micropollutant for attack by •OH (where the r^2 value was only 0.08). The slight correlation between the polarisability of the pesticide with k_{OH}, indicated that molecules able to acquire a dipole moment in an electric field are more likely to be attacked by •OH. Other chemical parameters such as the hydrophilicity expressed by log K_{OW}, the water solubility or the potential mobility from soil to water expressed by log K_{OC} do not correlate well with the reactivity of pesticides during AOPs. This makes it difficult for a simple classification of pesticide reactivity according to their chemical properties.

Although slight correlations have been identified, the overall observation is that no clear relationship exists between the physico-chemical properties of pesticides and their reactivity towards •OH and that a close look at the structure of the pesticides is required in order to evaluate the potential of AOPs for the removal of pesticides from drinking water.

The GCM developed by Minakata et al. (2009) is based on the chemical structure of a molecule. Some similarities in molecular structure can be seen for highly reactive pesticides (Table 2-4). 8 out of the 11 pesticides that exhibited the highest reactivity possess the moiety N-C=O in the molecule. This group has the greatest group contribution factor in the model as it is very effective in activating a methyl group that undergoes further H-atom abstraction (Minakata et al., 2009). In addition, compounds containing atoms such as sulphur (S) and nitrogen (N) are reactive due to the interactions of S- and N- with •OH. Moreover, the presence of C-H bonds in the molecule increases the reactivity of pesticides due to the H-atom abstraction. For example, the organochlorine pesticide endrin, which has 12 C-atoms fragments (CH-R1-R2-R3 or CH_2-R1-R2), exhibits a $k_{\bullet OH}$ of 1.73×10^{10} $M^{-1}.s^{-1}$, whilst clopyralid which has no C-atom fragment

exhibits a $k_{\bullet OH}$ of $1.15x10^{7}$ $M^{-1}.s^{-1}$. The reactivity due to H-atom abstraction becomes greater as the C-atom is saturated. In other words the specific rate constant follows the order $k_{CH\text{-}R1\text{-}R2\text{-}R3} > k_{CH2\text{-}R1\text{-}R2} > k_{CH3\text{-}R1}$ due to the greater stability of the primary carbon-centered radical. Flutriafol also exhibits a high reactivity of $1.56x10^{10}$ $M^{-1}.s^{-1}$ towards •OH despite the absence of N-C=O group and only one secondary carbon-centered group (Table 2-4). The reactivity here is mainly due to the presence of two aromatic rings which both have only two functional groups attached to them in the ortho-position. This structure favours the •OH additions on the two rings. On the contrary, compounds with low reactivity are those whose aromatic rings are saturated, decreasing the probability of •OH addition on the ring (Minakata et al., 2009). Carboxylic acid pesticides also exhibit relatively low reactivity as the -COOH group has an extremely low reactivity ($k_{\bullet COOH}$ of $7.0x10^{5}$ $M^{-1}.s^{-1}$) due to the polarity of oxygen which prevents •OH attacks to the -OH bond (Minakata et al., 2009). To summarise, one can expect a pesticide to have a high reactivity towards •OH with the presence of:

- an N-C=O group in the molecule;
- C-H bonds in the molecule (especially tertiary carbon-centered radicals);
- sulphur or nitrogen atoms in the molecule.

A pesticide will exhibit a low reactivity towards •OH with the:

- Presence of saturated aromatic rings in the molecule;
- Absence of C-H bonds in the molecule;
- Presence of –COOH group in the molecule.

According to the Environment Agency, the pesticides most frequently found above the drinking water limit of 0.1 $\mu g.L^{-1}$ include the phenoxycarboxylic acids: mecoprop, MCPA, 2,4-D or dichlorprop, and the ureas: diuron, isoproturon or chlortoluron (Environment Agency, 2012). Phenoxycarboxylic acids exhibit similar $k_{\bullet OH}$ due to the homogeneity of the structure, but appear at the bottom of the classification mainly due to the presence of the –COOH group and the absence of C-H bonds in the molecules. However, their reactivity ranges from $4.21x10^9$ to $5.11x10^9$ $M^{-1}.s^{-1}$ which is still very fast and means that they should be fairly easily removed by AOPs. The urea herbicides isoproturon and chlortoluron have high reactivity towards •OH ($1.12x10^{10}$ and $9.39x10^9$ $M^{-1}.s^{-1}$ respectively), whilst that of diuron is slower ($6.71x10^9$ $M^{-1}.s^{-1}$) due to the substitution of the CH-R groups present in the former molecules by –Cl atoms, but all of these should all be easily removed by AOPs. Finally, new pesticides such as metaldehyde or clopyralid, which are not readily removed by traditional technologies, both show lower reactivity in comparison to the majority of pesticides (Table 2-4). However, metaldehyde has a rate constant value of $4.36x10^9$ $M^{-1}.s^{-1}$, which is not much different from those observed for the urea and phenoxycarboxylic acid based herbicides, indicating that this pesticide should be degraded by AOPs. Clopyralid, on the other hand, contains a –COOH group and has a saturated ring has a reactivity two orders of magnitude lower ($k_{\bullet OH}=1.15x10^7$ $M^{-1}.s^{-1}$) than the next slowest compound and therefore is not likely to be treatable by AOPs.

Table 2-3 - Correlations between pesticides properties and $k_{\bullet OH}$

	Log Kow	Molecular weight ($g.mol^{-1}$)	Molar volume (cm^3)	Surface tension ($dyne.cm^{-1}$)	Polar surface area ($Å^2$)	Polarisability (10^{-24} cm^3)	Solubility ($mg.L^{-1}$)	Log Koc
r^2	0.0823	0.0773	**0.3265**	0.2018	0.0086	**0.3119**	0.0084	0.1335

Table 2-4 - Relationship between structure, chemical properties and reactivity of pesticides towards •OH.

Compound	Structure	Log Kow	MW ($g.mol^{-1}$)	Molar volume (cm^3)	Surface tension ($dyne.cm^{-1}$)	Polar surface area ($Å^2$)	Polarisability (10^{-24} cm^3)	Solubility ($mg.L^{-1}$)	Log Koc	$k_{•OH}$ ($M^{-1}.s^{-1}$)
Butachlor	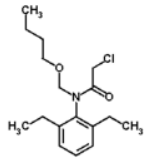	4.51	311.2	290.4	38.7	29.54	35.46	1.50	3.83	$2.83x10^{10}$
Alachlor	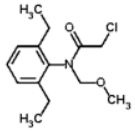	3.05	269.1	240.94	39.82	29.54	29.95	18.07	3.04	$2.46\ x10^{10}$
Fenamiphos	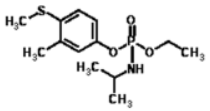	3.18	303.4	264.72	41.31	82.67	32.12	20.47	3.11	$2.00\ x10^{10}$
Molinate	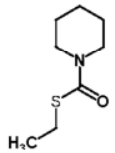	2.67	173.1	159.24	41.73	45.61	19.21	514.3	2.83	$1.98\ x10^{10}$
Vinclozolin	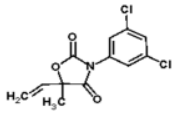	3.27	286.1	191.18	59.61	46.61	27.31	33.28	3.16	$1.85\ x10^{10}$
Metolachlor	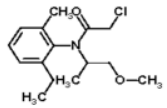	3.03	283.1	257.78	38.76	29.54	31.74	50.86	3.02	$1.77\ x10^{10}$

Table 2-4 (continued)

Compound	Structure	Log Kow	MW ($g.mol^{-1}$)	Molar volume (cm^3)	Surface tension ($dyne.cm^{-1}$)	Polar surface area ($Å^2$)	Polarisability (10^{-24} cm^3)	Solubility ($mg.L^{-1}$)	Log Koc	$k_{\bullet OH}$ ($M^{-1}.s^{-1}$)
Endrin	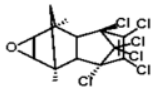	4.48	381.0	206	60.24	12.53	30.72	0.14	3.81	1.73×10^{10}
Bentazone	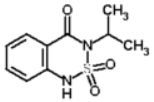	2.80	240.1	178.54	48.02	74.86	23.65	268.6	0.90	1.72×10^{10}
Metazachlor	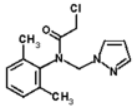	2.03	277.7	232.15	42.51	38.13	30.93	250.4	2.48	1.57×10^{10}
Flutriafol	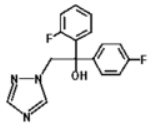	2.3	301.3	233.31	44.40	50.94	31.65	133.6	2.63	1.56×10^{10}
Propachlor	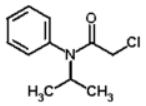	2.20	211.1	185.83	40.76	20.31	23.51	523.4	2.57	1.46×10^{10}

Table 2-4 (continued)

Compound	Structure	Log Kow	MW ($g.mol^{-1}$)	Molar volume (cm^3)	Surface tension ($dyne.cm^{-1}$)	Polar surface area ($Å^2$)	Polarisability (10^{-24} cm^3)	Solubility ($mg.L^{-1}$)	Log Koc	$k_{\bullet OH}$ ($M^{-1}.s^{-1}$)
Prometryn	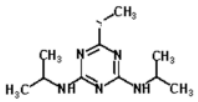	3.44	241.1	213.5	51.4	70.45	26.88	26.55	3.23	$1.40x10^{10}$
Terbufos	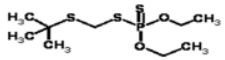	4.43	288.0	249.82	42.95	110.96	30.66	2.14	3.79	$1.39x10^{10}$
Thiodicarb	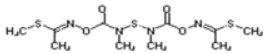	1.70	354.5	270.56	45.14	159.7	35.46	205.7	2.30	$1.39x10^{10}$
Disulfoton	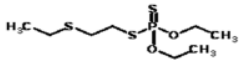	4.06	274.0	233.27	45.15	110.96	28.83	6.36	3.58	$1.34x10^{10}$
Trifluralin	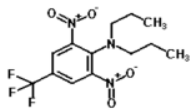	4.56	335.3	250.65	41.62	94.88	30.59	0.21	3.86	$1.27x10^{10}$

Table 2-4 (continued)

Compound	Structure	Log Kow	MW ($g.mol^{-1}$)	Molar volume (cm^3)	Surface tension ($dyne.cm^{-1}$)	Polar surface area ($Å^2$)	Polarisability (10^{-24} cm^3)	Solubility ($mg.L^{-1}$)	Log Koc	$k_{\bullet OH}$ ($M^{-1}.s^{-1}$)
Irgarol	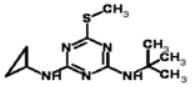	3.27	253.1	210.8	57.5	70.45	27.92	7.52	3.15	$1.19x10^{10}$
Profenofos	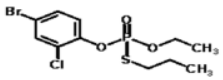	5.18	373.6	252.08	44.72	70.64	31.98	0.45	4.20	$1.18x10^{10}$
Isoproturon	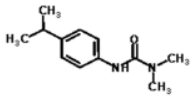	2.32	206.1	196.3	39.2	23.55	25.1	65	2.64	$1.12x10^{10}$
Triazophos	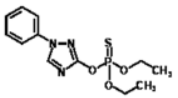	3.99	313.1	235.9	49.3	100.30	32.02	14.41	3.55	$1.06x10^{10}$
Prometon	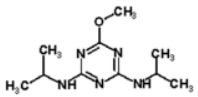	2.88	225.2	198.8	46.12	71.96	25.72	90.19	2.94	$1.02x10^{10}$

Table 2-4 (continued)

Compound	Structure	Log Kow	MW ($g.mol^{-1}$)	Molar volume (cm^3)	Surface tension ($dyne.cm^{-1}$)	Polar surface area ($Å^2$)	Polarisability (10^{-24} cm^3)	Solubility ($mg.L^{-1}$)	Log Koc	$k_{\bullet OH}$ ($M^{-1}.s^{-1}$)
Propazine	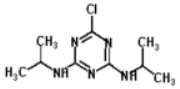	2.98	229.1	186.7	50.2	45.15	25.01	5.0	3.00	$1.00x10^{10}$
Metribuzin	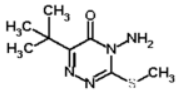	1.45	214.1	163.55	47.44	96.35	22.71	1304	2.16	$9.45x10^{9}$
Chlortoluron	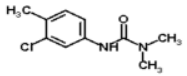	2.46	212.7	174.5	44.2	23.55	23.23	74	2.72	$9.39x10^{9}$
Tebuthiuron	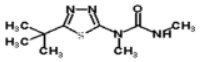	1.79	228.3	192.48	46.12	86.36	24.49	919.9	2.35	$9.34x10^{9}$
Acetochlor	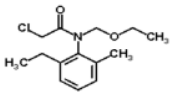	3.05	269.1	240.90	40.06	29.54	29.92	47.36	3.04	$9.12x10^{9}$
Malathion	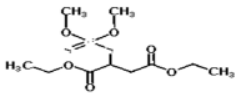	2.93	330.0	259.6	47.1	138.26	30.72	78.45	2.97	$9.11x10^{9}$

Table 2-4 (continued)

Compound	Structure	Log Kow	MW ($g.mol^{-1}$)	Molar volume (cm^3)	Surface tension ($dyne.cm^{-1}$)	Polar surface area ($Å^2$)	Polarisability (10^{-24} cm^3)	Solubility ($mg.L^{-1}$)	Log Koc	$k_{\bullet OH}$ ($M^{-1}.s^{-1}$)
Dichlofenthion	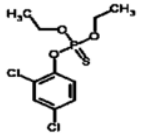	5.12	314.0	231.5	47.4	69.59	29.43	0.41	4.16	$8.66x10^9$
Methamidophos	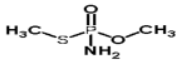	-0.82	141.0	109.7	44.4	64.65	12.47	200000	0.93	$7.40x10^9$
Atrazine	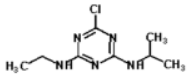	2.63	215.7	169.8	53.8	45.15	23.19	33	2.81	$7.38x10^9$
Captan	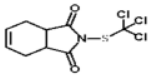	2.49	300.6	184.41	61.83	62.68	26.22	49.5	2.73	$7.02x10^9$
Diuron	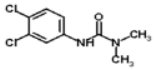	2.78	233.0	170.1	48.1	23.55	23.25	150.6	2.89	$6.71x10^9$
Parathion	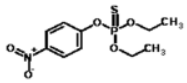	3.84	291.0	219.5	52.7	115.4	28.14	3.01	3.47	$6.68x10^9$
Linuron	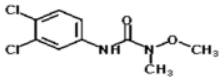	3.2	248.0	176.5	49.3	32.78	23.95	44.27	3.12	$6.28x10^9$

Table 2-4 (continued)

Compound	Structure	Log Kow	MW ($g.mol^{-1}$)	Molar volume (cm^3)	Surface tension ($dyne.cm^{-1}$)	Polar surface area ($Å^2$)	Polarisability (10^{-24} cm^3)	Solubility ($mg.L^{-1}$)	Log Koc	$k_{\bullet OH}$ ($M^{-1}.s^{-1}$)
Chlorfenvinphos	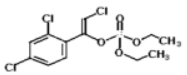	4.51	357.8	261.8	43.2	54.57	32.28	3.02	3.83	$6.17x10^9$
Acrolein	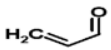	0.26	56.0	70.47	20.2	17.07	6.29	139700	1.52	$6.06x10^9$
Propyzamide	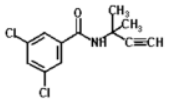	3.36	256.1	203.52	44.41	29.1	26.16	25.74	3.20	$6.05x10^9$
Chlorpyrifos	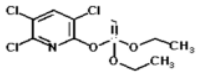	4.77	348.9	236.7	52.7	82.48	30.61	0.36	3.97	$5.29x10^9$
Dicamba	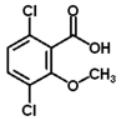	2.76	220.0	149.8	49.6	35.53	19.68	6100	0.05	$5.15x10^9$
Mecoprop	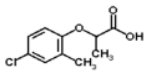	2.84	214.0	169.60	43.60	35.53	21.18	880	0.62	$5.11x10^9$
Aldicarb	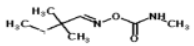	0.92	190.1	174.80	34.39	75.99	20.12	5312	1.88	$5.11x10^9$

Table 2-4 (continued)

Compound	Structure	Log Kow	MW ($g.mol^{-1}$)	Molar volume (cm^3)	Surface tension ($dyne.cm^{-1}$)	Polar surface area ($Å^2$)	Polarisability (10^{-24} cm^3)	Solubility ($mg.L^{-1}$)	Log Koc	$k_{\bullet OH}$ ($M^{-1}.s^{-1}$)
MCPA	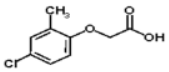	2.49	200.0	152.7	46.5	35.53	19.36	180.90	0.38	$4.66x10^9$
Dichlorprop	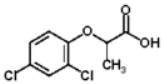	2.78	234.0	165.35	47.65	46.53	21.21	83.5	0	$4.66x10^9$
Metaldehyde	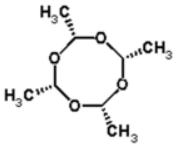	0.12	176.2	186	24.9	36.92	17.32	222	2.00	$4.36x10^9$
2,4-D	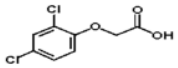	2.59	220.0	148.4	51.2	35.53	19.39	336.2	0.29	$4.21x10^9$
Dimethoate	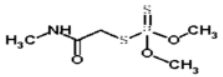	1.37	229.3	175.7	50.18	114.76	21.59	6626	2.12	$4.20x10^9$
Carbendazim	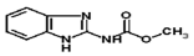	1.52	191.1	134.54	69.36	67.01	20.87	2441	2.19	$2.95x10^9$

Table 2-4 (continued)

Compound	Structure	Log Kow	MW ($g.mol^{-1}$)	Molar volume (cm^3)	Surface tension ($dyne.cm^{-1}$)	Polar surface area ($Å^2$)	Polarisability (10^{-24} cm^3)	Solubility ($mg.L^{-1}$)	Log Koc	$k_{.OH}$ ($M^{-1}.s^{-1}$)
Bromoxynil	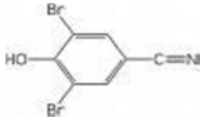	2.95	274.9	123.4	80.9	33.02	19.14	130	2.19	$2.36x10^{9}$
Pentachlorophenol	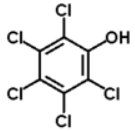	4.78	263.8	147.6	54.7	9.23	20.85	3.09	3.10	$2.12x10^{9}$
Lindane	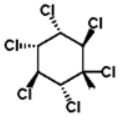	3.99	290.8	182.6	41.02	0	22.46	4.04	3.55	$1.64x10^{9}$
Clopyralid	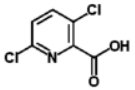	-2.63	192.0	119.1	62.83	50.19	16.28	5974	0	$1.15x10^{7}$

2.8 Scavenging rate

Apart from the pesticide structure the other variable which significantly impacts on the recorded rate constants is from the water matrix. The majority of the work which has assessed pesticide removal has been carried out in either laboratory grade water (LGW) or natural water (NW) (surface, ground or lake water). Laboratory grade water is typically used when evaluating kinetic parameters (such as the quantum yield and rate constants) and helps determine the optimum operational conditions for contaminant removal (Benitez et al., 2004). However, the use of natural waters is more representative of how the process may perform in real environmental conditions and therefore is a better evaluation of the true potential of any system. This is because in natural waters, not only is the target pesticide present but also many other competing organic and inorganic compounds (for example fulvic and humic acids, carbonate ions, other pesticides and metals).

A good example of how the results obtained from different water matrices impacts on removal rates is from the study of the photocatalytic degradation of chlorpyrifos in a variety of water types (Muhamad, 2010). The operating conditions were the same ([P]= 5 $mg.L^{-1}$, [TiO_2]= 0.2 $g.L^{-1}$) with the only difference being the water matrix. The first-order rate constants decreased in the order: distilled water > groundwater > lake water > river water (0.0139, 0.0117, 0.0112 and 0.0097 min^{-1} respectively). The rate constant was observed to decrease with an increase in the organic content. Benitez et al. (2004) reported the photooxidation of urea herbicides by UV/H_2O_2 and came to similar conclusions for three pesticides: diuron, isoproturon and linuron. First-order rate constants again followed the order: ultra-pure water > groundwater > lake water (20.7, 15.1 and 14.7 min^{-1} respectively for isoproturon). It is well documented that the presence of NOM and bicarbonates in natural waters will act as scavengers for •OH radicals (Haag and Hoigné, 1985).

Whilst •OH radicals are described as quasi-unselective and react with practically everything present in water, every organic molecule exhibits a different reactivity towards them (as represented by the $k_{\bullet OH}$ value). If a range of compounds are present in water, those with the highest $k_{\bullet OH}$ will preferentially react with •OH.

Although reactivity towards •OH is a key parameter in AOPs, the concentration of the different water constituents is also essential. In fact, a compound exhibiting a low $k_{\bullet OH}$ but present at high concentration in water will eventually scavenge more •OH than a highly reactive compound present at trace levels (Haag and Hoigné, 1985). In order to include the concentration of the different species present in water in the prediction of AOP efficiency, a parameter called scavenging rate has been developed (Haag and Hoigné, 1985). Scavenging rate (SR) or scavenging factor (SF) is the product of $k_{\bullet OH}$ and the concentration of a compound and is expressed in s^{-1}. The SR takes into consideration all of the species present in the water that could affect the degradation of a target micropollutant and has been previously used to determine the influence of water matrix on micropollutant degradation (Nakatani et al., 2007; Rosario-Ortiz et al., 2010; Katsoyiannis et al., 2011). It has been observed that a direct relationship exists between the scavenging rate and the effectiveness of AOPs where the greater the scavenging rate, the poorer the micropollutants removal by AOPs (Rosario-Ortiz et al., 2010). The main scavenging species in water are dissolved organic carbon (DOC), bicarbonate ions and nitrites (Rosario-Ortiz et al., 2010), such that the scavenging rate can be defined by:

$$SR_{water} = k_{\bullet OH\text{-}HCO_3^-} \times [HCO_3^-] + k_{\bullet OH\text{-}CO_3^{2-}} \times [CO_3^{2-}] + k_{\bullet OH\text{-}NOM} \times [NOM] + k_{\bullet OH\text{-}NO_2^-} \times [NO_2^-] \quad (2\text{-}31)$$

The values for the second-order rate constants with •OH are $k_{\bullet OH\text{-}HCO_3^-} = 8.5 \times 10^6\ M^{-1}.s^{-1}$, $k_{\bullet OH\text{-}CO_3^{2-}} = 3.9 \times 10^8\ M^{-1}.s^{-1}$, $k_{\bullet OH\text{-}NO_2^-} = 1.0 \times 10^{10}\ M^{-1}.s^{-1}$ (Buxton et al., 1988) and $k_{\bullet OH\text{-}NOMaveraged} = 3.6 \times 10^8$

$M^{-1}.s^{-1}$ = 2.5x10^4 L.$mgC^{-1}.s^{-1}$ (Hoigné, 1998). Even though the actual value of $k_{\bullet OH\text{-}NOM}$ depends on the nature of the DOC, its determination has been studied and it has been observed that the second-order rate constants between DOC and •OH is narrowly distributed and centered at 3.6x10^8 L.$mgC^{-1}.s^{-1}$ (Zepp et al., 1987; Hoigné, 1998; Westerhoff et al., 2007; Dong et al., 2010; Lee and von Gunten, 2010). The exception being humic acid which exhibits a higher value ($k_{\bullet OH,Humic\ acid}$ = 8.1 x 10^8 L.$(molC)^{-1}.s^{-1}$ (Westerhoff et al., 1999) although the use of an averaged value has been well accepted (Lee and von Gunten, 2010).

The phenomenon that occurs during treatment by •OH is based on a competition mechanism between the specified pesticide P and all organic and inorganic •OH scavengers (Si) present in the water, and can be represented by:

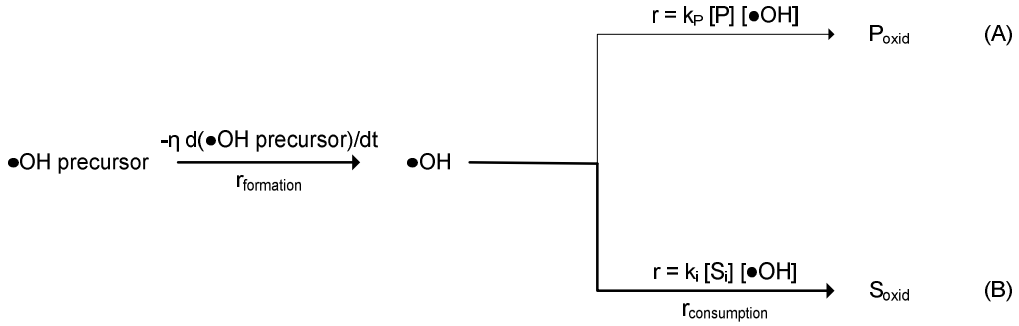

Figure 2-3 - Mechanism of •OH formation and their reaction with the different species present in water (adapted from Haag and Hoigné, 1985).

where η x d($•OH_{precurosor}$) = d(•OH), [•OH], [P] and [S_i] represent the molar concentrations of •OH, pesticide P and all organic and inorganic •OH scavengers S_i respectively, and k_P and k_i are the second-order rate constants for the reaction of •OH with the pesticide P and with all the different •OH scavengers S_i respectively.

In natural waters, P can be assumed to be very small compared to S_i (< µg.L^{-1} compared to > mg.L^{-1} respectively), and therefore the main consumption route of •OH will be via pathway B in

Figure 2-3. DOC nearly always represents the biggest •OH scavenger in a natural water; for example, Brezonik and Fulkerson-Brekken (1998) reported that DOC can represent 95% and 72% of all •OH scavengers in low and high alkalinity waters respectively.

2.8.1 Criticality of experimental concentrations

A wide range of scavenging rates have been observed, with values from $2.7x10^4$ to $5.85x10^5$ s^{-1} depending on the water quality (Table 2-6). The same concept of scavenging rate has been applied to the target micropollutant by multiplying the initial concentration by the second-order rate constant ($SR_p=k_{\bullet OH,P}$ x [P]) and values have been found to range from between 10.4 to $1.36x10^6$ s^{-1} (Table 2-6).

Pseudo-first order rate constants in laboratory grade water represent the ideal cases where no scavengers compete for •OH. Therefore, these constants were used as reference in the following analysis and the influence of the scavengers was evaluated by calculating the inhibition in rate constant between (LGW) and (NW) such that:

$$k'\,inhibition\ (\%) = \frac{k'_{LGW} - k'_{NW}}{k'_{LGW}} \times 100 \qquad (2\text{-}32)$$

where k'_{LGW} and k'_{NW} are the pseudo-first order rate constants in laboratory grade water and in natural water respectively.

Table 2-5 - Scavenging rate and rate constant inhibition of various micropollutants

Pollutant	[Pollutant] (M)	[DOC] ($mgC.L^{-1}$)	TA (mM $CaCO_3$)	pH	$k_{\bullet OH\ pollutant}$ ($M^{-1}.s^{-1}$)	SR_{water} (s^{-1})	SR_P (s^{-1})	•OH scavenged by water (%)	k' inhibition compared to LGW (%)	Reference
Isoproturon	$1.21x10^{-4}$	6.7	$3x10^{-4}$	7.1	$1.12x10^{10}$	$1.72\ x10^{5}$	$1.36x10^{6}$	11.23	29.0	Benitez et al., 2006; Benitez et al., 2009
Diuron	$1.07x10^{-4}$	6.7	$3x10^{-4}$	7.1	$6.71x10^{9}$	$1.72\ x10^{5}$	$7.18\ x10^{5}$	19.33	23.9	Benitez et al., 2006; Benitez et al., 2009
Linuron	$1.00x10^{-4}$	6.7	$3x10^{-4}$	7.1	$5.74\ x10^{9}$	$1.72\ x10^{5}$	$5.74\ x10^{5}$	23.06	15.1	Benitez et al., 2006; Benitez et al., 2009
Chlortoluron	$1.18x10^{-4}$	6.7	$3x10^{-4}$	7.1	$9.39x10^{9}$	$1.72\ x10^{5}$	$1.11\ x10^{6}$	13.42	17.1	Benitez et al., 2006; Benitez et al., 2009
Isoproturon	$1.21x10^{-4}$	2.6	$3.88x10^{-3}$	7.2	$1.12\ x10^{10}$	$7.55\ x10^{4}$	$1.36\ x10^{6}$	5.26	27.1	Benitez et al., 2006; Benitez et al., 2009
Diuron	$1.07x10^{-4}$	2.6	$3.88\ x10^{-3}$	7.2	$6.71\ x10^{9}$	$7.55\ x10^{4}$	$7.18\ x10^{5}$	9.51	23.4	Benitez et al., 2006; Benitez et al., 2009
Linuron	$1.00x10^{-4}$	2.6	$3.88\ x10^{-3}$	7.2	$5.74\ x10^{9}$	$7.55\ x10^{4}$	5.74E+05	11.62	13.5	Benitez et al., 2006; Benitez et al., 2009
Chlortoluron	$1.18x10^{-4}$	2.6	$3.88\ x10^{-3}$	7.2	$9.39\ x10^{9}$	$7.55\ x10^{4}$	$1.11\ x10^{6}$	6.37	19.9	Benitez et al., 2006; Benitez et al., 2009
Isoproturon	$1.21x10^{-4}$	1.2	0	7.0	$1.12\ x10^{10}$	$4.09\ x10^{4}$	$1.36\ x10^{6}$	2.92	1.0	Benitez et al., 2006; Benitez et al., 2009
Diuron	$1.07x10^{-4}$	1.2	0	7.0	$6.71\ x10^{9}$	$4.09\ x10^{4}$	$7.18\ x10^{5}$	5.39	21.2	Benitez et al., 2006; Benitez et al., 2009
Linuron	$1.00x10^{-4}$	1.2	0	7.0	$5.74\ x10^{9}$	$4.09\ x10^{4}$	$5.74\ x10^{5}$	6.65	7.1	Benitez et al., 2006; Benitez et al., 2009
Chlortoluron	$1.18x10^{-4}$	1.2	0	7.0	$9.39\ x10^{9}$	$4.09\ x10^{4}$	$1.11\ x10^{6}$	3.55	1.7	Benitez et al., 2006; Benitez et al., 2009

Table 2-5 (continued)

Pollutant	[Pollutant] (M)	[DOC] ($mgC.L^{-1}$)	TA (mM $CaCO_3$)	pH	$k_{\bullet OH\ pollutant}$ ($M^{-1}.s^{-1}$)	SR_{water} (s^{-1})	SR_P (s^{-1})	•OH scavenged by water (%)	k' inhibition compared to LGW (%)	Reference
Bromoxynil	3.60×10^{-6}	21	2.3E-03	8.4	2.36×10^{9}	5.85×10^{5}	8.50×10^{3}	98.57	53.8	Chelme-Ayala et al., 2010a
Trifluralin	3.00×10^{-6}	21	2.3E-03	8.4	1.27×10^{10}	5.85×10^{5}	3.81×10^{4}	93.89	42.9	Chelme-Ayala et al., 2010a
Bromoxynil	3.60×10^{-6}	3	1.36E-03	8.3	2.36×10^{9}	7.50E+04	8.50×10^{3}	89.82	20.0	Chelme-Ayala et al., 2010a
Trifluralin	3.00×10^{-6}	3	1.36E-03	8.3	1.27×10^{10}	7.50E+04	3.81×10^{4}	66.31	27.8	Chelme-Ayala et al., 2010a
E2	7.34×10^{-10}	0.892	2.83X10-4	7.6	1.41×10^{10}	2.69E+04	1.04×10^{1}	99.96	59.0	Chen et al., 2007
EE2	3.37×10^{-9}	0.892	2.83X10-4	7.6	1.02×10^{10}	2.69E+04	3.44×10^{1}	99.87	23.8	Chen et al., 2007
Propachlor	2.00×10^{-6}	15.1	nr	nr	1.07×10^{10}	3.78×10^{5}	2.14×10^{4}	94.64	25.9	Benitez et al., 2004
Metolachlor	2.00×10^{-6}	15.1	nr	nr	1.36×10^{10}	3.78×10^{5}	2.72×10^{4}	93.29	18.1	Benitez et al., 2004
Butachlor	2.00×10^{-6}	15.1	nr	nr	1.49×10^{10}	3.78×10^{5}	2.98×10^{4}	92.69	19.0	Benitez et al., 2004
Propachlor	2.00×10^{-6}	8.7	nr	nr	1.07×10^{10}	2.18×10^{5}	2.14×10^{4}	91.06	33.3	Benitez et al., 2004
Metolachlor	2.00×10^{-6}	8.7	nr	nr	1.36×10^{10}	2.18×10^{5}	2.72×10^{4}	88.91	27.7	Benitez et al., 2004
Butachlor	2.00×10^{-6}	8.7	nr	nr	1.49×10^{10}	2.18×10^{5}	2.98×10^{4}	87.97	28.6	Benitez et al., 2004

Table 2-5 (continued)

Pollutant	[Pollutant] (M)	[DOC] ($mgC.L^{-1}$)	TA (mM $CaCO_3$)	pH	$k_{\bullet OH\ pollutant}$ ($M^{-1}.s^{-1}$)	SR_{water} (s^{-1})	SR_P (s^{-1})	•OH scavenged by water (%)	k' inhibition compared to LGW (%)	Reference
Carbamazepine	1.00×10^{-6}	4.2	2.5×10^{-4}	7.0	5.85×10^{9}	1.09×10^{5}	5.85×10^{3}	94.92	81.9	Pereira et al., 2007(1)
Naproxen	1.00×10^{-6}	4.2	2.5×10^{-4}	7.0	8.61×10^{10}	1.09×10^{5}	8.61×10^{3}	92.70	66.3	Pereira et al., 2007(1)
Clofibric acid	1.00×10^{-6}	4.2	2.5×10^{-4}	7.0	5.72×10^{9}	1.09×10^{5}	5.72×10^{3}	95.03	50.7	Pereira et al., 2007(1)
Iohexol	3.00×10^{-6}	4.2	2.5×10^{-4}	7.0	3.81×10^{10}	1.09×10^{5}	1.14×10^{4}	90.54	28.1	Pereira et al., 2007(1)
Carbamazepine	1.00×10^{-6}	4.2	2.5×10^{-4}	7.0	5.85×10^{9}	1.09×10^{5}	5.85×10^{3}	94.92	75.2	Pereira et al., 2007(2)
Naproxen	1.00×10^{-6}	4.2	2.5×10^{-4}	7.0	8.61×10^{10}	1.09×10^{5}	8.61×10^{3}	92.70	74.8	Pereira et al., 2007(2)
Clofibric acid	1.00×10^{-6}	4.2	2.5×10^{-4}	7.0	5.72×10^{9}	1.09×10^{5}	5.72×10^{3}	95.03	87.2	Pereira et al., 2007(2)
Iohexol	3.00×10^{-6}	4.2	2.5×10^{-4}	7.0	3.81×10^{10}	1.09×10^{5}	1.14×10^{4}	90.54	16.9	Pereira et al., 2007(2)
Lindane	2.40×10^{-7}	6.14	0	7.0	3.34×10^{9}	2.89×10^{5}	1.00×10^{3}	99.65	87.6	Nienow et al., 2008
Lindane	3.00×10^{-7}	10.35	0	7.0	3.34×10^{9}	5.02×10^{5}	1.00×10^{3}	99.80	90.9	Nienow et al., 2008
Lindane	2.80×10^{-7}	5.43	0	7.0	3.34×10^{9}	3.67×10^{5}	1.00×10^{3}	99.73	81.4	Nienow et al., 2008
Lindane	3.10×10^{-7}	5.35	0	7.0	3.34×10^{9}	1.67×10^{5}	1.00×10^{3}	99.40	71.1	Nienow et al., 2008

nr: not recorded

Previous studies that have looked at the impact of water quality on micropollutant degradation have acknowledged that the scavenging rate is directly linked to the inhibition of micropollutant degradation (Haag and Hoigné, 1985; Pereira et al., 2007; Rosario-Ortiz et al., 2010). However, when data are compiled from various studies, the plot of these two parameters does not exhibit a clear relationship (Figure 2-4).

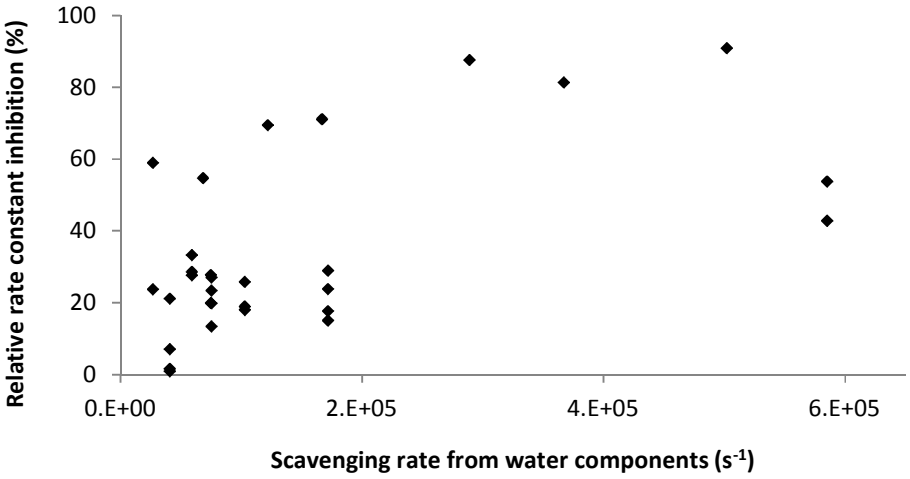

Figure 2-4 - Influence of scavenging rate on the rate constant inhibition.

As described above, the scavenging rate takes into account all of the different species that could affect the degradation of the target micropollutant, but does not take into consideration the micropollutant itself. The ratio between the micropollutant concentration and the other •OH scavengers can vary considerably from study to study. Therefore, the fraction of •OH scavenged by the water was calculated as:

$$\%\bullet OH \;\; scavenged \;\; by \;\; water = \frac{SR_{water}}{SR_{water} + SR_P} \times 100 \qquad (2\text{-}33)$$

where SR_{water} is the scavenging rate by all the water constituents as defined above in (2-31), and SR_p is the scavenging rate by the pollutant ($SR_p = k_{\bullet OH} \times [P]$).

The plot of the % of •OH scavenged by the water versus their influence on the inhibition of the pseudo-first order rate constant shows a good correlation between these two parameters (Figure 2-5). Interestingly, it highlights two very distinct zones: one where the fraction of •OH scavenged by water matrix constituents is relatively low (<85%) and a second for higher fractions of •OH scavenged by water matrix constituents (between 85% and 100%). In the first zone, the influence of water scavengers does not seem to have a major effect on micropollutant degradation. In fact, from 0 to 85% only a slow increase is observed in inhibition rates (between 1 and 28%). As a result, when the micropollutant represents >15% of •OH scavengers, its removal is not significantly affected by DOC and bicarbonates and exposing the water to slightly higher UV fluences would probably easily lead to the required concentration reduction.

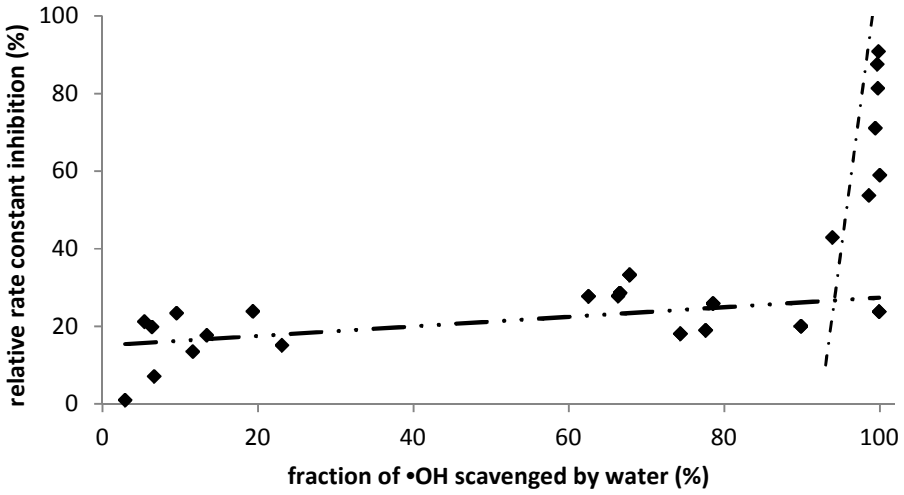

Figure 2-5 - Influence of the fraction of •OH scavenged by water components on the relative rate constant inhibition.

In the second zone, where •OH scavenged by water components represent more than 85%, the degradation of micropollutants can become highly influenced by DOC and bicarbonates. In this region, the inhibition in rate constant can be as high as 91%, in this case for the degradation of 76 $\mu g.L^{-1}$ of lindane with 10 $mg.L^{-1}$ of fulvic acid and 9.2 $mg.L^{-1}$ of humic acid (Nienow et al.,

2008). The trend shows that there is an increase of the rate constant inhibition with an increase of the fraction of •OH scavenged by water constituents which indicates that when a micropollutant is present at trace levels, its removal can be greatly affected by the water quality. A good example is the degradation of trifluralin in two natural waters; when the fraction of •OH scavenged by water constituents increased from 66.3% to 93.9% the inhibition of k' increased from 27.8% to 42.9% (Chelme-Ayala et al., 2010a). However, in the cases of bromoxynil and EE_2, the fractions of •OH scavenged by water constituents were 89.8 and 99.9% respectively and resulted in 20% and 23.8% rate constant inhibition. Interestingly, $k_{\bullet OH}$ values for bromoxynil and EE_2 were relatively high for micropollutants ($8.4x10^9$ and $1.1x10^{10}$ $M^{-1}.s^{-1}$ respectively) (Chelme-Ayala et al., 2010b; Rosenfeldt and Linden, 2004) which suggests that compounds having high reactivity are less affected by the background organic matter. On the contrary, micropollutants with low reactivity towards •OH such as lindane ($k_{\bullet OH}=5.2x10^8$ $M^{-1}.s^{-1}$) are highly affected by the DOC (Table 2-5) and will be hardly removed from natural waters.

2.8.2 Influence of the nature of water constituents on the •OH scavenging rate

According to its definition, the scavenging rate is directly linked to both the concentration of all water constituents and their reactivity towards •OH. Although it gives a fair idea of the relative impact the water quality will have on the degradation of micropollutants, some limitations are associated with this parameter. In fact, Nienow et al. (2008) studied the degradation of lindane in different synthetic waters: fulvic acid, humic acid and mixes of both at different concentrations (Nienow et al., 2008). They showed that humic acid has more of an inhibition effect than fulvic acid on the degradation of lindane ($k'_{lindane}= 1.8x10^{-3}$ and $2.8x10^{-3}$ s^{-1} respectively) indicating that waters with high humic substances will be more subject to •OH scavenging. This agrees with second-order rate constant data for the reaction of NOM isolates where humic acid exhibits a

high $k_{\bullet OH}$ compared to other NOM isolates (Westerhoff et al., 1999). In addition, Katsoyiannis et al. (2011) studied the degradation of pCBA in several natural waters and noticed important variations in rate of degradation of pCBA according to the nature of the water. For example, Lake Zurich and Lake Jonsvatnet waters exhibited similar scavenging rates but the pseudo-first order rate constant was 36% slower for Lake Jonsvatnet (Table 2-5). When looking at the composition of the water, it is observed that Lake Jonsvatnet has a higher concentration of DOC and lower alkalinity than for Lake Zurich, suggesting that the NOM has a greater influence than carbonate ions on •OH scavenging. However, Lake Jonsvatnet and Lake Greifensee waters had similar DOC concentrations but the latter had a much greater alkalinity and resulted in a reduction of the rate constant from $2.1x10^{-4}$ to $1.6x10^{-4}$ $m^2.J^{-1}$. Therefore, for similar scavenging rates, waters containing more organic matter will probably have a greater inhibition effect than alkalinity-rich waters on the degradation of micropollutants, especially for waters containing high concentrations of humic substances. However, the presence of alkalinity needs to be considered as it also impacts on the degradation of micropollutants.

Table 2-6 - Impact of alkalinity and NOM on the rate of degradation of pCBA in different lake waters. Reproduced from Katsoyiannis et al., 2011.

	Lake Zurich water	Lake Jonsvatnet water	Lake Greifensee water
Scavenging rate (s^{-1})	$6.1x10^{4}$	$6.2x10^{4}$	$10.4x10^{4}$
Alkalinity (mM)	2.6	0.4	4.0
[DOM] ($mgC.L^{-1}$)	1.3	3.0	3.1
k'_{pCBA} ($m^2.J^{-1}$)	$3.3x10^{-4}$	$2.1x10^{-4}$	$1.6x10^{-4}$

2.8.3 Practical significance of scavenging

The concentration of the target compound used in many studies are usually very high (often 1 $mg.L^{-1}$) and hence do not represent concentrations found in natural waters. Based on the maximum permissible concentration for single pesticides in drinking water in Europe

(0.1 μg.L^{-1}), a range of scenarios is presented below (Table 2-7). The mass concentration of pesticide in the source water was set at 0.2 μg.L^{-1} and the pH of the water at 7.6. The different scenarios look at the influence of NOM concentration, alkalinity and second-order rate constant of the pesticide on the scavenging rate. The three pesticides selected were chlortoluron ($k_{\bullet OH}$ = 9.39x10^9 $M^{-1}.s^{-1}$), metaldehyde ($k_{\bullet OH}$ = 4.36x10^9 $M^{-1}.s^{-1}$) and clopyralid ($k_{\bullet OH}$ = 1.15x10^7 $M^{-1}.s^{-1}$) and represent pesticides with high, medium and low reactivity towards •OH respectively. For NOM and alkalinity, low, medium and high concentrations have been selected (1,4 and 8 mg.L^{-1} of DOC and 20, 80 and 150 mg.L^{-1} as $CaCO_3$ for alkalinity).

Table 2-7 - Influence of water quality and pesticide reactivity on the percentage of •OH scavenged by water constituents. In brackets, percentage of •OH scavenged by NOM and alkalinity respectively.

Clopyralid

Alkalinity / NOM	low	medium	high
low	99.9984 (87.13/12.87)	99.9989 (62.84/37.16)	99.9991 (47.42/52.58)
medium	99.9996 (96.44/3.56)	99.9996 (87.12/12.88)	99.9996 (78.30/21.70)
high	99.9998 (98.19/1.81)	99.9998 (93.12/6.88)	99.9998 (87.83/12.17)

Metaldehyde

Alkalinity / NOM	low	medium	High
low	99.9905 (87.12/12.87)	99.9931 (62.83/37.15)	99.9948 (47.42/52.58)
medium	99.9974 (96.43/3.56)	99.9976 (87.12/12.88)	99.9979 (78.29/21.70)
high	99.9987 (98.18/1.81)	99.9987 (93.12/6.88)	99.9988 (87.83/12.17)

Chlortoluron

Alkalinity / NOM	low	medium	high
low	99.9683 (87.10/12.87)	99.9772 (62.83/37.15)	99.9828 (47.41/52.57)
medium	99.9912 (96.43/3.56)	99.9921 (87.11/12.88)	99.9929 (78.29/21.70)
high	99.9955 (98.18/1.81)	99.9958 (93.11/6.88)	99.9960 (87.82/12.17)

In all scenarios, the fraction of •OH scavenged by the water constituents is >99.9% (Table 2-6). Even in the most favourable case, where the pesticide is highly reactive towards •OH, and the water has a low DOC and low alkalinity, the value was still 99.97%. In comparison, for none of the studies mentioned above was the percentage of •OH scavenged by water constituents higher than in the most favourable case study (99.96 vs. 99.97%) and most of the values ranged between 3 and 95%. These observations suggest that for real waters, the water constituents will always scavenge more than any value presented in Figure 2-5. The first zone, where the water constituents have no major impact on micropollutants degradation, will never occur for most water sources, but will rather be at the top end of the second zone. Linked to the previous conclusions, this analysis shows that compounds such as clopyralid with low reactivities towards •OH are very unlikely to be removed by AOPs. However, it was noticed previously that highly reactive compounds were less affected by the scavenging effect of water constituents and therefore, for those compounds such as chlortoluron which may react 1-2 orders of magnitude faster than water constituents, AOPs will still be effective water treatment technologies for their removal.

2.9 Other parameters affecting the degradation of pesticides by UV/H_2O_2 and UV/TiO_2

The main characteristic and advantage of AOPs is their ability to transform organic compounds into minerals such as H_2O, CO_2 and inorganic salts. Many studies show that UV/H_2O_2 and UV/TiO_2 do not achieve degradation at the same rate for the same compound. In some cases, UV/H_2O_2 appears to be more effective while for others UV/TiO_2 is better. The influence of operational parameters on the effectiveness of the processes was studied over a wide range of pesticides belonging to various families of chemicals including organophosphates, organochlorines, ureas, s-triazines, phenoxycarboxylic acids, anilides and benzonitrile-based

pesticides. The rate constants are expressed in terms of UV fluence^{-1} ($cm^2.mJ^{-1}$) in order to standardise the dose of UV applied to the pollutant in many different configurations, from bench-scale quasi-collimated beam apparatus to pilot scale reactors.

2.9.1 Influence of irradiation wavelength on the rate of degradation

Typical lamps used in AOPs are monochromatic low pressure (LP) lamps emitting at 254, 300 or 365 nm. Polychromatic medium pressure (MP) lamps are also used which emit light over a broad range of wavelengths from 200 to 600 nm. Solar UV radiation can also be used to provide enough appropriate light energy into the system. The absorption of UV radiation by H_2O_2 is at its maximum in the range 180-200 nm and then steadily decreases up to 420 nm. The rate of degradation of the organophosphate insecticide parathion was five times faster with a LP lamp emitting at 254 nm than with a polychromatic MP lamp emitting in the range 253-578 nm (Figure 2-6). In the UV/TiO_2 system, any light emission in the UV range should be able to activate TiO_2 particles, as these particles absorb light below 380 nm (Hermann, 2005). Three studies reported the degradation of atrazine by UV/TiO_2 with three different irradiation sources, 254 nm, $300<\lambda<800$ nm and solar UV radiation (Sanches et al., 2010; Konstantinou et al., 2001; Maldonado et al., 2007) (Figure 2-6). The degradation efficiencies decreased in the order MP lamp > LP lamp > solar UV radiation. The solar UV radiation appears as the least effective due to the small proportion of UV light present in sunlight (≈6%) whilst the MP lamp was found to be significantly more efficient than the LP lamp. The degradation of simazine has been reported for two UV lamps emitting at 254 and 300 nm in the same study (Chu et al., 2009). The rate constants were $1.04x10^{-2}$ and $1.72x10^{-2}$ $cm^2.mJ^{-1}$ for wavelengths of 254 and 300 nm respectively, the 254 nm UV lamp being 41% less efficient than the 300 nm. These results suggest that irradiation at 254 nm and below, is necessary to split H_2O_2 into •OH whilst

irradiation in the range 280-315 nm which corresponds to UV-B light is the most suitable for UV/TiO_2 photocatalysis.

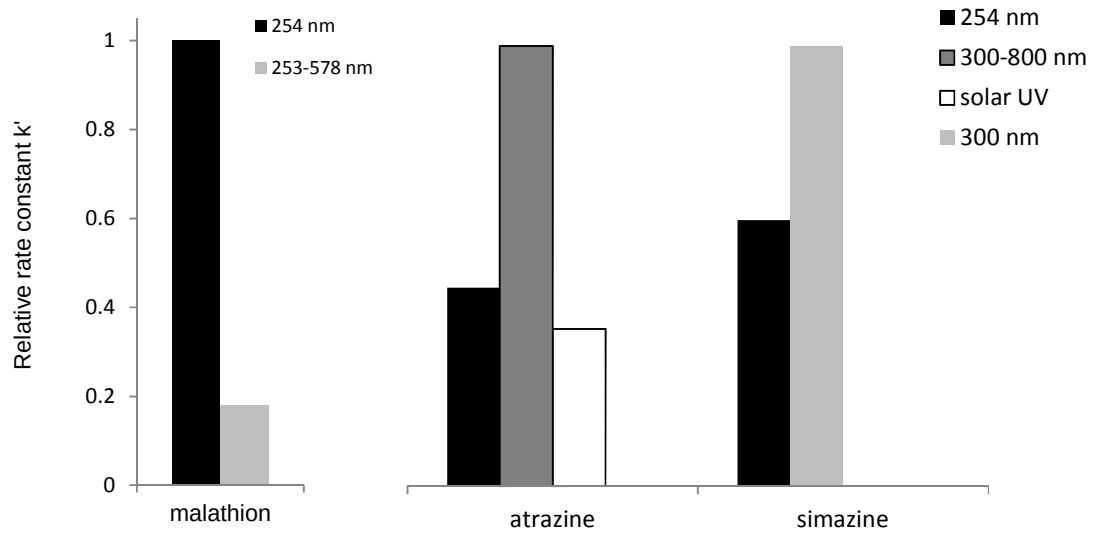

Figure 2-6 - Influence of wavelength on the degradation of pesticides by UV/H_2O_2 for the pesticide malathion and by UV/TiO_2 for the triazines atrazine and simazine.

2.9.2 Influence of pesticide concentration on the rate of degradation

Typical concentrations used in research studies are well above the levels found in groundwater and rivers (Table 2-SI-1), often for practical reasons such as the accurate following of kinetics, determination of by-products and the better precision of analytical instruments. However, the initial concentration has a significant influence on the rate of degradation because of the influence on the scavenging rate. A drop in rate constant is often observed with an increase of initial micropollutant concentration in laboratory grade water (Hu et al., 2007; Nienow et al., 2008; Tizaoui et al., 2011). In this scenario, no scavenger competes with the micropollutant for •OH and when the micropollutant concentration is increased, more organic molecules are present for the same amount of •OH formed. However, increasing the pollutant concentration in natural waters increases the ratio of •OH scavenged by the pollutant over other water constituents, and

should lead to higher reaction rate constants. However, to our knowledge, no study has been carried out in natural waters varying the initial concentration of micropollutant.

2.9.3 Influence of H_2O_2 and TiO_2 concentrations

The concentration of •OH precursors is a key parameter for the effectiveness of AOPs (Zalazar et al., 2008; Autin et al., 2012). In UV/H_2O_2 systems, [H_2O_2] reaches an optimum above which the effectiveness of the system is reduced (Figure 2-7-A). In fact, the rate of degradation initially increases with an increase of [H_2O_2], as more •OH are formed during irradiation. However, H_2O_2 is known to scavenge •OH, although at a lower rate than most micropollutants $k_{\bullet OH,H2O2}=2.7x10^7$ $M^{-1}.s^{-1}$ (Buxton et al., 1988).As [H_2O_2] becomes greater, a large number of the formed •OH will eventually react with H_2O_2 inhibiting the degradation of the target micropollutant. This inhibition can be as high as 75% with an increase of [H_2O_2] from 1 to 10 mM (Nienow et al., 2008). The optimum [H_2O_2] varies with the nature and the concentration of the pollutant and optimum ratios can be significantly different. As H_2O_2 does not absorb light very well, relatively high concentrations of the hydrogen peroxide are always required to form sufficient •OH. For example a molar ratio of 5:1 for H_2O_2 and dichloroacetic acid has been determined to be the optimum in order to effectively degrade 60 $mg.L^{-1}$ of dichloroacetic acid (Zalazar et al., 2008). This ratio goes up to 3850:1 for the degradation of 76 $\mu g.L^{-1}$ of lindane (Nienow et al., 2008). For UV/TiO_2 systems, at low TiO_2 concentrations, the effectiveness of the photocatalytic process is improved by increasing the TiO_2 dose due to the increased number of oxidative radicals formed during irradiation (Figure 2-7-B). However, at higher doses, an increase of TiO_2 concentration is not correlated to an enhancement of the process and the reaction rate often stabilises or even decreases. This has been explained to be mainly due to screening effects such that as the TiO_2 concentration increases, more and more particles prevent the penetration of the

light into the entire reactor volume, and hence part of the particles does not interact with any photons, leading to the stabilisation of the reaction rate. (Zalazar et al., 2008; Ahmed et al., 2011). Moreover, the optimal [TiO_2] is dependent on the catalyst and micropollutant properties (Zalazar et al., 2008) as well as the water quality. This is confirmed from Figure 2-7-B, where optimum doses vary from 0.1 $g.L^{-1}$ up to 1 $g.L^{-1}$ for drinking water applications, suggesting that the optimum concentration must be identified for each particular application.

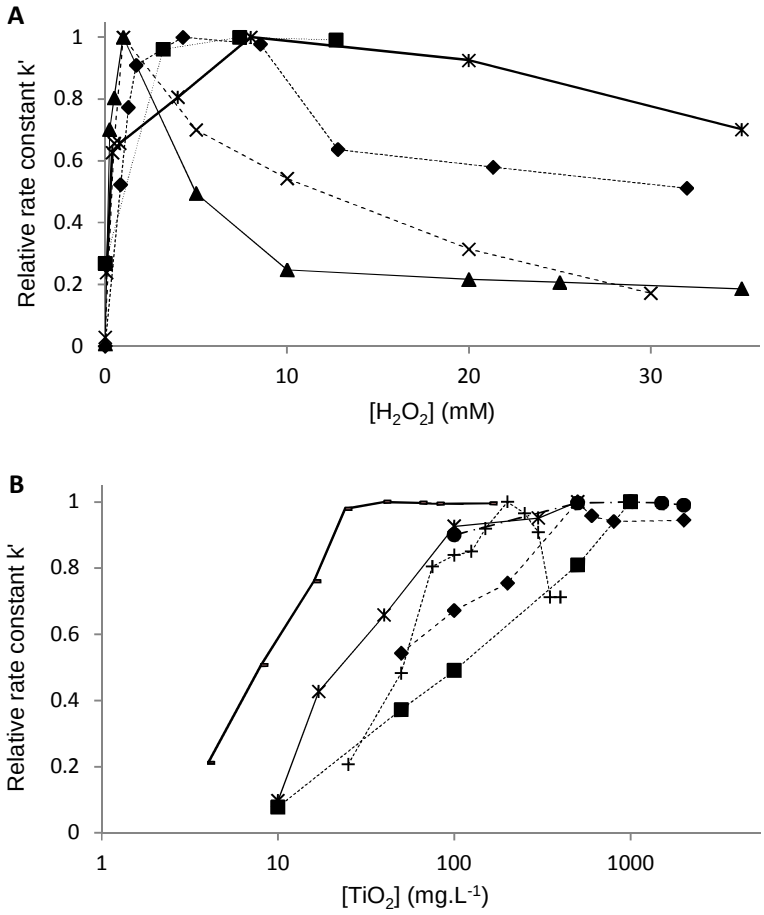

Figure 2-7 - Influence of A) [H_2O_2] and B) [TiO_2] on the rate constant of degradation of various pesticides. Summary of data from Esplugas et al., 2002; Hu et al., 2007; Bamba et al., 2008; Nienow et al., 2008; Zalazar et al., 2008; Chu et al., 2009; Muhamad et al., 2010; Autin et al., 2012.

2.10 Conclusion

This review highlights the critical points which need to be considered before implementing an AOP at full scale for the removal of micropollutants. The first step consists in the determination of the second order rate constant of the target micropollutant and its comparison to that of other well defined pesticides. This comparison will provide a global idea on how likely or unlikely the micropollutant is to be removed by AOPs. Although the micropollutant reactivity can suggest that AOPs may be suitable technologies for its removal from a water source, laboratory-scale trials are essential in the development of a technology and must be carried out for a better evaluation of its potential. However, this review demonstrated that the water quality had a critical impact on the rate of degradation of micropollutants. In fact, the fraction of •OH scavenged by the water constituents in natural waters are much higher than those used in research studies. Often, this is due to the use of high micropollutant concentrations for analytical reasons and accurate kinetics determination. But the findings suggest that data from research studies need to be handled with extra care and that it is essential to use natural water instead of laboratory grade water as it is to use appropriate micropollutant concentration or the risk of over estimation of the effectiveness of the technology becomes inevitable and unexpected errors will occur when full-scale pilot plant trials will be undertaken. Finally, optimal experimental parameters also need to be carefully determined as significant amounts of energy can be wasted by simply using an inappropriate oxidant concentration, or the wrong wavelength.

2.11 Acknowledgements

The authors would like to express their gratitude for the financial support for this project by Severn Trent Water Ltd.

2.12 References

Acero, J.L., Benitez, F.J., Real, F.J., Maya, C., 2003. Oxidation of acetamide herbicides in natural waters by ozone and by the combination of ozone/hydrogen peroxide: Kinetic study and process modeling. Ind. Eng. Chem. Res. 42(23), 5762-5769.

Ahmed, S., Rasul, M.G., Brown, R., Hashib, M.A., 2011. Influence of parameters on the heterogeneous photocatalytic degradation of pesticides and phenolic contaminants in wastewater: A short review. J. Environ. Manage. 92(3), 311-330.

Akpan, U.G., Hameed, B.H., 2009. Parameters affecting the photocatalytic degradation of dyes using TiO_2-based photocatalysts: A review. J. Hazard. Mater. 170(2-3), 520-529.

Al-Ekabi, H., Edwards, G., Holden, W., Safarazadeh-Amiri, A., Story, J., 1992. Water treatment by heterogeneous photocatalysis. In Eckenfelder, W.W., Bowers, A.R., Roth, J.A. Eds., Chemical oxidation: Technologies for the nineties, Vol. I, Pennsylvania, USA.

Armbrust, K.L., 2000. Pesticide hydroxyl radical rate constants: Measurements and estimates of their importance in aquatic environments. Environ. Toxicol. Chem. 19(9), 2175-2180.

Autin, O., Hart, J., Jarvis, P., MacAdam, J., Parsons, S.A., Jefferson, B., 2012. Comparison of UV/H_2O_2 and UV/TiO_2 for the degradation of metaldehyde: Kinetics and impact of background organics. Water Res. 46(17), 5655-5662.

Bamba, D., Atheba, P., Robert, D., Trokourey, A., Dongui, B., 2008. Photocatalytic degradation of the diuron pesticide. Environ. Chem. Lett. 6(3), 163-167.

Benitez, F.J., Acero, J.L., Real, F.J., Roman, S., 2004. Oxidation of MCPA and 2-4-D by UV radiation, Ozone, and the Combinations UV/H_2O_2 and O_3/H_2O_2. J. Environ. Sci. Health, Part B – Pestic., Food Contam., Agric. Wastes, B39(3), 393-409.

Benitez, F.J., Real, F.J., Acero, J.L., Garcia, C., 2006. Photochemical oxidation processes for the elimination of phenyl-urea herbicides in waters. J. Hazard. Mater. 138(2), 278-287.

Benitez, F.J., Real, F.J., Acero, J.L., Garcia, C., 2007. Kinetics of the transformation of phenyl-urea herbicides during ozonation of natural waters: Rate constants and model predictions. Water Res. 41(18), 4073-4084.

Benitez, F.J., Real, F.J., Acero, J.L., Roldan, G., 2009. Removal of selected pharmaceuticals in waters by photochemical processes. J. Chem. Technol. Biotechnol. 84(8), 1186-1195.

Beydoun, D., Amal, R., Low, G., McEvoy, S., 1999. Role of nanoparticles in photocatalysis. J. Nanopart. Res. 1(4), 439-458.

Brezonik, P.L., Fulkerson-Brekken, J., 1998. Nitrate-induced photolysis in natural waters: Controls on concentrations of hydroxyl radical photo-intermediates by natural scavenging agents. Environ. Sci. Technol. 32(19), 3004-3010.

Buxton, G.V., Greenstock, C.L., Helman, W.P., Ross, A.B., 1988. Critical review of rate constants for reactions of hydrated electrons, hydrogen atoms and hydroxyl radicals (•OH/•O^-) in aqueous solution. J. Phys. Chen. Ref. Data 17(2), 513-886.

Catalkaya, E.C., Kargi, F., 2009. Degradation and mineralization of simazine in aqueous solution by ozone/hydrogen peroxide advanced oxidation. J. Environ. Eng. 135(12), 1357-1364.

Caus, A., Vanderhaegen, S., Braeken, L., Van der Bruggen, B., 2009. Integrated nanofiltration cascades with low salt rejection for complete removal of pesticides in drinking water production. Desalination 241(1-3), 111-117.

Chelme-Ayala, P., El-Din, M.G., Smith, D.W., 2010a. Degradation of bromoxynil and trifluralin in natural water by direct photolysis and UV plus H_2O_2 advanced oxidation process. Water Res. 44(7), 2221-2228.

Chelme-Ayala, P., El-Din, M.G., Smith, D.W., 2010b. Kinetics and mechanism of the degradation of two pesticides in aqueous solution by ozonation. Chemosphere 78(5), 557-562.

Chen, H.-W., Ku, Y., Wu, C.-Y., 2007. Effect of LED optical characteristics of temporal behaviour of o-cresol decomposition by UV/TiO_2 process. J. Chem. Technol. Biot. 82(7), 626-635.

Chu, W., Wong, C.C., 2004. The photocatalytic degradation of Dicamba in TiO_2 suspensions with the help of hydrogen peroxide by different near UV irradiations. Water Res. 38(4), 1037-1043.

Chu, W., Rao, Y., Huy, W.Y., 2009. Removal of simazine in a UV/TiO_2 heterogeneous system. J. Agric. Food Chem. 57(15), 6944-6949.

De Laat, J., Maouala-Makata, P., Dore, M., 1996. Rate constants for reactions of ozone and hydroxyl radicals with several phenyl-ureas and acetamides. Environ. Technol. 17(7), 707-716.

Doll, T.E., Frimmel, F.H., 2005. Removal of selected persistent organic pollutants by heterogeneous photocatalysis in water. Catal. Today 101(3-4), 195-202.

Dorfman, L.M., Adams, G.E., 1973. Reactivity of the hydroxyl radical in aqueous solutions. National Standard Reference Data Series 46 (NSRDS-NBS46), (US National Bureau of Standards) US Government Printing Office, Washington, DC.

Environment Agency. Pesticide use in agriculture and horticulture, available at: http://www.environment-agency.gov.uk/cy/ymchwil/llyfrgell/data/34291.aspx (Accessed March, 2012).

Environment Agency, 2012. How do pesticides affect the environment? Available at: http://www.environment-agency.gov.uk/cy/ymchwil/llyfrgell/data/34397.aspx (Accessed November, 2012).

Esplugas, S., Gimenez, J., Contreras, S., Pascual, E., Rodriguez, M., 2002. Comparison of different advanced oxidation processes for phenol degradation. Water Res. 36(4), 1034-1042.

Foster, D. M., Rachwal, A. J., White, S. L., 1991. New treatment processes for pesticides and chlorinated organics control in drinking water. J. Inst. Water Env. Man. 5(4), 466-477.

Getoff, N., Solar, S., 1986. Radiolysis and pulse radiolysis of chlorinated phenols in aqueous solutions. Radiat. Phys. Chem. 28(5-6), 443-450.

Goslan, E.H., Krasner, S.W., Bower, M., Rocks, S.A., Holmes, P., Levy, L.S., Parsons, S.A., 2009. A comparison of disinfection by-products found in chlorinated and chloraminated drinking waters in Scotland. Water Res. 43(18), 4698-4706.

Gray, N. F., 2008. Drinking Water Quality: Problems and solutions, Chapter 6: Pesticides and organic micro-pollutants, second edition. Cambridge University Press, Cambridge, 137-168.

von Gunten, U., 2003. Ozonation of drinking water: Part I. Oxidation kinetics and product formation. Water Res. 37(7), 1443-1467.

Haag, W.R., Hoigné, J., 1985. Photo-sensitized oxidation in natural water via •OH radicals. Chemosphere 14(11-12), 1659-1671.

Haag, W.R., Yao, C.C.D., 1992. Rate constants for reaction of hydroxyl radicals with several drinking water contaminants. Environ. Sci. Technol. 26(5), 1005-1013.

Hall, T., Holden, B., Haley, J., 2011. Treatment for metaldehyde and other problem pesticides. 4th Developments in Water Treatment and Supply Conference, Cheltenham, June 7-8 2011.

Heberer, T., Dunnbier, U., 1999. DDT Metabolite Bis(Chlorophenyl)acetic Acid: The Neglected Environmental Contaminant. Environ. Sci. Technol. 33(14), 2346-2351.

Helaili, N., Bessekhouad, Y., Bouguelia, A., Trari, M., 2009. Visible light degradation of orange II using xCuyOz/TiO_2 heterojunctions. J. Hazard. Mater. 168(1), 484-492.

Herrmann, J. M., Disdier, J., Pichat, P., Malato, S. and Blanco, J., 1998. TiO2-based solar photocatalytic detoxification of water containing organic pollutants. Case studies of 2,4-Dichlorophenoxyaceticacid (2,4-D) and of benzofuran. Appl. Catal. B: Environ. 17(1-2), 15-23.

Herrmann, J.M., 2005. Heterogeneous photocatalysis: State of the art and present applications. Top. Catal. 34(1-4), 49-65.

Hladik, M. L., Roberts, A. L., Bouwer, E.J., 2005. Removal of neutral chloroacetamide herbicide degradates during simulated unit processes for drinking water treatment. Water Res. 39(20), 5033-5044.

Hossain, S., Guha, B. K., 2006. Removal of endrin from drinking water by GAC using batch study. Indian J. Environ. Prot. 26(5), 392-399.

Howe, R.F., 1998. Recent development in photocatalysis. Dev. Chem. Eng. Mineral Process 6(1), 55-84.

Hu, J. Y., Aizawa, T., Ookubo, Y., Morita, T., Magara, Y., 1998. Adsorptive characteristics of ionogenic aromatic pesticides in water on powdered activated carbon. Water Res. 32(9), 2593-2600.

Hu, L., Flanders, P.M., Miller, P.L., Strathmann, T.J., 2007. Oxidation of sulfamethoxazole and related antimicrobial agents by TiO_2 photocatalysis. Water Res. 41(12), 2612-2626.

Huston, P. L., Pignatello, J. J., 1999. Degradation of selected pesticide active ingredients and commercial formulations in water by the photo-assisted Fenton reaction. Water Res. 33(5), 1238-1246.

Hyde, R. A., 1989. Application of Granular Activated Carbon in the Water Industry. J. Inst. Water Env. Man. 3(2), 174-179.

Ijpelaar, G. F., Meijers, R. T., Hopman, R., Kruithof, J. C., 2000. Oxidation of herbicides in groundwater by the fenton process: A realistic alternative for O_3/H_2O_2 treatment. Ozone-Sci. Eng. 22(6), 607-616.

Ikehata, K., El-Din, M.G., 2005. Aqueous pesticide degradation by ozonation and ozone-based advanced oxidation processes: A review (part II). Ozone: Science and Engineering 27(3), 173-202.

Jiang, H., Adams, C., 2006. Treatability of chloro-s-triazines by conventional drinking water treatment technologies. Water Res. 40(8), 1657-1667.

Kasozi, G. N., Kiremire, B. T., Bugenyi, F. W. B., Kirsch, N. H., Nkedi-Kizza, P., 2006. Organochlorine residues in fish and water samples from Lake Victoria, Uganda. J. Environ. Qual. 35(2), 584-589.

Katsoyiannis, I.A., Canonica, S., von Gunten, U., 2011. Efficiency and energy requirements for the transformation of organic micropollutants by ozone, O_3/H_2O_2 and UV/H_2O_2. Water Res. 45(13), 3811-3822.

Kerst, C., Byloos, M., Leigh, W.J., 1997. Far-UV laser flash photolysis in solution. A time-resolved spectroscopic study of the chemistry of 1,1-dimethyl-1,3-(1-sila)-butadiene. Can. J. Chem. 75(7), 975-982.

Kiely, T., Donaldson, D., Grube, A., 2004. Pesticides industry sales and usage; 2000 and 2001 market estimates. US Environmental Protection Agency; Washington (DC). available at: http://www.epa.gov/opp00001/pestsales/01pestsales/market_estimates2001.pdf (Report EPA-733-R-04-001, Accessed February 2010).

Konstantinou, I.K., Sakellarides, T.M., Sakkas, V.A., Albanis, T.A., 2001. Photocatalytic degradation of selected s-triazine herbicides and organophosphorus insecticides over aqueous TiO_2 suspensions. Environ. Sci. Technol. 35(2), 398-405.

Kruithof, J. C., Kamp, P. C., Belosevic, M., 2002. UV/H_2O_2-treatment: The ultimate solution for pesticide control and disinfection. Water Sci. Technol.: Water Supply 2(1), 113-122.

Lee, Y., von Gunten, U., 2010. Oxidative transformation of micropollutants during municipal wastewater treatment: Comparison of kinetic aspects of selective (chlorine, chlorine dioxide, ferrate^{VI}, and ozone) and non-selective oxidants (hydroxyl radical). Water Res. 44(2), 555-566.

Lopez, M.C., Fernandez M.I., Rodriguez, S., Santaballa, J.A., Steenken, S., Vulliet, E., 2005. Mechanisms of direct and TiO_2 photocatalised UV degradation of phenylurea herbicides. ChemPhysChem 6(10), 2064-2074.

MacAdam, J., Parsons, S.A., 2009. An investigation into advanced oxidation of three chlorophenoxy pesticides in surface water. Water Sci. Technol. 59(8), 1665-1671.

Maldonado, M.I., Passarinho, P.C., Oller, I., Gernjak, W., Fernández, P., Blanco, J., Malato, S., 2007. Photocatalytic degradation of EU priority substances: A comparison between TiO_2 and Fenton plus photo-Fenton in a solar pilot plant. J. Photochem. Photobiol. A 185(2-3), 354-363.

Meijers, R. T., Van der Veer, A. J., Kruithof, J. C., 1993. Degradation of pesticides by ozonation and advanced oxidation. Water Supply 11(3-4), 309-320.

Mezyk, S.P., Cooper, W.J., Bartels, D.M., O'Shea, K.E., Wu, T., 2001. Radiation chemistry of alternative fuel oxygenates: Substituted ethers. J. Phys. Chem. A 105(14), 3521-3526.

Miglioranza, K. S. B., Gonzales Sagrario, M. A., Aizpun de Moreno, J. E., Moreno, V. J., Escalante, A. H., Osterrieth, M. L., 2002. Agricultural Soil as a Potential Source of Input of Organochlorine Pesticides into a Nearby pond. Environ. Sci. Pollut. R. 9(4), 250-256.

Minakata, D., Li, K., Westerhoff, P., Crittenden, J., 2009. Development of a group contribution method to predict aqueous phase hydroxyl radical (HO•) reaction rate constants. Environ. Sci. Technol. 43, 6220-6227.

Minero, C., 1999. Kinetic analysis of photoinduced reactions at the water semiconductor interface. Catal. Today 54(2-3), 205-216.

Montoya, J.F., Velasquez, J.A., Salvador, P., 2009. The direct-indirect kinetic model in photocatalysis: a reanalysis of phenol and formic acid degradation rate dependence on photon flow and concentration in TiO_2 aqueous dispersions. Appl. Catal. B: Environ. 88(1-2), 50-58.

Muhamad, S.G., 2010. Kinetic studies of catalytic photodegradation of chlorpyrifos insecticide in various natural waters. Arab. J. Chem. 3(2), 127-133.

Nakatani, N., Hashimoto, N., Shindo, H., Yamamoto, M., Kikkawa, M., Sakugawa, H., 2007. Determination of photoformation rates and scavenging rate constants of hydroxyl radicals in natural waters using an automatic light irradiation and injection system. Anal. Chim. Acta 581(2), 260-267.

Nienow, A.M., Bezares-Cruz, J.C., Poyer, I.C., Hua, I., Jafvert, C.T., 2008. Hydrogen peroxide-assisted UV photodegradation of lindane. Chemosphere 72(11), 1700-1705.

Ormad, P., Cortes, S., Puig, A., Ovelleiro, J. L., 1997. Degradation of organochloride compounds by O_3 and O_3/H_2O_2. Water Res. 31(9), 2387-2391.

Ormad, M. P., Miguel, N., Claver, A., Matesanz, J. M., Ovelleiro, J. L., 2008. Pesticides removal in the process of drinking water production. Chemosphere 71(1), 97-106.

Orzel, L., Jańczyk, A., Brindell, M., Stopa, G., Stochel, G., 2010. New trends in the application of laser-flash photolysis- case studies. J. Coord. Chem. 63(14-16), 2695-2714.

Parsons, S.A., 2004. Advanced Oxidation Processes for Water and Wastewater Treatment, IWA, UK.

Peller, J., Kamat, P.V., Radiolytic transformations of chlorinated phenols and chlorinated phenoxyacetic acids. J. Phys. Chem. A 109(42), 9528-9535.

Pereira, V.J., Weinberg, H.S., Linden, K.G., Singer, P.C., 2007. UV degradation kinetics and modelling of pharmaceutical compounds in laboratory grade and surface water via direct and indirect photolysis at 254nm. Environ. Sci. Technol. 41(5), 1682-1688.

Pereira, V.J., Linden, K.G., Weinberg, H.S., 2007. Evaluation of UV irradiation for photolytic and oxidative degradation of pharmaceutical compounds in water. Water Res. 41(19), 4413-4423.

Pimentel, D., Lehman, H., Eds., 1993. The Pesticide Question: Environment, Economics and Ethics. Chapman & Hall, New York and London.

Pirbazari, M., Badriyha, B.N., Miltner, R.J. 1991. GAC adsorber design for removal of chlorinated pesticides. J. Environ. Eng. 117(1), 80-100.

Ravishankara, A.R., Wine, P.H., Langford, A.O., 1979. Absolute rate constant for the reaction $OH + HBr \rightarrow H_2O + Br$. Chem. Phys. Lett. 63(3), 479-484.

Rosario-Ortiz, F.L., Wert, E.C., Snyder, S.A., 2010. Evaluation of UV/H_2O_2 treatment for the oxidation of pharmaceuticals in wastewater. Water Res. 44(5), 1440-1448.

Rosenfeldt, E.J., Linden, K.G., 2004. Degradation of endocrine disrupting chemicals bisphenol A, ethinyl estradiol, and estradiol during UV photolysis and advanced oxidation processes. Environ. Sci. Technol. 38(20), 5476-5483.

Rosenfeldt, E.J., Linden, K.G., 2007. The $R_{OH,UV}$ concept to characterize and the model UV/H_2O_2 process in natural waters. Environ. Sci. Technol. 41(7), 2548-2553.

Sanches, S., Barreto-Crespo, M.T., Pereira, V.J., 2010. Drinking water treatment of priority pesticides using low pressure UV photolysis and advanced oxidation processes. Water Res. 44(6), 1809-1818.

Scaiano, J.C., 1982. Laser flash photolysis studies of some 1,4-biradicals. Acc. Chem. Res. 15(8), 252-258.

Shemer, H., Linden, K.G., 2006. Degradation and by-product formation of diazinon in water during UV and UV/H_2O_2 treatment. J. Hazard. Mater. 136(3), 553-559.

Tanghe, N., Benezet-Toulze, M., Bouillot, P., Druoton, P., Levi, Y., Paillard, H. and Philipps, F., 1992. Study on the industrial application of ozone-hydrogene peroxyde oxidation coupling for the elimination of triazines in water treatment. Water Supply, 10(2), 121-132.

Tizaoui, C., Mezughi, K., Bickley, R., 2011. Heterogeneous photocatalytic removal of the herbicide clopyralid and its comparison with UV/H_2O_2 and ozone oxidation techniques. Desalination 273(1), 197-204.

Thuy, P.T., Moons, K., Van Dijk, J.C., Viet Anh, N., Van Der Bruggen, B., 2008. To what extent are pesticides removed from surface water during coagulation-flocculation?. Water Environ. J. 22(3), 217-223.

U.S.EPA Office of Pesticide Programs, 2001. The incorporation of water treatment effects on pesticide removal and transformations in food quality protection. Available at: http://www.epa.gov/oppfead1/trac/science/water_treatment.pdf (Act (FQPA) Drinking Water Assessments, accessed February 2010).

Valencia, S., Catano, F., Rios, L., Restrepo, G., Marin, J., 2011. A new kinetic model for heterogeneous photocatalysis with titanium dioxide: Case of non-specific adsorption considering back reaction. Appl. Catal. B - Environ 104(3-4), 300-304.

Van der Bruggen, B., Schaep, J. Maes, W., Wilms, D., Vandecasteele, C., 1998. Nanofiltration as a treatment method for the removal of pesticides from ground waters. Desalination 117(1-3), 139-147.

Westerhoff, P., Aiken, G., Amy, G., Debroux, J., 1999. Relationships between the structure of natural organic matter and its reactivity towards molecular ozone and hydroxyl radicals. Water Res. 33(10), 2265-2276.

Westerhoff, P., Mezyk, S.P., Cooper, W.J., Minakata, D. 2007. Electron pulse radiolysis determination of hydroxyl radical rate constants with Suwannee River fulvic acid and other dissolved organic matter isolates. Environ. Sci. Technol. 41(13), 4640-4646.

World Health Organisation, 2004. Guidelines for drinking-water quality, Vol.1: Recommendations, World Health Organisation, 3rd edition, Geneva.

Wu, C., Shemer, H., Linden, K.G., 2007. Photodegradation of metolachlor applying UV and UV/H_2O_2. J. Agric. Food Chem. 55(10), 4059-4065.

Yeung, K.L., Javier Maira, A., Stolz, J., Hung, E., Ho, N.K.-C., Wei, A.C., Soria, J., Chao, K.-J., Yue, P.L., 2002. Ensemble effects in nanostructured TiO_2 used in the gas-phase photooxidation of trichloroethylene. J. Phys. Chem. B 106(18), 4608-4616.

Zalazar, C.S., Satuf, M.L., Alfano, O.M., Cassano, A.E., 2008. Comparison of H_2O_2/UV and heterogeneous photocatalytic processes for the degradation of dichloroacetic acid in water. Environ. Sci. Technol. 42(16), 6198-6204.

Zepp, R.G., Hoigné, J., Bader, H., 1987. Nitrate-induced photooxidation of trace organic chemicals in water. Environ. Sci. Technol. 21(5), 443-450.

Zheng, S., Cai, Y., O'Shea, K.E., 2010. TiO_2 photocatalytic degradation of phenylarsonic acid. J. Photochem. Photobio. A: Chem. 210(1), 61-68.

2.13 Supporting Information.

Table 2-SI-1 - Comparison of experimental and theoretical second-order rate constant for a range of pesticides

Compound	Experimental $k_{\bullet OH}$ ($M^{-1}.s^{-1}$)	Theoretical $k_{\bullet OH}$ ($M^{-1}.s^{-1}$)	$k_{\bullet OH}$ theo/exp	Method	Reference
prometon	2.9×10^{9}	1.02×10^{10}	3.52	Competition kinetics using nitrobenzene as reference compound	Shemer et al., 2006
terbacil	7.4×10^{9}	1.90×10^{10}	2.57	Competition kinetics using nitrobenzene as reference compound	Shemer et al., 2006
disulfoton	1.5×10^{10}	1.34×10^{10}	0.89	Competition kinetics using nitrobenzene as reference compound	Shemer et al., 2006
terbufos	1.3×10^{10}	1.39×10^{10}	1.10	Competition kinetics using nitrobenzene as reference compound	Shemer et al., 2006
diazinon	9.0×10^{9}	5.84×10^{9}	0.65	Competition kinetics using nitrobenzene as reference compound	Shemer et al., 2006
diuron	9.9×10^{9}	6.70×10^{9}	0.68	Competition kinetics using nitrobenzene as reference compound	Shemer et al., 2006
linuron	1.0×10^{10}	5.29×10^{9}	0.53	Competition kinetics using nitrobenzene as reference compound	Shemer et al., 2006
linuron	4.20×10^{9}	5.29×10^{9}	1.26	Laser flash photolysis of Ar-saturated H_2O_2	Lopez et al., 2005
monolinuron	2.60×10^{9}	7.10×10^{9}	2.73	Laser flash photolysis of Ar-saturated H_2O_2	Lopez et al., 2005
fenuron	1.60×10^{9}	7.50×10^{9}	4.69	Laser flash photolysis of Ar-saturated H_2O_2	Lopez et al., 2005
monuron	3.10×10^{9}	7.16×10^{9}	2.31	Laser flash photolysis of Ar-saturated H_2O_2	Lopez et al., 2005
Diuron	2.90×10^{9}	6.70×10^{9}	2.31	Laser flash photolysis of Ar-saturated H_2O_2	Lopez et al., 2005

Table 2-SI-1(Continued)

Compound	Experimental $k_{\bullet OH}$ ($M^{-1}.s^{-1}$)	Theoretical $k_{\bullet OH}$ ($M^{-1}.s^{-1}$)	$k_{\bullet OH}$ theo/exp	Method	Reference
fluomethuron	3.20 x10^{10}	8.14 x10^{9}	0.25	Laser flash photolysis of Ar-saturated H_2O_2	Lopez et al., 2005
isoproturon	1.30 x10^{10}	1.12 x10^{10}	0.86	Laser flash photolysis of Ar-saturated H_2O_2	Lopez et al., 2005
MCPA	6.27 x10^{9}	4.66 x10^{9}	0.74	Competition kinetics using pCBA as reference compound	Benitez et al., 2004
2,4-D	5.20 x10^{9}	4.21 x10^{9}	0.81	Competition kinetics using pCBA as reference compound	Benitez et al., 2004
simazine	2.10 x10^{9}	4.76 x10^{9}	2.27	Competition kinetics using H_2O_2 as reference compound	Beltran et al., 2000
parathion	9.70 x10^{9}	4.51 x10^{9}	0.46	Competition kinetics using nitrobenzene as reference compound	Wu et al., 2010
lindane	5.20 x10^{9}	3.34 x10^{9}	0.64	Photo-Fenton using DBCP as reference compound	Haag and Yao, 1992
atrazine	2.60 x10^{9}	7.38 x10^{9}	2.84	Photo-Fenton using acetophenone as reference compound	Haag and Yao, 1992
simazine	2.80 x10^{9}	4.76 x10^{9}	1.70	Photo-Fenton using acetophenone as reference compound	Haag and Yao, 1992
aldicarb	8.10 x10^{9}	2.32 x10^{9}	0.29	Photo-Fenton using acetophenone as reference compound	Haag and Yao, 1992
carbendazim	2.20 x10^{9}	2.95 x10^{9}	1.34	Competition kinetics using H_2O_2 as reference compound	Mazellier et al., 2002
dichlorprop	5.20 x10^{9}	4.66 x10^{9}	0.90	Pulse radiolysis	Peller and Kamat, 2005
2,4-dichlorophenol	7.40 x10^{9}	5.24 x10^{9}	0.71	Pulse radiolysis	Peller and Kamat, 2005

Table 2-SI-1(Continued)

Compound	Experimental $k_{\bullet OH}$ ($M^{-1}.s^{-1}$)	Theoretical $k_{\bullet OH}$ ($M^{-1}.s^{-1}$)	$k_{\bullet OH}$ theo/exp	Method	Reference
2,4-D	5.20 x10^9	4.21 x10^9	0.81	Pulse radiolysis	Peller and Kamat, 2005
mecoprop	2.50 x10^9	5.11 x10^9	2.04	Competition kinetics using acetophenone as reference compound	Armbrust, 2009
dicamba	1.30 x10^9	5.15 x10^9	3.96	Competition kinetics using acetophenone as reference compound	Armbrust, 2009
molinate	2.10 x10^9	2.00 x10^{10}	9.52	Competition kinetics using acetophenone as reference compound	Armbrust, 2009
thiobencarb	1.90 x10^9	2.42 x10^{10}	12.74	Competition kinetics using acetophenone as reference compound	Armbrust, 2009
acetochlor	6.30 x10^9	9.12 x10^9	1.45	Competition kinetics using pCBA as reference compound	Acero et al., 2003
metolachlor	6.70 x10^9	1.80 x10^{10}	2.69	Competition kinetics using pCBA as reference compound	Acero et al., 2003
propachlor	4.60 x10^9	1.41 x10^{10}	3.07	Competition kinetics using pCBA as reference compound	Acero et al., 2003
butachlor	7.44 x10^9	1.49 x10^{10}	2.00	Competition kinetics using pCBA as reference compound	Acero et al., 2003
atrazine	2.10 x10^9	7.38 x10^9	3.51	Competition kinetics using atrazine as reference compound	De Laat et al., 1996
chlortoluron	4.30 x10^9	9.40 x10^9	2.19	Competition kinetics using atrazine as reference compound	De Laat et al., 1996
diuron	4.60 x10^9	6.70 x10^9	1.46	Competition kinetics using atrazine as reference compound	De Laat et al., 1996
isoproturon	5.20E+09	1.12 x10^{10}	2.15	Competition kinetics using atrazine as reference compound	De Laat et al., 1996

Table 2-SI-1(Continued)

Compound	Experimental $k_{\bullet OH}$ ($M^{-1}.s^{-1}$)	Theoretical $k_{\bullet OH}$ ($M^{-1}.s^{-1}$)	$k_{\bullet OH}$ theo/exp	Method	Reference
linuron	4.30×10^9	5.29×10^9	1.23	Competition kinetics using atrazine as reference compound	De Laat et al., 1996
alachlor	5.00×10^9	1.12×10^{10}	2.24	Competition kinetics using atrazine as reference compound	De Laat et al., 1996
metolachlor	5.10×10^9	1.80×10^{10}	3.53	Competition kinetics using atrazine as reference compound	De Laat et al., 1996
propachlor	4.30×10^9	1.41×10^{10}	3.28	Competition kinetics using atrazine as reference compound	De Laat et al., 1996
carbofuran	2.20×10^9	9.46×10^9	4.30	Competition kinetics using PNDA as reference compound	Mabury and Crosby, 1996
MCPA	1.70×10^9	4.66×10^9	2.74	Competition kinetics using PNDA as reference compound	Mabury and Crosby, 1996
2,4-D	1.60×10^9	4.21×10^9	2.63	Competition kinetics using PNDA as reference compound	Mabury and Crosby, 1996
propanil	1.60×10^9	4.54×10^9	2.84	Competition kinetics using PNDA as reference compound	Mabury and Crosby, 1996
molinate	8.50×10^8	2.00×10^{10}	23.53	Competition kinetics using PNDA as reference compound	Mabury and Crosby, 1996
atrazine	8.20×10^8	7.40×10^9	9.02	Competition kinetics using PNDA as reference compound	Mabury and Crosby, 1996
simazine	2.10×10^9	4.80×10^9	2.29	Competition kinetics using chlorobenzene as reference compound	Chramosta et al., 1993
propazine	1.20×10^9	1.00×10^{10}	8.33	Competition kinetics using chlorobenzene as reference compound	Chramosta et al., 1993
atrazine	1.70×10^9	7.40×10^9	4.35	Competition kinetics using chlorobenzene as reference compound	Chramosta et al., 1993

Table 2-SI-1(Continued)

Compound	Experimental $k_{\bullet OH}$ ($M^{-1}.s^{-1}$)	Theoretical $k_{\bullet OH}$ ($M^{-1}.s^{-1}$)	$k_{\bullet OH}$ theo/exp	Method	Reference
metolachlor	9.10×10^{9}	1.80×10^{10}	1.98	Competition kinetics using nitrobenzene as reference compound	Wu et al., 2007
chlortoluron	6.90×10^{9}	9.40×10^{9}	1.36	Competition kinetics using pCBA as reference compound	Benitez et al., 2007
diuron	6.60×10^{9}	6.70×10^{9}	1.02	Competition kinetics using pCBA as reference compound	Benitez et al., 2007
isoproturon	7.90×10^{9}	1.12×10^{10}	1.42	Competition kinetics using chlortoluron as reference compound	Benitez et al., 2007
linuron	5.90×10^{9}	5.29×10^{9}	0.90	Competition kinetics using diuron as reference compound	Benitez et al., 2007
atrazine	7.30×10^{9}	7.40×10^{9}	1.01	Competition kinetics using pCBA as reference compound	Sanches et al., 2010
isoproturon	8.00×10^{8}	1.12×10^{10}	14.00	Competition kinetics using pCBA as reference compound	Sanches et al., 2010
diuron	1.27×10^{10}	6.70×10^{9}	0.53	Competition kinetics using pCBA as reference compound	Sanches et al., 2010
alachlor	5.40×10^{9}	1.12×10^{10}	2.07	Competition kinetics using pCBA as reference compound	Sanches et al., 2010
2-chlorophenol	1.2×10^{10}	6.27×10^{9}	0.52	Pulse radiolysis	Getoff and Solar, 1986

CHAPTER 3 COMPARISON OF UV/H_2O_2 AND UV/TiO_2 FOR THE DEGRADATION OF METALDEHYDE: KINETICS AND IMPACT OF BACKGROUND ORGANICS

CHAPTER 3: COMPARISON OF UV/H_2O_2 AND UV/TiO_2 FOR THE DEGRADATION OF METALDEHYDE: KINETICS AND IMPACT OF BACKGROUND ORGANICS

Olivier Autin [a], *Julie Hart* [b], *Peter Jarvis* [a], *Jitka MacAdam* [a], *Simon A. Parsons* [a], *Bruce Jefferson* [a]

[a] Cranfield Water Science Institute, Department of Environmental Science and Technology, Cranfield University, Bedfordshire, MK43 0AL, UK.

[b] Severn Trent Water LTD., Severn Trent Centre, PO Box 5309, Coventry, West Midlands, CV3 9FH, UK.

3.1 Abstract

The kinetics of photodegradation of the pesticide metaldehyde by UV/H_2O_2 and UV/TiO_2 in laboratory grade water and a natural surface water were studied. Experiments were carried out in a bench scale collimated beam device using UVC radiation. Metaldehyde was efficiently degraded by both processes in laboratory grade water at identical rates of degradation (0.0070 and 0.0067 $cm^2.mJ^{-1}$ for UV/TiO_2 and UV/H_2O_2 respectively) when optimised doses were used. The ratio between oxidant and metaldehyde was significantly higher for H_2O_2 due to its low photon absorption efficiency at 254 nm. However, the presence of background organic compounds in natural water severely affected the rate of degradation, and whilst the pseudo first-order rate constant of degradation by UV/H_2O_2 was slowed down (0.0020 $cm^2.mJ^{-1}$), the degradation was completely inhibited for the UV/TiO_2 process (k'=0.00007 $cm^2.mJ^{-1}$) due to the blockage of active sites on TiO_2 surface by the background organic material.

Keywords: Metaldehyde, Advanced Oxidation Processes, Hydrogen peroxide, Titanium dioxide, Kinetics, Natural Organic Matter.

3.2 Introduction

Advanced oxidation processes (AOP) represent a group of destructive reaction processes that have shown promise for the treatment of micropollutants. This includes a range of compounds that have been identified to be difficult to treat through conventional drinking water treatment flow sheets (Parsons, 2004). One sub-set of the AOPs utilises UV irradiation to activate a selection of different chemicals to produce highly reactive and quasi-unselective hydroxyl radicals (•OH). These processes include titanium dioxide (TiO_2), hydrogen peroxide (H_2O_2) and Fenton's reagent (H_2O_2/Fe^{3+}) (Evgenidou and Fytianos, 2002; Thomson et al., 2002; Sharpless and Linden, 2003; Toepfer et al., 2006; Sanches et al., 2010). The photolysis of H_2O_2 at 254 nm yields the formation of two •OH per photon absorbed (Baxendale and Willson, 1957) whilst the irradiation of TiO_2 with light waves having an energy greater than the band gap energy creates electron-hole pairs. The excited electron and hole move to the surface of the TiO_2 and react with adsorbed substances (Fotiadis et al., 2007); the holes can oxidise HO^- ions and H_2O molecules into reactive radicals or react directly with pollutants in the water. The excited electron has to react with a scavenger (invariably dissolved oxygen in water) quickly enough, or it will recombine with the hole and the catalyst activity will be lost. In both processes, organic molecules need to be in close proximity of the formed •OH radicals in order for a reaction to occur. The main difference between the two processes is the phase in which the reactions occur. In the UV/H_2O_2 process, •OH are formed in the liquid phase and can directly react in solution. TiO_2 is a solid catalyst where •OH are formed at its surface. Therefore, the adsorption of organics

onto, or very close to the surface of TiO_2 particles is critical and is the determining step of UV photocatalysis (Minero et al., 1992; Linsebigler et al., 1995; Thompson and Yates Jr., 2005). A number of previous studies have already looked at the comparison of these two processes for the best technology to treat a range of different target organic compounds generally in one type of background water, often laboratory grade water with no competing organic compounds (Ruppert et al., 1994; Alaton et al., 2002; Stepnowskiand Zaleska, 2005; Bobu et al., 2006; Tizaoui et al., 2011). The different studies have shown cases where one or other of the processes is the most effective. However, direct comparison across the studies is complicated as in most cases a relatively limited range of concentrations of the •OH forming material (e.g. H_2O_2 or TiO_2) are considered. Further, when adjusted in terms of the mole ratio of the added •OH forming chemical (e.g. H_2O_2 or TiO_2) in relation to the moles of pollutant, the two processes are generally tested over different ranges making a fair comparison very difficult. For instance typical ratios used in UV/H_2O_2 experiments range between 50-420 moles H_2O_2 per mole of pollutant compared to 7-60 moles of TiO_2 per mole of pollutant for photocatalysis (Chen et al., 1998; Sanches et al., 2010; Benitez et al., 2011). Zalazar et al. (2008) highlighted a similar challenge when comparing the two processes in the development of kinetic models for the degradation of dichloroacetic acid and therefore extended the factors to consider to include differences in nominal lamp input power. The work compared the two processes based on three normalisation criteria including fixed retention time, quantum efficiency and the specific energy consumption to degrade 50% of the initial TOC. The authors concluded that H_2O_2/UV was the most effective of the AOPs but acknowledged that these findings may change for different target compounds and in natural water matrices.

The objective of the current study was to build on these previous comparisons by directly comparing the influence of H_2O_2 and TiO_2 concentrations in both laboratory grade and surface water exposed to the same levels of irradiation to investigate the oxidation kinetics of the two processes and then discuss the design implications. The context of the current study relates to degradation of the pesticide metaldehyde, the active ingredient found in most slug pellets. Metaldehyde is not new and was first introduced in 1940 and has been widely used since the 1970s in agriculture, horticulture, and domestic gardens (Iglesias et al., 2001). At first sight, metaldehyde is a simple compound and is moderately soluble in water (188 $mg.L^{-1}$) with a low Log K_{ow} (1.14). In 2007, Bristol Water in the UK identified metaldehyde in treated drinking water and it has been subsequently shown to be widely detected in groundwater and surface water (Water UK, 2009). Significantly, metaldehyde is very poorly removed across most drinking water treatment plants to the degree that in 2010, a third of the 1,103 failures of drinking water standards reported in England and Wales by the Drinking Water Inspectorate (DWI) were due to metaldehyde. To illustrate, current water treatment practice is to use activated carbon to remove such compounds but in the case of metaldehyde uneconomic operation of granular activated carbon beds is seen. Modeling work has shown that virgin GAC may only have a 44 day bed life before the drinking water standard of 0.1 $\mu g.L^{-1}$ standard is exceeded (Hall, 2010). A recent review of the problems facing UK water utilities in relation to metaldehyde concluded that although concentrations of the pesticide have been lower in raw water over past 2 years, water treatment works can only achieve 30-50% removal of metaldehyde and it is difficult to achieve the 0.1 $\mu g.L^{-1}$ standard if raw water concentrations of metaldehyde were above 0.15 $\mu g.L^{-1}$ (Hall et al., 2011). Consequently the traditional solution to

removing the majority of pesticides in the UK (granular activated carbon and ozone) appears unsuitable as removal barrier for metaldehyde. Previous studies on the removal of metaldehyde in surface water (0.17-0.27 $\mu g.L^{-1}$) showed that direct photolysis (low power UV) could only achieve 15% removal whereas combination with 10 $mg.L^{-1}$ H_2O_2 enabled between 55 and 60% removal to be possible (Lamming, 2010).

3.3 Experimental section

3.3.1 Chemicals and reagents

Metaldehyde, hydrogen peroxide (35% w/w), and analytical grade methanol, dichloromethane and acetonitrile were purchased from Fisher Scientific (Loughborough, UK). Para-chlorobenzoic acid (pCBA) and an aqueous solution of bovine liver catalase with 40000-60000 $units.mg^{-1}$ protein (1 unit decomposes 1 μmol of H_2O_2 per minute as described by the supplier) were purchased from Sigma Aldrich (Poole, UK). Titanium dioxide (Aeroxide® TiO_2 P25 Degussa) was purchased from Lawrence Industries (Tamworth, UK). Laboratory grade water (LGW) was produced by a Purelab Option- S7/15 system (Elga process water, Buckinghamshire, UK). The surface water, characterized by its relatively high non-purgeable organic carbon (NPOC) concentration of 8.7 $mgC.L^{-1}$ and alkalinity of 140 mg $CaCO_3.L^{-1}$, was collected from a reservoir in the Severn Trent Water region (UK) and stored in the dark at 4˚C. Prior to experiments, the water was filtered (0.45 μm, Fisher Scientific, UK).

3.3.2 Irradiation procedures

UV experiments were all conducted in a Wedeco AG bench scale quasi-collimated beam apparatus (Herford, Germany) fitted with four 30 W low pressure Hg lamps that emit monochromatic light at 254 nm. A warm up time of 30 min was allowed to ensure

consistent light output before irradiating the solution. A volume of 250 mL of test solution was placed in a Petri dish 22 cm away from the light source and stirred with a magnetic stirrer. In many studies, the degradation of micropollutants is often expressed as a function of time which does not take into consideration the experimental set up and therefore results cannot be directly compared with other studies. The expression of a micropollutant degradation as a function of UV fluence instead of irradiation time standardizes UV processes which enables comparison of data from different studies with higher confidence and was thus used in this study (Bolton and Linden, 2003). UV irradiance from the collimated beam was determined to be 22.6 $W.m^{-2}$ using the uridine actinometry method as described by von Sonntag and Schuchmann (1992). The required volumes of solution were withdrawn at 7 UV fluences, depending on the experiment being carried out, in order to quantify the concentrations of metaldehyde and pCBA by GCMS and HPLC respectively. In all experiments, the pH was the natural pH of the different solutions tested.

It has been reported that although TiO_2 particles are activated at $\lambda<380$ nm (Herrmann, 2005; Chiron et al., 2000; Pirkanniemi and Sillanpaa, 2002), the optimum wavelength for their activation is $300< \lambda<310$ nm (Li Puma and Yue, 1999; Chu and Wong, 2004; Chu et al., 2009). In this study, an irradiation wavelength of 254 nm has been chosen as H_2O_2 cannot be photolysed at wavelengths higher than 280 nm (Urey et al., 1929) and still enables the activation of TiO_2.

3.3.3 Determination of second-order rate constants

The second-order rate constant between metaldehyde and •OH was determined by competition kinetics using pCBA as the probe compound ($k_{\bullet OH}$ = 5.0 x 10^9 $M^{-1}.s^{-1}$) (Neta and Dorfman, 1968), as it does not undergo direct photolysis and has been widely

applied in similar experiments (Pereira et al., 2007; Sutherland and Adams, 2007; Sanches et al., 2010). Competition kinetics experiments were conducted in laboratory grade water spiked with 1 mg.L^{-1} of metaldehyde in order to follow its degradation and 0.5 mg.L^{-1} of pCBA was added to the solution in order to determine indirectly the second-order rate constant (Sanches et al., 2010) with 5 mg.L^{-1} of H_2O_2 as the source of •OH. The reaction of the two organic compounds (the reference pCBA (R) and the target metaldehyde (T)) with •OH can be described by the following kinetic equations:

Metaldehyde + •OH → Products

$$r_T = k_{\bullet OH,T} \times [T] \times [\bullet OH] = k'_T \times [T] \quad (3\text{-}1)$$

pCBA + •OH → Products

$$r_R = k_{\bullet OH,R} \times [R] \times [\bullet OH] = k'_R \times [R] \quad (3\text{-}2)$$

Where r_T and r_R are the reactions rates of metaldehyde and pCBA respectively, in M.s^{-1}, [-] denote molar concentrations, $k_{\bullet OH}$ represents the second-order rate constant in $M^{-1}.s^{-1}$ and k' is the pseudo-first-order rate constant in s^{-1}.

The oxidation of both compounds followed the pseudo-first-order kinetic model and therefore:

$$\ln (C/C_0) = - k' \times t \quad (3\text{-}3)$$

The slopes of the straight lines give the pseudo-first-order rate constants. Subsequently, the second-order rate constant between metaldehyde and •OH was obtained substituting (3-1) and (3-2):

$$k'_T / k_{\bullet OH,T} = k'_R / k_{\bullet OH,R} \quad (3\text{-}4)$$

3.3.4 UV/TiO_2

The same procedure was used for the photocatalytic removal of metaldehyde where the appropriate amount of metaldehyde stock solution was spiked to achieve initial concentrations of 1 mg.L^{-1}. Such high concentrations were used in order to accurately follow the kinetics of metaldehyde degradation. A series of tests has been repeated at lower metaldehyde concentration, and although the rate constants were slower, the same profiles were observed (data not shown). TiO_2 was then added at concentrations varying from 0.8 to 160 mg.L^{-1} (corresponding to 0.01 to 2 mM). Molar concentrations are used here for a direct comparison between the two processes, even though the authors acknowledge that it leads to overestimation of the molar concentration of TiO_2 as only the surface of TiO_2 is active and the internal mass of TiO_2 particles should be excluded. A contact time of 10 minutes was given between the TiO_2 and the contaminant(s) before irradiation. Adsorption experiments in the dark and direct photolysis experiments were also performed to determine the influence of these two parameters on the photocatalytic process. At determined UV fluences, an aliquot was withdrawn and directly filtered through a Millex-HA 0.45 μm syringe filter to separate the suspended TiO_2 prior to solid phase extraction (SPE) and analysis.

3.3.5 UV/H_2O_2

The UV/H_2O_2 tests followed the same experimental set-up as the UV/TiO_2 with the exception that H_2O_2 (from 0.08 to 100 mM) was added to the solution instead of TiO_2. Samples were collected and directly quenched with the enzyme catalase in order to stop the reaction between H_2O_2 and the reactants before SPE extraction and analysis. For the quenching, a conservative approach was used and 1 mg of enzyme catalase was added

to the 250 mL of irradiated solution and left in contact for at least 30 minutes to ensure that all the H_2O_2 was destroyed.

3.3.6 Analytical methods

Metaldehyde was analysed using a method described by the Environment Agency (2009). Metaldehyde was extracted from aqueous samples by SPE (styrene-divinylbenzene cartridges, Strata, 200 mg/3 mL, Phenomenex, UK). The cartridge was first conditioned using 10 mL of methanol followed by 2 mL of ultrapure water. 1 mL of sample was then passed through the cartridge and rinsed with 2 mL of ultrapure water. The cartridge was then dried by passing air through it for 30 minutes. An appropriate glass tube was then placed under the cartridge and 2 mL of dichloromethane were added to the cartridge, collecting the eluate. A further 1 mL was added to ensure that all the metaldehyde was eluted, and the cartridge was dried for 10 minutes. The fraction was then evaporated by nitrogen, reconstituted with dichloromethane and analysed by gas chromatography-mass spectrometry (GC-MS) using an Agilent 6890N gas chromatograph coupled with a Agilent 5973 mass selective detector with a limit of detection of 0.175 $\mu g.L^{-1}$ (GC-MS + SPE). A HP-5MS column was used (Capillary 30.0 m x 250 µm x 0.25 µm nominal), the oven was programmed from 35 to 260˚C at 15˚C.min^{-1} and from 260 to 310˚C at 25˚C.min^{-1} and the carrier gas was helium used at 1 mL.min^{-1}. 1,4-dichlorobenzene-d_4 was used as internal standard.

pCBA was analysed by high performance liquid chromatography (HPLC) using a Kontron system equipped with a variable ultraviolet absorbance detector (SCI-tek instruments, Buckinghamshire, UK) which was set at 240 nm. The column was a Gemini 5 µm C18 110A (150 x 4.6 mm) (Phenomenex, Cheshire, UK), and the mobile

phase was a mixture of 60% methanol and 40% water adjusted at pH 2 with phosphoric acid and the flow rate was 1 mL.min^{-1}.

DOC was measured in the non-purgeable organic carbon (NPOC) mode using a Shimadzu 5000-A TOC analyser.

For all of the analyses, a new calibration curve was generated before each sequence and showed good linearity in the concentration ranges studied ($r^2 > 0.99$). Standards were also measured after every ten samples to ensure good quality control of the data produced and all of the experiments were duplicated.

3.4 Results and Discussion

3.4.1 Photodegradation of metaldehyde by direct photolysis

The direct photolysis of metaldehyde achieved only 2% removal at a maximum dose of 1750 mJ.cm^{-2} (Figure 3-1-A) consistent with the molar absorption coefficient for metaldehyde of 21.4 M^{-1}.cm^{-1} at 254 nm, demonstrating that the compound does not absorb light at this wavelength. In comparison, pesticides such as isoproturon and chlorfenvinphos (which are treatable by direct photolysis) have molar absorption coefficients of 5944 and 8656 M^{-1}.cm^{-1} respectively (Sanches et al., 2010). The investigation of the adsorption/desorption of metaldehyde onto the TiO_2 surface over a one hour contact time shows that after an initial 40% metaldehyde adsorption during the first minute of contact, equilibrium was reached after 10 min, and that metaldehyde was not readily adsorbed onto TiO_2 (Figure 3-1-B). Heterogeneous photocatalysis is a surface phenomenon and the majority of the reactions occur at the TiO_2/liquid interface or very near the surface of the TiO_2 aggregate (Linsebigler et al., 1995; Thompson and Yates Jr., 2005) thus requiring close contact for a reaction to occur. The low uptake of

photons by metaldehyde defined by a quantum yield of 0.000017 mol.einstein^{-1} and its poor adsorption mean that neither UV alone nor TiO_2 alone are able to remove metaldehyde and that alternative approaches are required, confirming the need to consider AOPs.

3.4.2 Influence of H_2O_2 and TiO_2 concentrations on the degradation of metaldehyde in laboratory grade water

Addition of H_2O_2 enhances the degradation of metaldehyde (Figure 3-1-A) as expected due to the photolysis of H_2O_2 which leads to the formation of the strongly oxidising •OH radical. Therefore, the oxidation by •OH can be determined as the main degradation mechanism for metaldehyde. A pseudo-first order decay was observed for all of the conditions tested with the H_2O_2 concentration exerting a significant influence on metaldehyde degradation. For example, with an irradiation dose of 600 mJ.cm^{-2} and 100 mM H_2O_2 concentration, 41% metaldehyde removal was achieved compared to 95% at an 8 mM dose. Interestingly, the higher H_2O_2 concentrations tested in this study did not result in improved removal consistent with the fact that H_2O_2 acts as a scavenger for •OH producing the much less effective •HO_2 radical. The combination of UV/TiO_2 also leads to complete degradation of metaldehyde within 600 mJ.cm^{-2} (Figure 3-1-C) with a TiO_2 concentration of 24 mg.L^{-1} (0.3 mM). However, only 20% removal is reached at 1500 mJ.cm^{-2} irradiation with a TiO_2 dose of 0.8 mg.L^{-1} (0.01 mM). For each concentration, the degradation follows a pseudo-first order decay up to a UV dose of 600 mJ.cm^{-2}. The concentration of photocatalyst is a key parameter in the degradation rate of organic contaminants by UV/TiO_2 (Chu et al., 2009; Ahmed et al., 2011) and the degradation rate increases with an increase in TiO_2 concentration between 0 and 0.3

mM. However, further addition of TiO_2 did not enhance the degradation of metaldehyde with TiO_2 concentrations from 0.3 to 2 mM resulting in similar profiles of degradation.

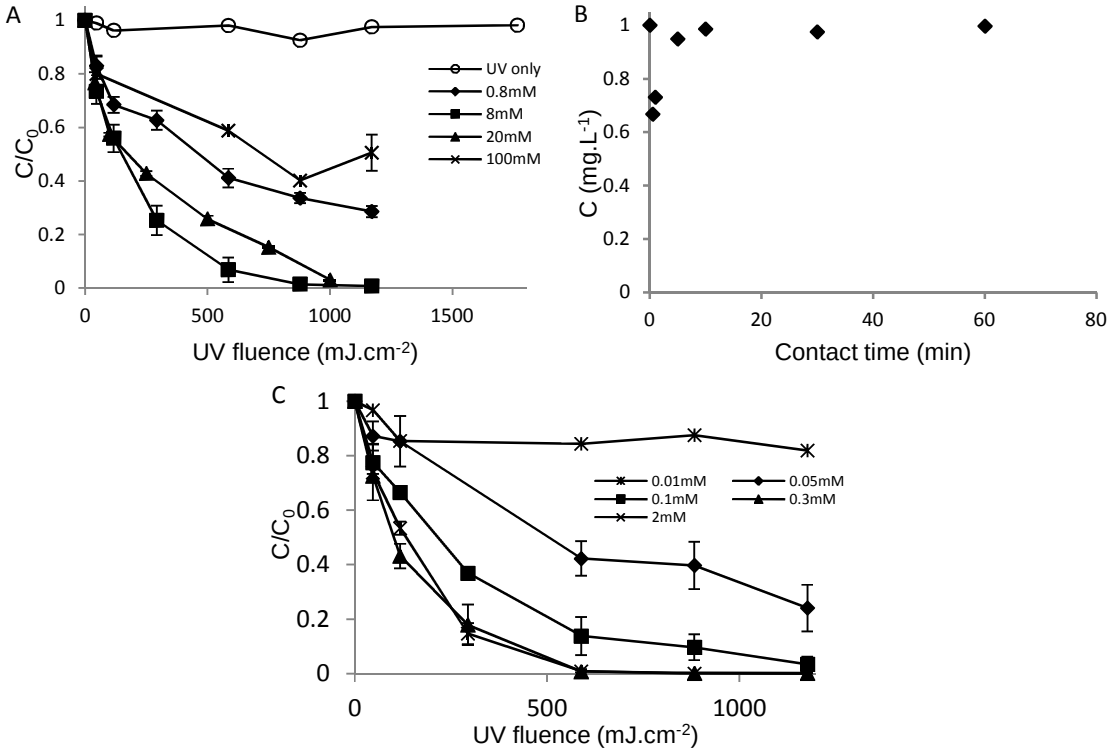

Figure 3-1 - (A) Direct photolysis and influence of hydrogen peroxide concentration on the photodegradation of metaldehyde (B) dark adsorption on TiO_2 surface $[TiO_2]$=100 mg.L^{-1} and (C) influence of TiO_2 concentration on the photocatalytic degradation of metaldehyde. $[metaldehyde]_0$=1 mg.L^{-1} in LG water.

Considering the efficacy of both processes in terms of mineralisation rather than removal of the parent compounds provide a different insight. The removal of DOC was similar for both processes, with 30% DOC removal at 3500 mJ.cm^{-2} (Figure 3-2). Increasing the UV dose to 14,000 mJ.cm^{-2} resulted in no more than 40% DOC removal suggesting that metaldehyde by-products are less treatable than metaldehyde in both processes indicating a reaction limitation as opposed to issues related to adsorption of the degradation products. Analysis of the data in terms of a second-order rate expression revealed a rate constant of 1.3x10^9 M^{-1}.s^{-1} for the reaction between metaldehyde and

•OH ($k_{•OH}$). Comparison of this rate constant with reported values for other pesticides such as isoproturon ($1.3x10^{10}$ $M^{-1}.s^{-1}$; Lopez et al., 2005), 2,4-D ($5.0x10^{9}$ $M^{-1}.s^{-1}$; Benitez et al., 2004) or atrazine ($2.6x10^{9}$ $M^{-1}.s^{-1}$; Haag and David Yao, 1992) shows that metaldehyde is less easily treated by AOPs and that the presence of other synthetic pesticides in the water will slow down metaldehyde removal.

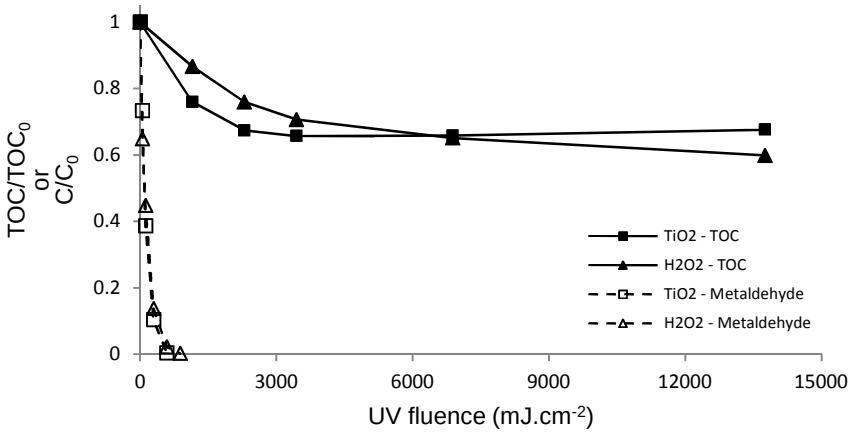

Figure 3-2 - Mineralisation of metaldehyde by UV/H_2O_2 and UV/TiO_2 processes; $[TOC]_0$=1.2 mg.L^{-1} in LG water, $[H_2O_2]$=8 mM, $[TiO_2]$=0.3 mM.

3.4.3 Photochemical oxidation of metaldehyde in surface water

The previous results have shown that both processes are effective at metaldehyde degradation in laboratory grade water where metaldehyde will be the only organic compound present initially and so always able to react with the available •OH. Similar experiments carried out in surface waters containing a background DOC of 8.7 mgC.L^{-1} (in comparison to the 0.55 mgC.L^{-1} that the metaldehyde provided), revealed a very different response (Figure 3-3-A). In the case of UV/H_2O_2 the process remained effective with 92% removal at 1,200 mJ.cm^{-2} whereas at the same UV dose, only 7% removal was possible with TiO_2 (Figure 3-3-B). These results show that background DOC has a significantly bigger impact on the inhibition of metaldehyde degradation during UV/TiO_2 than UV/H_2O_2. Such findings are consistent with the work of Philippe

et al. (2010) who showed that TiO_2 was a good adsorbent for specific types of NOM such that the background organic materials can block the available active sites on TiO_2 surface restricting the access of metaldehyde to the formed •OH. To illustrate, batch adsorption trials of NOM surrogates revealed 85% removal of tannic acid (hydrophobic anionic) compared to 25 and 40% respectively for L-glutamic and L-aspartic acids (hydrophilic anionic compounds). In the current case background organic matter represented 94% of the total dissolved carbon content in the water. Even if only 40% of the available DOC adsorbed onto the TiO_2, this was still 3.5 $mg.L^{-1}$ of DOC, over six times greater than the initial metaldehyde concentration. The results above show that 600 $mJ.cm^{-2}$ are required to degrade 0.55 $mgC.L^{-1}$ of metaldehyde. The adsorbed background DOC reacts with •OH six times slower than metaldehyde does, which would result in an irradiation dose of 22,000 $mJ.cm^{-2}$ to degrade the adsorbed DOC. Assuming that once the adsorbed DOC has reacted, the rate of degradation of metaldehyde becomes identical to that of UV/H_2O_2, it would require 24,000 $mJ.cm^{-2}$ to remove 90% of the metaldehyde, beyond the operational limits of our trial work.

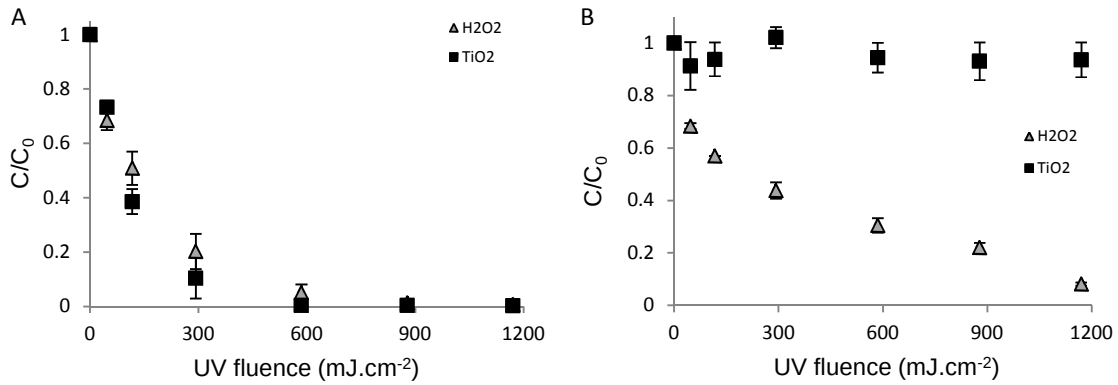

Figure 3-3 - Photooxidation of metaldehyde in (A) laboratory grade water and (B) surface water. $[Metaldehyde]_0$=1 $mg.L^{-1}$; $[H_2O_2]_0$=8 mM; $[TiO_2]$=0.3 mM.

In the case of UV/H_2O_2 an increase in UV dose was required but the overall process was still able to degrade metaldehyde (Figure 3-3-B). This was consistent with the fact that

the second order rate constant for metaldehyde is higher than those for the background organics with reported ranges between 1.4 and 4.5 x 10^8 $M^{-1}.s^{-1}$ and averaged 2.2 x 10^8 $M^{-1}.s^{-1}$ (Westerhoff et al., 2007). Comparison across the two processes suggests that the influence of background organic material is related more to adsorption than the reaction with •OH such that under current UV delivery technologies the addition of H_2O_2 is likely to be a more economically effective method. However, the rapid development of UV LED light sources means that lower cost delivery of UV is likely in the near future. It is predicted reduced costs for LEDs will result in a lowering by 1-2 orders in the total costs of the system when compared to traditional UV light sources such that the high doses required with TiO_2 will become economically possible (Shie et al., 2008) as clean TiO_2 can be sustainably retained with a membrane unit (Rivero et al., 2006). Thus the development of UV LED offers an implementation route for a non-chemical solution to the problem.

3.4.4 Kinetic comparison of UV/H_2O_2 and UV/TiO_2

In laboratory grade water, analysis of the data in terms of the impact of the molar concentration of H_2O_2 and TiO_2 on the photodegradation kinetic rate revealed significantly different profiles (Figure 3-4). The comparative plot has a logarithmic scale of molar concentration, reflecting a 1-2 order of magnitude difference in the concentrations required for TiO_2 and H_2O_2. This is best illustrated in terms of the required dose to reach the maximum degradation rate constant, which was 0.3 mM for TiO_2 compared to 8 mM for H_2O_2. Significantly, the rate constant was similar in both cases (0.0067 and 0.0070 $cm^2.mJ^{-1}$ for UV/H_2O_2 and UV/TiO_2 respectively) indicating that both processes are capable of delivering the same levels of reaction under optimum conditions.

In the case of UV/H_2O_2, the initial photodegradation rate of metaldehyde increased between the range 0.08 and 8 mM H_2O_2 beyond which the rate decreased for all further concentrations tested up to the maximum H_2O_2 dose of 100 mM due to the influence of residual H_2O_2 scavenging the available •OH (Figure 3-4). To illustrate, an increase of H_2O_2 concentration from 8 to 100 mM leads to an 8-fold decrease in the first-order reaction rate constant from 0.0067 to 0.0008 $cm^2.mJ^{-1}$. From this work, the optimum dose was identified at 8 mM and at this concentration, 86% of the metaldehyde was degraded at a UV fluence of 300$mJ.cm^{-2}$ and 95% at 600 $mJ.cm^{-2}$. The shape of the curve reflects a need to consider dose control of H_2O_2 if the maximum removal rate is to be maintained. To illustrate, a 50% change in the molar concentration of H_2O_2 (4-12 mM) equating to 136-408 $mg.L^{-1}$ of H_2O_2, resulted in an 18% reduction in rate if under dosed and only a 3% decrease in the rate constant if overdosed.

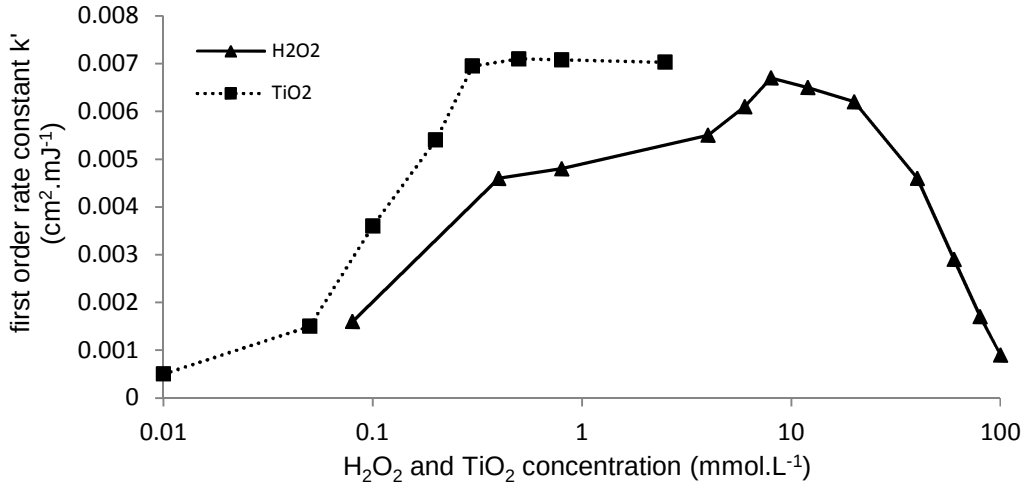

Figure 3-4 - Influence of H_2O_2 and TiO_2 concentrations on the first order rate constant k'; $[Metaldehyde]_0$=1 $mg.L^{-1}$.

For heterogeneous photocatalytic degradation, the pseudo-first-order rate constant increases linearly in the TiO_2 range 0-0.3 mM, up to 0.0070 $cm^2.mJ^{-1}$ which was due to the increasing photon absorption by TiO_2 particles. Further increases in TiO_2

concentration did not accelerate the degradation which was consistent with reports concerning the increase in opacity and to light scattering effects as the particle concentration was increased (Ahmed et al., 2011). Although the profiles of degradation were very different, at optimum concentration of H_2O_2 and TiO_2, the rates of degradation were very similar (0.0067 and 0.0070 $cm^2.mJ^{-1}$ respectively) suggesting that under optimum conditions the two processes are dominated by the reaction of •OH and so respond similarly. The rate constant was higher for TiO_2 compared to H_2O_2 for all comparative doses (Figure 3-4) suggesting that TiO_2 is a more effective •OH producer at any given UV dose. The explanation for the differences relates to the relative efficiency of photon absorption as defined by the decadic molar extinction coefficient (ε). In the case of H_2O_2 ε is 19.6 $M^{-1}.cm^{-1}$ compared to 2255 $M^{-1}.cm^{-1}$ for TiO_2 at 254 nm. This is balanced against recombination and the greater influence of background material. The greater influence of the latter is confirmed by the pseudo first-order rate constants in natural water measured at 0.002 and 0.00007 $cm^{-2}.mJ^{-1}$ for H_2O_2 and TiO_2 respectively.

3.5 Conclusions

Comparison of UV/H_2O_2 and UV/TiO_2 for the degradation of metaldehyde has shown that in pure systems both processes can deliver the equivalent rate of treatment under optimised conditions. In such cases significantly more moles of H_2O_2 are required due to its low photon absorption efficiency. However, in natural waters containing background organic matter and alkalinity the TiO_2 process was severely inhibited due to factors such as the adsorption of non-target organic molecules blocking contact between metaldehyde and •OH. Consequently, under current UV delivery system, H_2O_2 will be the more effective system which will continue until, for example, the development of

UV LED light sources enables very high UV doses to be delivered economically. The practical implications of this finding are that application of UV based AOPs remain a relatively high cost option (compared to conventional processes), but provide the only reliable means of metaldehyde removal. At the present time, such treatment is likely to be limited to niche cases where the significance of the problem justifies the higher costs involved. Larger scale uptake is likely only once methods to reduce the required energy input have been established and tested.

3.6 Acknowledgements

The authors would like to express their gratitude for the financial support for this project by Severn Trent Water Ltd.

3.7 References

Ahmed, S., Rasul, M.G., Brown, R., Hashib, M.A., 2011. Influence of parameters on the heterogeneous photocatalytic degradation of pesticides and phenolic contaminants in wastewater: A short review. J. Environ. Manage. 92(3), 311-330.

Alaton, I.A., Balcioglu, I.A., Bahnemann, D.W., 2002. Advanced oxidation of a reactive dyebath effluent: Comparison of O_3, H_2O_2/UV-C and TiO_2/UV-A processes. Water Res. 36(5), 1143-1154.

Baxendale, J.H., Willson, J.A., 1957. Photolysis of hydrogen peroxide at high light intensities. Trans. Faraday Soc. 53, 344-356.

Benitez, F.J., Acero, J.L., Real, F.J., Roman, S., 2004. Oxidation of MCPA and 2-4-D by UV radiation, Ozone, and the Combinations UV/H_2O_2 and O_3/H_2O_2. J. Environ. Sci. Health, Part B – Pestic., Food Contam., Agric. Wastes, B39(3), 393-409.

Benitez, F.J., Acero, J.L., Real, F.J., Roldan, G., Casas, F., 2011. Comparison of different chemical oxidation treatments for the removal of selected pharmaceuticals in water matrices. Chem. Eng. J. 168(3), 1149-1156.

Bobu, M., Wilson, S., Greibrokk, T., Lundanes, E., Siminiceanu, I., 2006. Comparison of advanced oxidation processes and identification of monuron photodegradation products in aqueous solution. Chemosphere 63(10), 1718-1727.

Bolton, J.R., Linden, K.G., 2003. Standardization of methods for fluence (UV dose) determination in bench-scale UV experiments. J. Environ. Eng. 129(3), 209-215.

Chiron, S., Fernandez-Alba, A., Rodriguez, A, Garcia-Calvo, E., 2000. Pesticide chemical oxidation: State-of-the-art. Water Res. 34(2), 366-377.

Chen, T.-F., Doong, R.-A., Lei, W.-G., 1998. Photocatalytic degradation of parathion in aqueous TiO_2 dispersion: The effect of hydrogen peroxide and light intensity. Water Sci. Technol. 37(8), 187-193.

Chu, W., Wong, C.C., 2004. The photocatalytic degradation of dicamba in TiO_2 suspensions with the help of hydrogen peroxide by different near UV irradiations. Water Res. 38(4), 1037-1043.

Chu, W., Rao, Y., Huy, W.Y., 2009. Removal of simazine in a UV/TiO_2 heterogeneous system. J. Agric. Food Chem. 57(15), 6944-6949.

Environment Agency, 2009. The determination of metaldehyde in waters using chromatography with mass spectrometric detection, [online] Available from http://www.environment-agency.gov.uk/static/documents/Research/Metaldehyde-226b.pdf (accessed August 2010).

Evgenidou, E., Fytianos, K., 2002. Photodegradation of triazine herbicides in aqueous solutions and natural waters. J. Agric. Food Chem. 50(22), 6423-6427.

Fotiadis, C., Xekoukoulotakis, N.P., Mantzavinos, D., 2007. Photocatalytic treatment of wastewater from cottonseed processing: Effect of operating conditions, aerobic biodegradability and ecotoxicity. Catal. Today 124(3-4), 247-253.

Haag, W.R., David Yao, C.C., 1992. Rate constants for reaction of hydroxyl radicals with several drinking water contaminants. Environ. Sci. Technol. 26(5), 1005-1013.

Hall, T., 2010. Removal of metaldehyde and other pesticides, CIWEM Drinking Water Quality Conference on Emerging Contaminants and Advanced Treatment Technologies, March 23rd 2010.

Hall, T., Holden, B., Haley, J., 2011. Treatment for metaldehyde and other problem pesticides, 4th Developments in Water Treatment and Supply Conference, Cheltenham, June 7-8 2011.

Herrmann, J.M., 2005. Heterogeneous photocatalysis: State of the art and present applications. Top. Catal. 34(1-4), 49-65.

Iglesias, J., Castillejo, J., Castro, R., 2001. Mini-plot field experiments on slug control using biological and chemical control agents. Ann. Appl. Biol. 139(3), 285-292.

Lamming, E.M., 2010. Ultra Violet (UV) and Hydrogen Peroxide Treatment of Metaldehyde, Master's Thesis, Cranfield University.

Li Puma, G., Yue, P.L., 1999. Comparison of the effectiveness of photon-based oxidation processes in a pilot falling film photoreactor. Environ. Sci. Technol. 33(18), 3210-3216.

Linsebigler, A.L., Lu, G., Yates Jr., J.T., 1995. Photocatalysis on TiO_2 surfaces: Principles, mechanisms, and selected results. Chem. Rev. 95(3), 735-758.

Lopez, M.C., Fernandez, M.I., Rodriguez, S., Santaballa, J.A., Steenken, S., Vulliet, E., 2005. Mechanisms of direct and TiO_2-photocatalysed UV degradation of phenylurea herbicides. ChemPhysChem 6(10), 2064-2074.

Minero, C., Catozzo, F., Pelizzetti, E., 1992. Role of adsorption in photocatalyzed reactions of organic molecules in aqueous TiO_2 suspensions. Langmuir 8(2), 481-486.

Neta, P., Dorfman, L., 1968. Pulse radiolysis studies. XIII. Rate constants for the reaction of hydroxyl radicals with aromatic compounds in aqueous solutions. Adv. Chem. Ser. 81(15), 222-230.

Parsons, S.A., 2004. Advanced Oxidation Processes for Water and Wastewater Treatment, IWA, UK.

Pereira, V.J., Weinberg, H.S., Linden, K.G., Singer, P.C., 2007. UV degradation kinetics and modelling of pharmaceutical compounds in laboratory grade and surface water via direct and indirect photolysis at 254 nm. Environ. Sci. Technol. 41(5), 1682-1688.

Pirkanniemi, K., Sillanpaa, M., 2002. Heterogeneous water phase catalysis as an environment application: A review. Chemosphere 48(10), 1047-1060.

Philippe, K.K., Hans, C., MacAdam, J., Jefferson, B., Hart, J., Parsons, S.A., 2010. Photocatalytic oxidation of natural organic matter surrogates and the impact on trihalomethane formation potential. Chemosphere 81(11), 1509-1516.

Rivero, M.J., Parsons, S.A., Jeffrey, P., Pidou, M., Jefferson, B., 2006. Membrane chemical reactor (MCR) combining photocatalysis and microfiltration for grey water treatment. Water Sci. Technol. 53(3), 173-180.

Ruppert, G, Bauer, R, Heisler, G., 1994. UV-O_3, UV-H_2O_2, UV-TiO_2 and the photo-Fenton reaction comparison of advanced oxidation processes for wastewater treatment. Chemosphere 28(8), 1447-1454.

Sanches, S., Barreto-Crespo, M.T., Pereira, V.J., 2010. Drinking water treatment of priority pesticides using low pressure UV photolysis and advanced oxidation processes. Water Res. 44(6), 1809-1818.

Sharpless, C., Linden, K., 2003. Experimental and model comparisons of low and medium pressure Hg lamps for the direct and H_2O_2 assisted UV photodegradation of N-nitrosodimethylamine in simulated drinking water. Environ. Sci. Technol. 37(9), 1933-1940.

Shie, J.-L., Lee, C.-H., Chiou, C.-S., Chang, C.-T., Chang, C.-C., Chang, C.-Y., 2008. Photodegradation kinetics of formaldehyde using light sources of UVA, UVC and UVLED in the presence of composed silver titanium oxide photocatalyst. J. Hazard. Mater. 155(1-2), 164-172.

von Sonntag, C., Schuchmann, H.P., 1992. UV disinfection of drinking water and by-product formation - some basic considerations. J. Water Supply Res. Technol. - Aqua 41(2), 67-74.

Stepnowski, P., Zaleska, A., 2005. Comparison of different advanced oxidation processes for the degradation of room temperature ionic liquids. Journal of Photochemistry and Photobiology A: Chemistry 170(1), 45-50.

Sutherland, J., Adams, C., 2007. Determination of Hydroxyl Radical Rate Constants for Fuel Oxygenates. Environ. Eng. Sci. 24(8), 998-1005.

Thomson, J., Roddick, F., Drikas, M., 2002. Natural organic matter removal by enhanced photo-oxidation using low pressure mercury vapour lamps. Water Sci. Technol. Water Supply 2(5-6), 435-443.

Thompson, T.L., Yates Jr., J.T., 2005. TiO_2-based photocatalysis: Surface defects, oxygen and charge transfer. Top. Catal. 35(3-4), 197-210.

Tizaoui, C., Mezughi, K., Bickley, R., 2011. Heterogeneous photocatalytic removal of the herbicide Clopyralid and its comparison with UV/H_2O_2 and ozone oxidation techniques. Desalination 273(1), 197-204.

Toepfer, B., Gora, A., Li Puma, G., 2006. Photocatalytic oxidation of multicomponent solutions of herbicides: Reaction kinetics analysis with explicit photon absorption effects. Appl. Catal. B-Environ. 68(3-4), 171-180.

Urey, H.C., Dawsey, L.H., Rice, F.O., 1929. The absorption spectrum and decomposition of hydrogen peroxide by light. J. Am. Chem. Soc. 51(5), 1371-1383.

Water UK, 2009. Water Company Proposed PR09 Catchment Management schemes, November 2009, 15-16.

Westerhoff, P., Mezyk, S.P., Cooper, W.J., Minakata, D. 2007. Electron pulse radiolysis determination of hydroxyl radical rate constants with Suwannee River fulvic acid and other dissolved organic matter isolates. Environ. Sci. Technol. 41(13), 4640-4646.

Zalazar, C.S., Satuf, M.L., Alfano, O.M., Cassano, A.E., 2008. Comparison of H_2O_2/UV and heterogeneous photocatalytic processes for the degradation of dichloroacetic acid in water. Environ. Sci. Technol. 42(16), 6198-6204.

CHAPTER 4 THE IMPACT OF BACKGROUND ORGANIC MATTER AND ALKALINITY ON THE DEGRADATION OF THE PESTICIDE METALDEHYDE BY TWO ADVANCED OXIDATION PROCESSES: UV/H_2O_2 AND UV/TiO_2

CHAPTER 4: THE IMPACT OF BACKGROUND ORGANIC MATTER AND ALKALINITY ON THE DEGRADATION OF THE PESTICIDE METALDEHYDE BY TWO ADVANCED OXIDATION PROCESSES: UV/H_2O_2 AND UV/TiO_2

Olivier Autin [a], *Julie Hart* [b], *Peter Jarvis* [a], *Jitka MacAdam* [a], *Simon A. Parsons* [a], *Bruce Jefferson* [a]

[a] Cranfield Water Science Institute, Department of Environmental Science and Technology, Cranfield University, Bedfordshire, MK43 0AL, UK.

[b] Severn Trent Water LTD., Severn Trent Centre, PO Box 5309, Coventry, West Midlands, CV3 9FH, UK.

4.1 Abstract

The impact of background constituents on the degradation of trace levels of micropollutants by two advanced oxidation processes: UV/H_2O_2 and UV/TiO_2 was studied. Experimental results demonstrated that the background scavenging rate rather than the concentration of micropollutant controls the required UV irradiation dose. The character of the natural organic matter had a limited impact on scavenging when the water source remains unchanged, however, a periodic bleed of hydrophobic material may substantially increase the minimum UV dose required to reach the desired micropollutant concentration. Moreover, in the case of UV/TiO_2, high concentrations of background organic matter do not only act as scavengers but also saturate the TiO_2 surface. Alkalinity inhibits the efficacy of UV/TiO_2 photocatalysis due to the formation of large TiO_2 aggregates. The study also demonstrated that the use of synthetic waters for treatability test purposes was an acceptable approach as long as both the background organic matter and the alkalinity were matched to that of the projected

application. Finally spiking micropollutants at higher concentrations does not alter the significance of the findings as long as the background constituents represent more than 85% of the total scavenging rate.

Keywords: metaldehyde, natural organic matter, alkalinity, scavenging, titanium dioxide, hydrogen peroxide.

4.2 Introduction

Advanced oxidation processes (AOPs) are based on the formation of highly reactive hydroxyl radicals (•OH) that are quasi-unselective and react with a wide range of organic compounds including micropollutants (MP) in surface or ground waters (Benitez et al., 2006; Chelme-Ayala et al., 2010). Consequently AOPs have been suggested for the treatment of otherwise recalcitrant micropollutants such as metaldehyde and clopyralid that have been causing significant treatment problems (Hall et al., 2011). However, uptake of AOP technology is limited (Li Puma and Yue, 2003) as the majority of the •OH are used up (scavenged) by the natural organic matter (NOM) and carbonate ions present in the water. These background components slow down the degradation of the target micropollutant. For instance, Wu and Linden (2010) noticed a reduction in the rate constant by 50% when the alkalinity increased from 25 to 500 $mg.L^{-1}$ as $CaCO_3$ during the treatment of two organophosphate pesticides (parathion and chlorpyriphos) by UV/H_2O_2. A more pronounced inhibition effect was observed by He et al. (2011) for the degradation of 1 µM of microcystin-LR in UV/H_2O_2 system where a 35-70% reduction in the rate constant was observed by the addition of 50 $mg.L^{-1}$ as $CaCO_3$ and a 54-74% reduction in the presence of 2.5-4.0 $mg.L^{-1}$ dissolved organic carbon (DOC). Limited removal of the background DOC is generally observed (less than 20%), whereas UV_{254} levels drop more significantly indicating that the parent DOC molecules are oxidised, with the subsequent degradates continuing to scavenge •OH (Metz et al., 2011; Lamsal et al., 2011). In contrast, removal of the target micropollutant requires only

a single •OH attack to generate a loss of identity of the molecule making the impact of the background water critical to the efficacy of AOPs for micropollutant removal.

Limitations associated with the sensitivity of the analytical instruments used for micropollutant measurement have meant that the majority of studies on the impact of background constituents have spiked elevated micropollutants concentrations into the target waters. For instance, the typical range of mass ratios investigated is between 9 and 20,000 $\mu g_{MP}.mg_{DOC}^{-1}$ whereas the target applications have mass ratios below 0.8 $\mu g_{MP}.mg_{DOC}^{-1}$. Two previous studies have operated within this range looking at removal of endocrine disruptors (Chen et al., 2007) and pesticides (Ijpelaar et al., 2002) and have observed a more significant impact due to the background organic materials. Consequently, questions around the significance of spiking and the impact of DOC character on the efficacy of AOPs exist which require resolution to better define how and where AOP_S should be used in drinking water treatment flowsheets.

The current paper aims to build on these earlier studies to better understand the role of the background constituents and assess the potential at translating findings at high mass ratios to more practically significant levels. The current work investigates this by monitoring the degradation of a target micropollutant (metaldehyde) in the presence of alkalinity and three surrogates of NOM. These contaminants can be individually monitored enabling differentiation between the influences of the reactivity and the concentration of all the components that undergo •OH attack. The chosen surrogates have been selected from the groups listed by Croué et al. (2000) to represent a post coagulated organic residual (Bond et al., 2009). The analogues were leucine and serine to represent hydrophilic material not removed by coagulation and resorcinol to represent the residual bleed of hydrophobic material that can occur following inadequate coagulation (Sharp et al., 2006a). In addition to

the composition of the water, the surrogates were selected according to their relative adsorption capacities and reactivity towards •OH compared to the pesticide metaldehyde (Table 4-1). These model compounds have already been successfully used to evaluate the potential of UV/H_2O_2 and UV/TiO_2 for NOM removal where effective and rapid DOC removal by UV/TiO_2 was observed with 80-90% DOC removed after 1-5 min irradiation using a 630 W MP lamp and 2 $g.L^{-1}$ of TiO_2 (Philippe et al., 2010). The removal of NOM by UV/H_2O_2 was complete after 30 000 $mJ.cm^{-2}$ irradiation with a 120 W LP lamp irradiating at 254 nm and 2 mM H_2O_2 (Bond et al., 2009). The target micropollutant, metaldehyde, was chosen as it is a common contaminant of water supplies in the UK but is not readily removed by traditional water treatment technologies. A previous study showed that 1 $mg.L^{-1}$ of metaldehyde was effectively removed in laboratory grade water by both UV/H_2O_2 and UV/TiO_2 at similar rates of degradation and within 500 $mJ.cm^{-2}$ when optimum doses were used, but similar experiments in surface water showed a slowdown of the UV/H_2O_2 process and a total inhibition of the UV/TiO_2 process (Autin et al., 2012a) and so is indicative of the findings from previous studies.

Table 4-1 - Second order rate constant k•OH.

Organic compound	Structure	$k_{•OH}$ ($M^{-1}.s^{-1}$)	Log K_{ow}	ξ at 254 nm ($M^{-1}.cm^{-1}$)
Metaldehyde	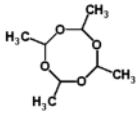	$1.3x10^{9}$ [a]	0.12[d]	19.0
Serine	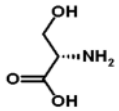	$3.2x10^{8}$ [b]	-3.07[d]	0.3
Leucine	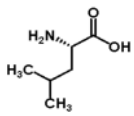	$1.7x10^{9}$ [b]	-1.52[d]	0.5
Resorcinol		$1.2x10^{10}$ [c]	0.80[d]	559.8

a: value from Autin et al., 2012a; b: values from Xu and Chance, 2005; c: value from Minakata et al., 2009; d: values from Chemspider chemical data base search. Available at: http://www.chemspider.com.

4.3 Material and methods

4.3.1 Chemicals and reagents

Metaldehyde, serine, leucine, hydrogen peroxide (35% w/w) and $NaHCO_3$ were obtained from Fisher Scientific and resorcinol from Sigma-Aldrich at analytical purity or above. Titanium dioxide (Aeroxide® TiO_2 P25 Degussa) was purchased from Lawrence Industries (Tamworth, UK). All solutions were prepared in ultrapure water (Purelab Option – S7/15, 18.2 MΩ cm and TOC < 3 ppb).

4.3.2 Synthetic and natural water characteristics and fractionation

For synthetic water experiments, stock solutions of serine, leucine and resorcinol were initially prepared in ultrapure water (UPW) at 500 $mg.L^{-1}$, and metaldehyde at 1 $mg.L^{-1}$. The appropriate volume of each solution was then spiked into UPW to achieve the required concentrations for UV experiments. The natural water was collected from a drinking water treatment works in the Severn Trent Water region, UK. The water was collected post-GAC treatment and had a DOC of 3.5 $mg.L^{-1}$ (26.5%, 25.3% and 48.3% of hydrophobic, transphilic and hydrophilic fractions respectively) and an alkalinity of 120 $mg.L^{-1}$ as $CaCO_3$. The water was stored in the dark at 4˚C until used for experiments.

4.3.3 Irradiation procedure

UV experiments were all conducted in a Wedeco AG bench scale quasi-collimated beam apparatus (Herford, Germany) equipped with four 30 W UV-C low pressure lamps emitting monochromatic light at 254 nm. A volume of 250 mL of test solution was placed in a Petri dish at 22 cm from the light source and stirred. UV irradiance was determined to be 23.3 $W.m^{-2}$ using the potassium ferrioxalate method as described by Hatchard and Parker (1956). Samples were withdrawn at UV fluences of approximately 0, 500, 1000, 1500, 2000 and 3000 $mJ.cm^{-2}$ to quantify the concentration of the different compounds. All experiments were

carried out at natural pH (7.8-8.2 with the exception of synthetic water without $NaHCO_3$ where the pH was 6.7-7.0) and room temperature (20-22˚C).

Depending on the characteristics and concentrations of both the NOM and the pesticide, the molar ratio between a micropollutant and the background organic matter can vary significantly. For practical reasons, the maximum ratio used in this study was 1:10,000, to accurately follow the kinetics of degradation of metaldehyde. In the first part of the study, four different ratios were studied decreasing the NOM concentration by one order of magnitude down to a 1:10 ratio. This approach was taken in order to identify if a critical ratio existed above which the AOPs could not effectively remove traces of micropollutants. In the second part, four different ratios 1:500, 1:1,000, 1:2,000 and 1:5,000 have been studied, 1) varying [DOC] at fix [metaldehyde] and 2) varying [metaldehyde] at fix [DOC], in order to identify whether the ratio between the micropollutant and the background organic matter, the concentration of micropollutant or the concentration of background organic matter was critical in micropollutant degradation.

4.3.4 Sample analysis

For UV/TiO_2, samples were filtered through 0.45 μm syringe filters (Millex-HA) to separate the suspended TiO_2 prior to analysis, and were directly analysed after UV/H_2O_2 experiments. The analyses were performed using a Waters 2695 LC system coupled with a Waters Quattro Premier Xe MS-MS. The aqueous mobile phase A consisted of 5 mM ammonium acetate/0.1% formic acid and the organic mobile phase B was acetonitrile/0.1% formic acid. The flow rate was set to 0.2 $mL.min^{-1}$ and the conditions were 50% A and 50% B held for 2 min. The Quattro Premier Xe tandem quadruple mass spectrometer was operated under positive electrospray ionisation mode for metaldehyde, leucine and serine and negative electrospray ionisation mode for resorcinol. The instrument was operated in multiple reaction monitoring set to monitor ions m/z 194 for metaldehyde, m/z 131.7 for leucine, m/z 105.7 for

serine and m/z 108.5 for resorcinol. Source conditions were as follows: capillary 3.5 kV, source temperature 120˚C, desolvation temperature 350˚C, and nitrogen drying gas 1000 $L.h^{-1}$. Calibration curves were generated prior to each new sequence for each compound and the concentrations were determined using Micromass QuantLynx.

The alkalinity was measured by HCl titrimetric method 2320B (APHA, 1992). The absorbance at 254 nm was measured with a UV-Vis spectrophotometer (Jenway, UK) and the the decadic molar absorption coefficient for each compound was defined using:

$$A_{254,i} = \xi_i \times l \times C_i \quad (4\text{-}1)$$

where $A_{254,i}$ is the absorbance of the compound i at 254 nm (in cm^{-1}), ξ_i is the decadic molar absorption coefficient of i at 254 nm (in $M^{-1}.cm^{-1}$), l is the path length in the spectrophotometer (1 cm) and C_i is the concentration of I (in M). The size of the TiO_2 aggregates was measured using a laser diffraction instrument (Malvern Mastersizer 2000, Malvern Instruments, UK).

4.4 Results

4.4.1 Degradation of metaldehyde in single and multi-component modes

In the absence of competing species the degradation of metaldehyde exceeded 80% in both systems when irradiated with 1000 $mJ.cm^{-1}$ and >95% removal when irradiated with 1500 $mJ.cm^{-1}$ (Figure 4-1-A). In the presence of one competing organic compound, irrespective of the NOM surrogate involved, the degradation of metaldehyde was reduced such that a UV dose of 2000 $mJ.cm^{-2}$ was required to achieve a 90% removal of metaldehyde (Figure 4-1-B-D). In comparison, the degradation profile for each surrogate compound was significantly different from one another. The sequence was consistent with their respective second-order rate constants (Table 4-1) such that serine was removed at a lower rate than metaldehyde,

leucine was removed slightly faster than the pesticide and resorcinol was removed much more quickly and was completely degraded within 500 mJ.cm^{-2} for UV/H_2O_2 (Figure 4-1-D). Comparison of the degradation profiles for the two AOPs reveals similar profiles in the case of metaldehyde and leucine and slight differences in the case of resorcinol and serine suggesting that whilst •OH oxidation is the main degradation pathway for both systems other factors are also involved. Importantly, across all of the trials the metaldehyde concentration was two orders of magnitude lower than the competing species but was still degraded faster than serine suggesting that the rate of degradation is more sensitive to the reactivity rather than the concentration of a micropollutant (although significantly less •OH are required to degrade 5.68x10^{-8} M of metaldehyde compared to 5.68x10^{-6} M of serine).

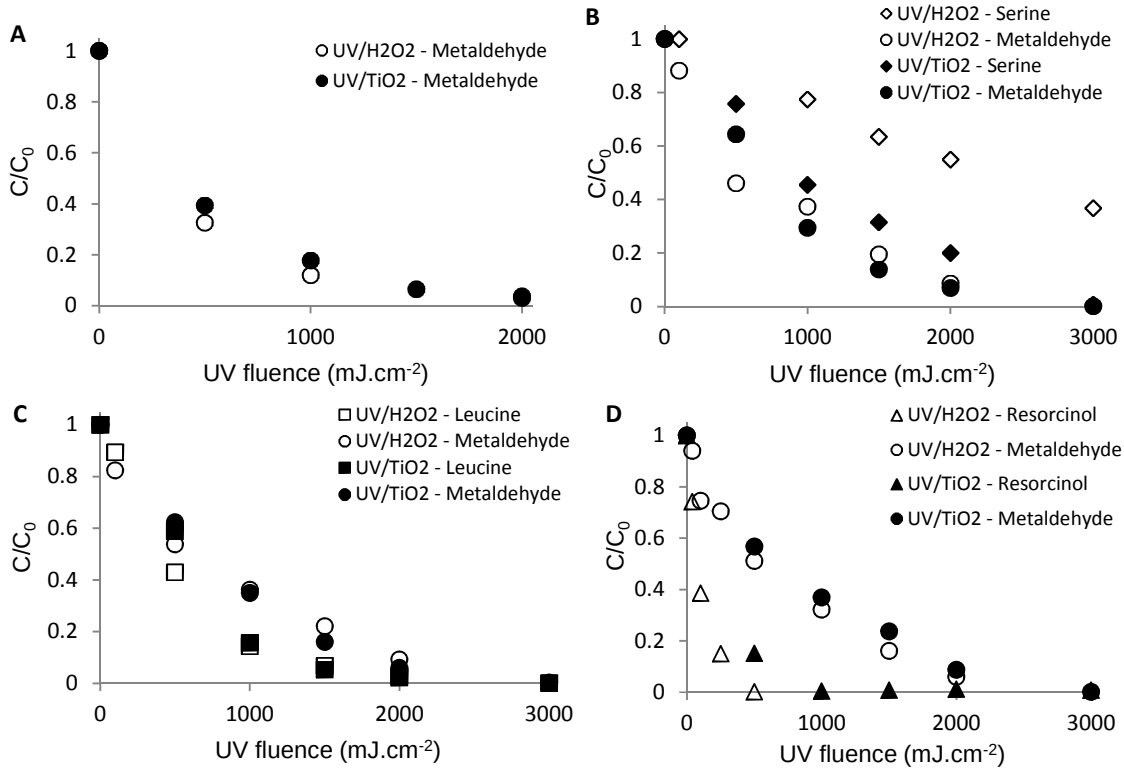

Figure 4-1 - Degradation of metaldehyde by UV/TiO_2 and UV/H_2O_2 in A) single component mode and in competition with B) Serine, C) Leucine and D) Resorcinol. [Metaldehyde]= 5.68x10^{-8} M, [NOM surrogate]= 5.68x10^{-6} M, [TiO_2]=100 mg.L^{-1}, [H_2O_2]= 8 mM.

4.4.2 Impact of the ratio between NOM and metaldehyde

The metaldehyde rate constant decreased as the mole ratio of the surrogate compound to metaldehyde increased (Figure 4-2-A,B). No significant difference was observed in relation to the different surrogate compounds used indicating that the inhibitory nature of the background NOM is more related to concentration than the reactivity of the competing species. In the case of UV/TiO_2, a linear decrease in rate constant was observed up to a mole ratio of 1:100 where the presence of organics reduced the rate of metaldehyde degradation by an average value of 13% and 38% for ratios 1:10 and 1:100 respectively. Increasing the ratio further led to greater inhibition as observed in terms of the rate constant which was reduced by 84% and 96% for ratios of 1:1,000 and 1:10,000.

In the case of UV/H_2O_2, the rate constant linearly decreased with an increase of NOM surrogate to metaldehyde ratio (Figure 4-2-B). To illustrate, an inhibition in the rate constant from 24% to 86% was observed as the mole ratio increased from 10:1 to 10,000:1. A clearer differentiation was observed between the two systems in regards to inhibition based on changing background organic concentration, reflecting the differences in treatment pathways that exist. In the UV/H_2O_2 system, the reactions between •OH and the organic material occurs in the aqueous phase such that any increase in background concentration is reflected in a commensurate increase in the scavenging rate thus reducing the number of •OH available to react with metaldehyde. In the UV/TiO_2 system, reactions occur at the TiO_2/liquid interface and so organic material can block access to the surface in addition to scavenging. At low mole ratios, only scavenging appears to be important but once the ratio reached 1,000:1 the probability of close proximity between metaldehyde and TiO_2 is reduced, leading to greater inhibition of metaldehyde degradation. Ultimately, the results suggest a limiting permissible amount of background organic compounds to avoid blockage of the catalyst, which in the current case lies between mole ratios of 1:100 and 1:1,000.

4.4.3 Impact of NOM characteristics

The inhibitory nature of the background NOM on metaldehyde degradation appears insensitive to differences in the NOM characteristics (Figure 4-2-A,B). To illustrate, at a mole ratio of 1:100 the rate constant observed with UV/H_2O_2 was $1.16x10^{-3}$, $1.05x10^{-3}$ and $1.13x10^{-3}$ $cm^2.mJ^{-1}$ for serine, leucine and resorcinol respectively. In contrast, the rate constant of the individual compounds varied significantly at $2.8x10^{-4}$ $cm^2.mJ^{-1}$ for serine, $1.6x10^{-3}$ $cm^2.mJ^{-1}$ for leucine and $1.0x10^{-2}$ $cm^2.mJ^{-1}$ for resorcinol. Consequently, the character of an individual compounds appears to influence its own degradation by •OH but has a more limited influence on the degradation of trace micropollutants.

The influence of the mole ratio on the degradation of the NOM surrogates was system specific with different responses observed with UV/TiO_2 compared to UV/H_2O_2 (Figure 4-2-C,D). In the case of UV/H_2O_2 the rate constants were unaffected by changes in the mole ratio until a ratio of 1:10,000 where they all merged at a value of 0.1-$0.4x10^{-3}$ $cm^2.mJ^{-1}$.For UV/TiO_2, the rate constants converged at a lower mole ratio of 1:1,000, with a value between $0.3x10^{-3}$ and $0.8x10^{-3}$ $cm^2.mJ^{-1}$. Below mole ratios of 1:1,000 a clear difference in rate constant was observed which is consistent with their reactivity towards •OH. As the ratio increased, resorcinol was the most affected as it decreased from $6.9x10^{-3}$ $cm^2.mJ^{-1}$ at a mole ratio of 1:10 to $0.5x10^{-3}$ $cm^2.mJ^{-1}$ at a mole ratio of 1:1,000 (Figure 4-2-C). The increase sensitivity to mole ratio for the UV/TiO_2 over UV/H_2O_2 reflects the additional inhibitory impact of surface blockage over just scavenging as seen with UV/H_2O_2.

To further examine the impact of NOM character on the process the total scavenging rate SR (s^{-1}) was calculated as the sum of the individual components:

$$SR = k_{\bullet OH,M}[M] + k_{\bullet OH,S}[S] + k_{\bullet OH,H_2O_2}[H_2O_2] \quad (4\text{-}2)$$

where [-] is the molar concentration of either metaldehyde [M], the competing species (NOM surrogate) [S] or hydrogen peroxide [H_2O_2], and $k_{\bullet OH,-}$ is the second order rate constant of each component ($M^{-1}.s^{-1}$). Analysis of the data reveals that the choice of NOM surrogate significantly influences the relationship between increasing mole ratio and the total scavenging rate (Table 4-2). To illustrate, as the mole ratio of serine increased from 1:10 to 1:10000 the overall scavenging rate increased from $2.16x10^4$ s^{-1} to $3.98x10^4$ s^{-1} compared to $2.23x10^4$ s^{-1} to $70.3x10^4$ s^{-1} in the case of resorcinol reflecting differences in the reactivity of the different surrogates to •OH (Table 4-2). As all other components are fixed the change in total scavenging rate commensurately affected the percentage contribution of scavenging derived from the NOM surrogate. When the mole ratio was low, in other words at low concentration of NOM, most of the •OH were scavenged by H_2O_2. For instance, at a ratio of 1:10, H_2O_2 provided between 96.9 and 99.9 % of the total scavenging rate (Table 4-2). As the surrogate concentration was increased to a mole ratio of 1:10,000 the percentage of •OH scavenged by the organic surrogates increased to 45.7%, 81.7% and 96.9% for serine, leucine and resorcinol respectively. The impact of increased scavenging rate was a reduction in the percentage of •OH associated to scavenging by metaldehyde which varied between 0.034% and 0.001% of the total scavenging rate and corresponded to inhibition in the degradation rate constant of between 14 and 81% compared to the rate without competing species. However, the impact of scavenging rate was different depending on the NOM compound indicating a clear impact associated with NOM character, where greater inhibition was observed for the least reactive surrogate when normalised on the basis of percentage of the scavenging rate derived by the NOM surrogate.

Table 4-2 - Fraction of •OH scavenged by the different species present in water during UV/H_2O_2 treatment when metaldehyde is in competition with serine, leucine and resorcinol.

Serine	Ratio 1:10	Ratio 1:100	Ratio 1:1 000	Ratio 1:10 000
Overall SR (s^{-1})	$2.16x10^4$	$2.18x10^4$	$2.34x10^4$	$3.98x10^4$
$SR_{Metaldehyde}$ (%)	0.034	0.034	0.032	0.019
SR_{Serine} (%)	0.084	0.83	7.76	45.7
SR_{H2O2} (%)	99.88	99.13	92.21	54.28
Leucine	1:10	1:100	1:1 000	1:10 000
Overall SR (s^{-1})	$2.17x10^4$	$2.26x10^4$	$3.13x10^4$	$11.8x10^4$
$SR_{Metaldehyde}$ (%)	0.034	0.033	0.024	0.006
$SR_{Leucine}$ (%)	0.44	4.28	30.89	81.71
SR_{H2O2} (%)	99.52	95.69	69.08	18.28
Resorcinol	1:10	1:100	1:1 000	1:10 000
Overall SR (s^{-1})	$2.23x10^4$	$2.84x10^4$	$8.98x10^4$	$70.3x10^4$
$SR_{Metaldehyde}$ (%)	0.033	0.026	0.008	0.001
$SR_{Resorcinol}$ (%)	3.06	23.97	75.93	96.93
SR_{H2O2} (%)	96.90	76.00	24.06	3.07

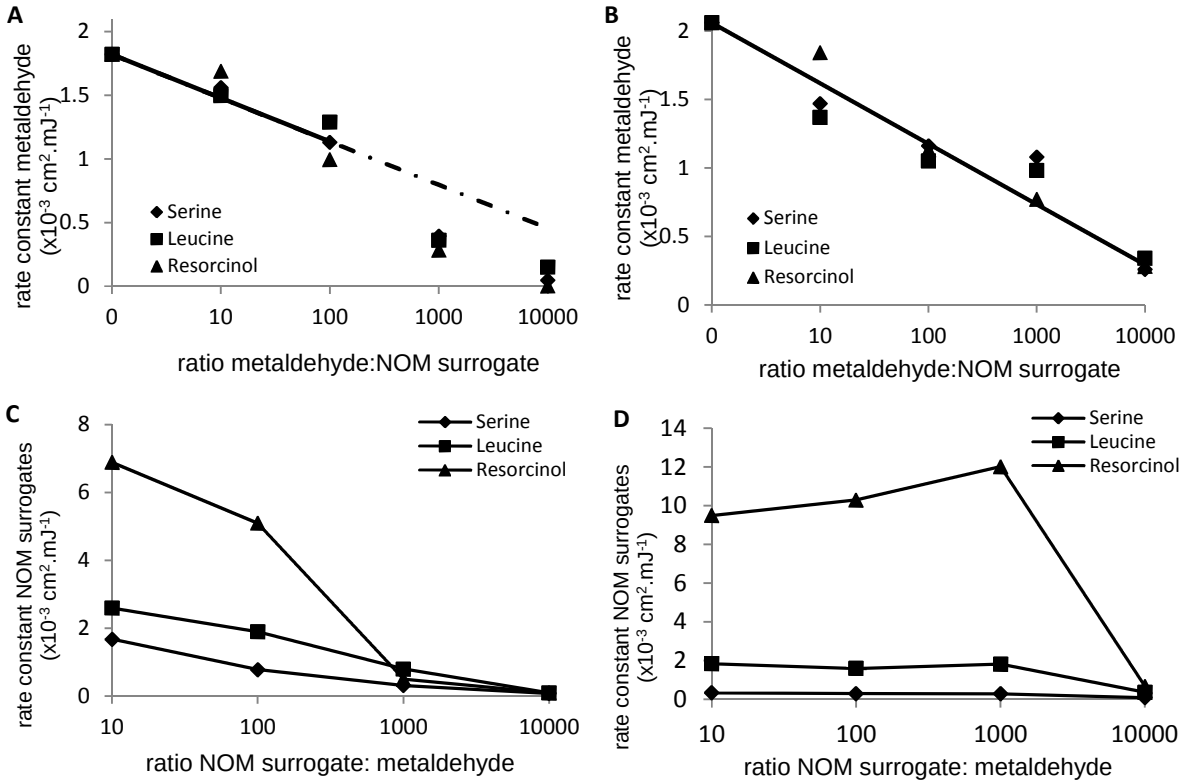

Figure 4-2 - Impact of the nature and concentration of natural organic matter on the pseudo-first order rate constant of A) metaldehyde by UV/TiO_2, B) metaldehyde by UV/H_2O_2, C) NOM surrogates by UV/TiO_2, D) NOM surrogates by UV/H_2O_2. [metaldehyde] = $5.68x10^{-8}$ M, [TiO_2] = 100 mg.L^{-1}, [H_2O_2] = 8 mM. Ratio NOM surrogate: metaldehyde = 0 is metaldehyde alone in single component.

4.4.4 Influence of NOM and metaldehyde concentrations in a mixture of NOM surrogates

The compounds were then all mixed together in order to better represent a natural water, where various organic compounds are present. The experiments were carried out at four different mole ratios between metaldehyde and the background DOC and under two regimes: (1) varying [DOC] at fixed [metaldehyde] and (2) varying [metaldehyde] at fixed [DOC]. For bothUV/H_2O_2 and UV/TiO_2, increasing the [DOC] (which also increased the ratio of NOM: metaldehyde) resulted in a substantial inhibition of metaldehyde degradation and this effect was more pronounced for UV/TiO_2 (Figure 4-3). To illustrate, the metaldehyde degradation rate constant varied from $0.97x10^{-3}$ to $0.18x10^{-3}$ $cm^2.mJ^{-1}$ when the mole ratio increased from 1:500 to 1:2,000, resulting in a strong inhibition of metaldehyde removal with only 43% metaldehyde removal at 3000 $mJ.cm^{-2}$ for the ratio of 1:2,000. However, when the [DOC] was kept constant at 3.5 $mg.L^{-1}$ and the [metaldehyde] decreased no negative effect on metaldehyde degradation was observed as a function of increasing mole ratio. For instance, the rate constant increased from $0.61x10^{-3}$ to $1.13x10^{-3}$ $cm^2.mJ^{-1}$ for the UV/TiO_2 system as the ratio increased from 1:500 and 1:5000. Comparison of the two AOPs revealed that under both regimes the UV/H_2O_2 systems generated a higher rate constant again demonstrating the impact of other factors on the TiO_2 over and above just scavenging of •OH.

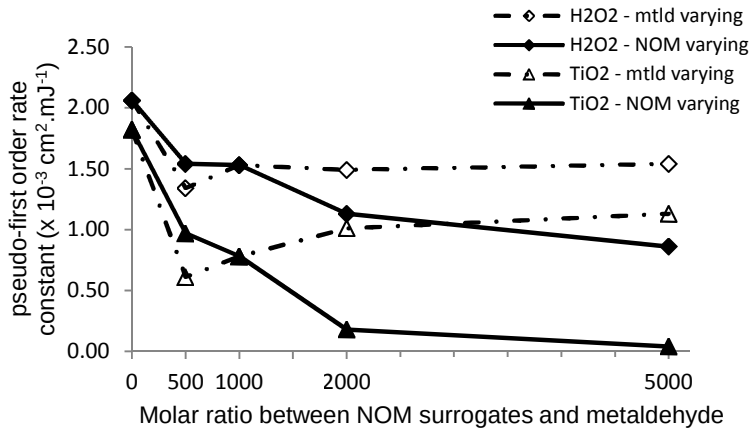

Figure 4-3 - Rate of degradation of metaldehyde by UV/TiO_2 and UV/H_2O_2 for different NOM: metaldehyde ratios varying [metaldehyde] or [NOM].

4.4.5 Influence of alkalinity

The presence of carbonate ions had no major influence on the degradation of metaldehyde and the three NOM surrogates by UV/H_2O_2. To illustrate, metaldehyde removal decreased from 90% without carbonate ions to 84% in the presence of alkalinity after 1500 mJ.cm^{-2} of irradiation, corresponding to a diminution of the rate constant from 1.53x10^{-3} to 1.38x10^{-3} cm^2.mJ^{-1} (Figure 4-4-B). In contrast, addition of alkalinity reduced the degradation of metaldehyde in the UV/TiO_2 system to 45% compared to the system without alkalinity, where 93% of the metaldehyde was degraded (Figure 4-4-A). The difference in impact on the two processes indicates that the role of alkalinity on the UV/TiO_2 system is not principally about scavenging of •OH. Analysis of the possible inhibition mechanism revealed that it was not due to carbonate ion adsorption onto the surface of the catalyst as only 3.5-4% of the available total carbonate mass was removed. However, measurement of the size of the catalyst particles revealed that significant aggregation occurs in the presence of alkalinity. To illustrate, when dispersed in clean water the TiO_2 particle have a mean aggregate size of 3 μm which was not significantly altered when either metaldehyde or any of the NOM surrogates where added (Figure 4-5). In contrast, in the presence of alkalinity the average size of the aggregates increased from 3 μm to 450 μm. The impact of alkalinity on the UV/TiO_2 process was confirmed as the metaldehyde degradation rate was the same for systems containing alkalinity with or without the background surrogate compounds, at a rate of 0.21x10^{-3} cm^2.mJ^{-1} (Figure 4-4-A). Similar particle size determination has been carried out using NaOH for pH adjustment and showed no changes in particles size (i.e. average particle size = 3 μm, data not shown). The form under which alkalinity is present does not seem to change the behaviour at the TiO_2 surface. Indeed, similar TiO_2 particle size of 450 μm was observed in presence of alkalinity with and without pH adjustment (i.e. at pH 7.0 and 8.1) which resulted in similar degrees of degradation observed at pH 7.0 and 8.1 in the presence of alkalinity

($0.21x10^{-3}$ $cm^2.mJ^{-1}$). In addition, in the absence of alkalinity, a change of pH did not result in TiO_2 aggregation as the average particle size was 3.5 µm at pH 8.1 and resulted in similar rate of metaldehyde degradation than at pH 7.0 ($0.72x10^{-3}$ $cm^2.mJ^{-1}$). Titanium dioxide has a point of zero charge of 6.4 and here all the experiments have been undertaken above this pH, hence, the surface of TiO_2 was in all tests negatively charged. Regardless of the conditions used (i.e. presence or absence of alkalinity, pH between 6.7 and 8.1) the zeta potential was always in the range -16 to -18 mV indicating that the mechanism for the aggregation is not due to the compression of electrical double layer but could rather be attributed to complexation reaction. This type of reaction has already been observed in activated sludge where cations such as calcium and magnesium enhanced the flocculation of activated sludge (Nguyen et al., 2008).

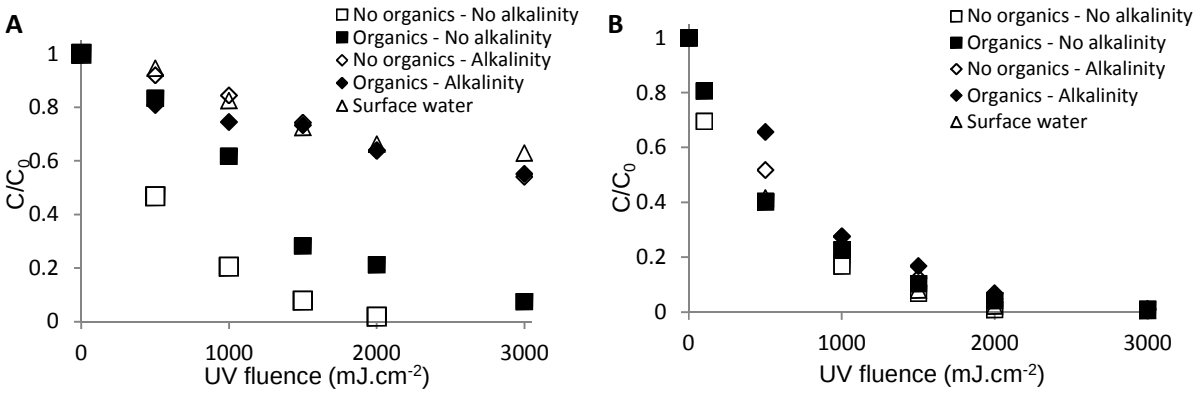

Figure 4-4 - Degradation of metaldehyde by A) UV/TiO_2 and B) UV/H_2O_2, metaldehyde only (black symbols), in the presence of NOM surrogates, 3.5 mg.L^{-1} DOC, ratio 1: 1 000 (grey symbols) and in the presence of NOM surrogates and carbonate ions, alkalinity= 120 mg.L^{-1} as $CaCO_3$. [metaldehyde]=10 µg.L^{-1}, [TiO_2]= 100 mg.L^{-1}, [H_2O_2]= 8 mM.

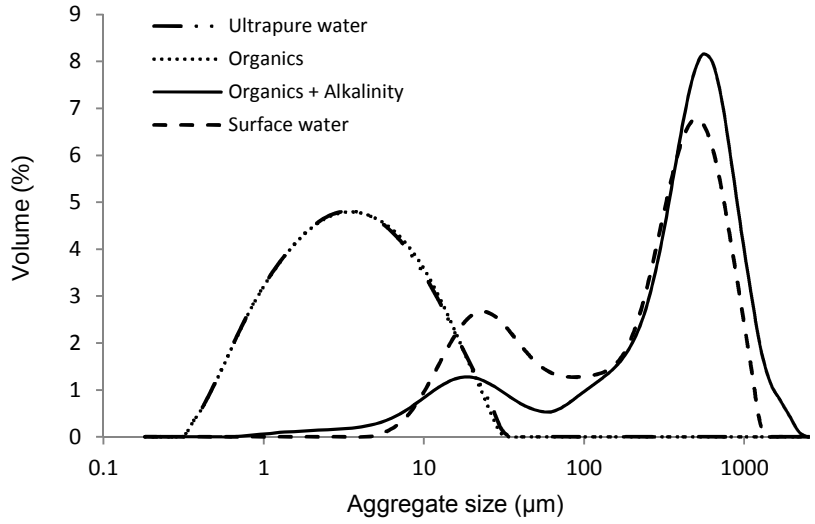

Figure 4-5 - Impact of organics and alkalinity on the size of TiO_2 aggregates. Synthetic solutions prepared in ultrapure water. [TiO_2]= 100 mg.L^{-1}; [metaldehyde]= 10 µg.L^{-1}; ratio [metaldehyde]/[NOM surrogates]= 1:1,000; alkalinity= 120 mg.L^{-1} as $CaCO_3$.

4.5 Discussion

The results presented in this work show that both the background organic matter and the alkalinity of a water source can be critical influences on the efficacy of AOPs for micropollutant removal. In the case of UV/H_2O_2 the principal influence is on scavenging and hence the background organics are the dominant factor. Previous studies have reported a link between scavenging rate and the efficacy of micropollutant removal in real waters for both drinking water and wastewater treatment (Haag and Hoigné, 1985; Rosario-Oritz et al., 2010; Muhamad, 2010). For instance, the degradation rate constant of urea herbicides by UV/H_2O_2 decreased in the order ultra-pure water>groundwater>lake water (Benitez et al., 2004). The use of surrogates in the current study has enabled refinements of these findings by being able to differentiate between concentration, character and mole ratio of the background organic scavengers. Importantly, the results demonstrate that both the concentration and character of the background organic compounds are important rather than the molar ratio between micropollutant and background DOC. The implication of which is that the background scavenging rate controls the required UV dose rather than the actual concentration of

micropollutant. This is evidenced in terms of the very small percentage contribution (a maximum of 0.08%) that the micropollutant makes to the total scavenging rate. Changes in the concentration of an individual surrogate commensurately increased the scavenging rate and this directly impacted on the inhibition of metaldehyde degradation consistent with studies on the inhibition of trifluralin in natural waters (Chelme-Ayala et al., 2010). However, the picture is complicated through the influence of NOM characteristics due to the differences in their reactivity with •OH influencing the change in the overall scavenging rate (Table 4-2). Support for this is also provided from work on the degradation of lindane in the presence of humic and fulvic acids where greater inhibition was observed in the case of humic acid commensurate with its high reactivity to •OH (Nienow et al., 2008). Similarly, Katsoyiannis et al. (2011) demonstrated differences in the degradation of pCBA in different natural waters as a consequence of differences in their character. The implications of such findings are that if the character of the organics in a water source remains unchanged then the impact of DOC is understood and can be confidently managed. However, if the character of the water changes, through either catchment impacts or pre-treatment, then the impact in changes in DOC will be less predictable. Both are known to routinely occur, restricting the confidence placed with regards to the efficacy of AOPs for micropollutant removal (Sharp et al., 2006b). A hypothetical example would be where an AOP is placed after coagulation which periodically bleeds 1-2 $mg.L^{-1}$ DOC in the form of hydrophobic materials due to variation in the incoming load (Sharp et al., 2006b). Based on the findings in this study, assuming a base DOC of 2 $mg.L^{-1}$, an additional UV dose of 240 $mJ.cm^{-2}$ would be required to maintain a 90% removal of the micropollutant otherwise a 5% reduction in removal at a fixed dose would be observed.

In the case of UV/TiO_2, high concentrations of organic matter further inhibit degradation of the target micropollutant beyond just the impact of scavenging by simultaneously saturating

the TiO_2 surface and reducing the photonic efficiency resulting in photocatalytic deactivation (Chong et al., 2010; Ahmed et al., 2011). More significantly, alkalinity inhibits the efficacy of the process which has previously been attributed to the scavenging properties of HCO_3^-/CO_3^{2-} in aqueous solutions (Schmelling et al., 1997; Bhatkhande et al., 2002) or to the inhibition of the surface activity of TiO_2 particles (Chong et al., 2010). To our knowledge, the impact of alkalinity on the aggregation of TiO_2 particles has not been previously considered and the work here suggests that it may have a significant impact. Alkalinity derived aggregation causes a reduction in reactive surface area by 150 times compared to the cases where alkalinity was not present. Amelioration of such impacts can potentially be delivered through imparting elevated shear into the reactor space to break up the aggregates (Jefferson et al., 2012). Until such technology is developed the inhibitory nature of alkalinity appears to limit the practical use of photocatalysis for micropollutant removal.

The results presented in this work also provide support for appropriate testing of AOPs for micropollutant removal. Firstly, comparison of the micropollutant degradation profiles when using synthetic waters containing both organic matter and alkalinity closely matched those of real site surface water (Figure 4-4). Consequently, confidence can be assigned to treatability tests on synthetic waters where both the background organic concentration and the alkalinity have been matched to the proposed application. Secondly, the concentration of background organic matter was shown to be more important than the mole ratio (Figure 4-3) such that spiking micropollutants into water for improved analytic precision should not influence the significance of the findings. This is consistent with analysis of previously reported data which suggests that as long as the background water represents 85% of the total scavenging rate then changes in micropollutant concentration have negligible impacts on the observed degradation kinetics (Autin et al., 2012b).

4.6 Conclusions

It was shown that whilst both the background organic matter and alkalinity act as •OH scavengers in the UV/H_2O_2 process reducing the rate of degradation of micropollutants, the inhibitory role of alkalinity in UV/TiO_2 photocatalysis is much more pronounced due to the formation of large TiO_2 aggregates. It was demonstrated that AOPs are controlled by the background scavenging rate regardless of the concentration of micropollutant which means that a small variation in organic matter concentration will have a significant influence on the rate of degradation of the micropollutant. The large difference in concentration between the micropollutant and NOM means that for a given NOM concentration, its character does not have a great influence on micropollutant removal. However, a seasonal increase of hydrophobic material will have a greater inhibitory effect than that of hydrophilic material. Finally, it was shown that both micropollutant spiking and using synthetic water to evaluate the treatability of micropollutants agreed with the findings for removal from natural water systems.

4.7 Acknowledgements

The authors would like to express their gratitude for the financial support for this project by Severn Trent Water Ltd.

4.8 References

Ahmed, S., Rasul, M.G., Brown, R., Hashib, M.A., 2011. Influence of parameters on the heterogeneous photocatalytic degradation of pesticides and phenolic contaminants in wastewater: A short review. J. Environ. Manage. 92(3), 311-330.

APHA (1992) Standard Methods. 18th Edition, American Public Health Association, Washington DC, USA.

Autin, O., Hart, J., Jarvis, P., MacAdam, J., Parsons, S.A., Jefferson, B., 2012a. Comparison of UV/H_2O_2 and UV/TiO_2 for the degradation of metaldehyde: Kinetics and impact of background organics. Water Res. 46(17), 5655-5662.

Autin, O., Jarvis, P., Jefferson, B., 2012b. Understanding the reactivity of pesticides towards •OH in drinking water treatment by advanced oxidation processes. Crit. Rev. Environ. Sci. Technol. Submitted.

Bhatkhande, D.S., Pangarkar, V.G., Beenackers, A.A.C.M., 2002. Photocatalytic degradation for environmental applications – A review. J. Chem. Technol. Biotechnol. 77(1), 102-116.

Benitez, F.J., Acero, J.L., Real, F.J., Roman, S., 2004. Oxidation of MCPA and 2-4-D by UV radiation, Ozone, and the Combinations UV/H_2O_2 and O_3/H_2O_2. J. Environ. Sci. Health, Part B – Pestic., Food Contam., Agric. Wastes, B39(3), 393-409.

Benitez, F.J., Real, F.J., Acero, J.L., Garcia, C., 2006. Photochemical oxidation processes for the elimination of phenyl-urea herbicides in waters. J. Hazard. Mater. 138(2), 278-287.

Bond, T., Goslan, E.H., Jefferson, B., Roddick, F., Fan, L., Parsons, S.A., 2009. Chemical and biological oxidation of NOM surrogates and effect on HAA formation. Water Res. 43(10), 2615-2622.

Chelme-Ayala, P., El-Din, M.G., Smith, D.W., 2010. Degradation of bromoxynil and trifluralin in natural water by direct photolysis and UV plus H_2O_2 advanced oxidation process. Water Res. 44(7), 2221-2228.

Chemspider, 2012. Chemical data base search. Available at http://www.chemspider.com (Accessed February 2012).

Chen, P.-J., Rosenfeldt, E.J., Kullman, S.W., Hinton, D.E., Linden, K.G., 2007. Biological assessments of a mixture of endocrine disruptors at environmentally relevant concentrations in water following UV/H_2O_2 oxidation. Sci. Total Environ. 376(1-3), 18-26.

Chong, M. N., Jin, B., Chow, C.W.K., Saint, C., 2010. Recent developments in photocatalytic water treatment technology: A review. Water Res. 44(10), 2997-3027.

Croué, J.P., Korshin, G.V., Benjamin, M., 2000. Characterization of natural organic matter in drinking water, Report 90780. AWWA Research Foundation, USA.

Haag, W.R., Hoigné, J., 1985. Photo-sensitized oxidation in natural water via •OH radicals. Chemosphere 14(11-12), 1659-1671.

Hall, T., Holden, B., Haley, J., 2011. Treatment for metaldehyde and other problem pesticides, 4th Developments in Water Treatment and Supply Conference, Cheltenham, June 7-8 2011.

Hatchard, C.G., Parker, C.A., 1956. A new sensitive chemical actinometer. II. Potassium ferrioxalate as a standard chemical actinometer. Proc. R. Soc. Lond. A 235(1203), 518-536.

He, X., Pelaez, M., Westrick, J.A., O'Shea, K.E., Hiskia, A., Triantis, T., Kaloudis, T., Stefan, M.I., de la Cruz, A.A., Dionysou, D.D., 2011. Efficient removal of microcystin-LR by UV-C/H_2O_2 in synthetic and natural water samples. Water Res. 46(5), 1501-1510.

Ijpelaar, G.F., Groenendijk, M., Hopman, R., Kruithof, J.C., 2002. Advanced oxidation technologies for the degradation of pesticides in ground water and surface water. Water Sci. Technol. 2(1), 129-138.

Jefferson, B., Pidou, M., Autin, O., MacAdam, J., Parsons, S.A., Bayer, C., Follmann, M., Melin, T., Wienk, I.M., Cuperus, F.P., 2012. Membrane-based processes, 179-212. In Innovative and integrated technologies for the treatment of industrial wastewater, Lopez, A., Di Iaconi, C., Mascolo, G., Pollice, A.; IWA publishing, London.

Katsoyiannis, I.A., Canonica, S., von Gunten, U., 2011. Efficiency and energy requirements for the transformation of organic micropollutants by ozone, O_3/H_2O_2 and UV/H_2O_2. Water Res. 45(13), 3811-3822.

Lamsal, R., Walsh, M.E., Gagnon, G.A., 2011. Comparison of advanced oxidation processes for the removal of natural organic matter. Water Res. 45(10), 3263-3269.

Li Puma, G., Yue, P.L., 2003. Modelling and design of thin-film slurry photocatalytic reactors for water purification. Chem. Eng. J. 58(11), 2269-2281.

Metz, D.H., Meyer, M., Dotson, A., Beerendonk, E., Dionysou, D.D., 2011. The effect of UV/H_2O_2 treatment on disinfection by-product formation potential under simulated distribution system conditions. Water Res. 45(13), 3969-3980.

Minakata, D., Li, K., Westerhoff, P., Crittenden, J., 2009. Development of a group contribution method to predict aqueous phase hydroxyl radical (HO•) reaction rate constants. Environ. Sci. Technol. 43, 6220-6227.

Muhamad, S.G., 2010. Kinetic studies of catalytic photodegradation of chlorpyrifos insecticide in various natural waters. Arab. J. Chem. 3(2), 127-133.

Nguyen, T.P., Hilal, N., Hankins, N.P., Novak, J.T., 2008. Determination of the effect of cations and cationic polyelectrolytes on the characteristics and final properties of synthetic and activated sludge. Desalination 222(1-3), 307-317.

Nienow, A.M., Bezares-Cruz, J.C., Poyer, I.C., Hua, I., Jafvert, C.T., 2008. Hydrogen peroxide-assisted UV photodegradation of lindane. Chemosphere 72(11), 1700-1705.

Philippe, K.K., Hans, C., MacAdam, J., Jefferson, B., Hart, J., Parsons, S.A., 2010. Photocatalytic oxidation of natural organic matter surrogates and the impact on trihalomethane formation potential. Chemosphere 81(11), 1509-1516.

Rosario-Ortiz, F.L., Wert, E.C., Snyder, S.A., 2010. Evaluation of UV/H_2O_2 treatment for the oxidation of pharmaceuticals in wastewater. Water Res. 44(5), 1440-1448.

Sanches, S., Barreto-Crespo, M.T., Pereira, V.J., 2010. Drinking water treatment of priority pesticides using low pressure UV photolysis and advanced oxidation processes. Water Res. 44(6), 1809-1818.

Satuf, M.L., Brandi, J., Cassano, A.E., Alfano, O.M., 2007. Scaling-up of slurry reactors for the photocatalytic degradation of 4-chlorophenol. Catal. Today 129(1-2), 110-117.

Schmelling, D.C., Gray, K.A., Kamat, P.V., 1997. The influence of solution matrix on the photocatalytic degradation of TNT in TiO_2 slurries. Water Res. 31(6), 1439-1447.

Sharp, E.L., Jarvis, P., Parsons, S.A., Jefferson, B., 2006a. Impact of fractional character on the coagulation of NOM. Colloid Surface A 286(1-3), 104-111.

Sharp, E.L., Parsons, S.A., Jefferson, B., 2006b. Seasonal variations in natural organic matter and its impact on coagulation in water treatment. Sci. Total Environ. 363(1-3), 183-194.

Wu, C., Linden, K.G., 2010. Phototransformation of selected organophosphorus pesticides: Roles of hydroxyl and carbonate radicals. Water Res. 44(12), 3585-3594.

Xu, G., Chance, M.R., 2005. Radiolytic modification and reactivity of amino acid residues serving as structural probes for protein footprinting. Anal. Chem. 77(14), 4549-4555.

CHAPTER 5 COMPARISON OF UV/TiO_2 AND UV/H_2O_2 PROCESSES IN AN ANNULAR PHOTOREACTOR: INFLUENCE OF WATER PARAMETERS ON METALDEHYDE REMOVAL, QUANTUM YIELDS AND ENERGY CONSUMPTION

CHAPTER 5: COMPARISON OF UV/TiO_2 AND UV/H_2O_2 PROCESSES IN AN ANNULAR PHOTOREACTOR: INFLUENCE OF WATER PARAMETERS ON METALDEHYDE REMOVAL, QUANTUM YIELDS AND ENERGY CONSUMPTION

Olivier Autin [a], *Julie Hart* [b], *Peter Jarvis* [a], *Jitka MacAdam* [a], *Simon A. Parsons* [a], *Bruce Jefferson* [a]

[a] Cranfield Water Science Institute, Department of Environmental Science and Technology, Cranfield University, Bedfordshire, MK43 0AL, UK.

[b] Severn Trent Water LTD., Severn Trent Centre, PO Box 5309, Coventry, West Midlands, CV3 9FH, UK.

5.1 Abstract

Advanced oxidation processes have proven their efficacy in the removal of micropollutants but the role of background constituents on the kinetics of degradation is not well understood. Investigation into the role of alkalinity and background organic matter as defined by three surrogate compounds – serine, leucine and resorcinol – on the degradation of metaldehyde was conducted with a continuous flow photoreactor operated as either UV/TiO_2 or UV/H_2O_2. The presence of alkalinity only influenced the UV/TiO_2 system through the aggregation of the catalyst from 3.5 μm to 400 μm median size. Background organic compounds inhibited the process through scavenging such that reaction rates were on average reduced by 19%. Modelling the radiation field enabled the quantum yield to be determined indicating that metaldehyde contributed to 0.1% of the total quantum yield under realistic background organic matter concentrations. Examination of models in term of electrical energy per order suggested that ideal reactor width of 3 mm for TiO_2 and 11.7 cm are required.

Keywords: metaldehyde, natural organic matter, alkalinity, quantum yield, advanced oxidation processes.

5.2 Introduction

Advanced oxidation processes (AOPs) have been successfully used at lab and pilot scale for the degradation of micropollutants in drinking water applications (Pereira et al., 2007; Katsoyiannis et al., 2011). Existing models describing the radiation field in the reaction space have been successfully applied for the degradation of single component and even multicomponent mixtures of organic contaminants in laboratory grade water (Li Puma and Yue, 1999; Satuf et al., 2007, Li Puma et al., 2007, Zalazar et al., 2008). However, most of these studies excluded the presence of natural scavengers such as natural organic matter (NOM) or carbonate ions which have shown inhibitory effects in AOPs (Rosenfeldt and Linden, 2007; Pereira et al., 2007) resulting in over-prediction of the destruction rates (Song et al., 2008). Previous work at bench scale has demonstrated that the high concentration of organic and carbonate scavengers commonly present in background water reduces the proportion of available •OH that reacts with the target micropollutant down to less than 0.05% of those produced (Autin et al., 2012). Incorporation of this impact has enabled effective prediction of the degradation of micropollutants in a UV/H_2O_2 pilot plant (Song et al., 2008). In such work it is common to use measurements of the bulk NOM concentration such as absorbance at 310 nm restricting understanding on the impact of organic character on the process. The organic make-up of the background NOM is known to be highly variable and the impact of this on the degradation of micropollutants at bench scale has revealed that both the concentration and character of the organics is important through their combined impact on the overall scavenging rate (Autin et al., 2012). The impact of NOM was shown to be common across AOPs but specific issues in relation to alkalinity were observed only with

UV/TiO_2 where loss of reactive surface area due to catalyst aggregation was observed in the presence of alkalinity.

The current study aims to incorporate such findings at pilot scale in order using the previously developed model by Li Puma et al. (2007) to evaluate the potential of AOPs for micropollutant removal. The work extends previous studies by directly comparing two AOPs: UV/H_2O_2 and UV/TiO_2 in order to establish process specific features and their impact on the overall suitability of the technology for micropollutant removal.

For both processes, the local volumetric rate of photon absorption (LVRPA) which informs on how and where the reactions occur in the reactor was determined. From the LVRPA and experimental data, the quantum yields and energy requirement were determined for the different scenarios. Finally, the rate constants independent of photon absorption were determined for both systems in order to standardize them to any reactor configuration.

Nomenclature

a	model parameter SFM
b	model parameter SFM
c_{cat}	photocatalyst concentration ($kg.m^{-3}$)
C_i	metaldehyde or NOM surrogate concentration ($mol.m^{-3}$)
C_{0i}	initial concentration of metaldehyde or NOM surrogate ($mol.m^{-3}$)
H	length of the reactor (m)
I	radiation intensity (or radiative flux) ($W.m^{-2}$)
k_T	kinetic rate constant independent of radiation absorbed ($m^3.e^{-1}$)
L	lamp length (m)
$VRPA$	volumetric rate of photon absorption (W or $e.s^{-1}$)
$LVRPA$	local volumetric rate of photon absorption ($W.m^{-3}$ or $e.s^{-1}.m^{-3}$)
m	order of the reaction with respect to the LVRPA
p_b	probability of scattering in the backward direction
p_f	probability of scattering in the forward direction
p_s	probability of scattering in the side direction
r	radial coordinate (m)
r^*	dimensionless radial coordinate (=r/R)
r_l	lamp radius (m)
r_i	reaction rate with respect to substrate I ($mol.s^{-1}.m^{-3}$)
R	external radius of annulus (m)
S_l	radiation emission of lamp per unit time per unit length ($W.m^{-1}$)
t	time (s)
V_t	total volume of fluid in recirculation system (m^3)
V_r	reactor volume (m^3)
z	axial coordinate (m)
z^*	dimensionless axial coordinate (=z/H)

Greek letters

α	geometrical parameter (=H/L)
β	geometrical parameter (=$L/\eta R$)
γ	dimensionless parameter SFM
δ	reaction space radial coordinate (m)
δ^*	dimensionless reaction space radial coordinate (=ζ/δ)
η	ratio of internal radius to external radius of annulus
κ	specific mass absorption coefficient at 254 nm ($m^2.kg^{-1}$)
λ	radiation wavelength (m)
σ	specific mass scattering coefficient at 254 nm ($m^2.kg^{-1}$)
τ	optical thickness
τ_{app}	apparent optical thickness
Φ	quantum yield ($mol.e^{-1}$)
ω	scattering albedo (=$\sigma/\sigma+\kappa$)
ω_{corr}	corrected scattering albedo SFM

5.3 Material and methods

5.3.1 Chemicals

Metaldehyde, serine, leucine, hydrogen peroxide (35% w/w), $NaHCO_3$ were obtained from Fisher Scientific (Loughborough, UK) and resorcinol from Sigma-Aldrich (Poole, UK) at analytical purity or above. Titanium dioxide P25 Degussa was purchased from Lawrence Industries (Tamworth, UK). Laboratory grade water (LGW) was produced by a Purelab Option (S7/15, 18.2 MΩ and TOC< 3 ppb). The surface water was collected post-GAC from a drinking water treatment works in the Severn Trent Water region, UK and had a DOC of 3.5 $mg.L^{-1}$ and an alkalinity of 120 $mg.L^{-1}$ as $CaCO_3$. The water was stored in the dark at 4˚C until used for experiments.

Table 5-1 - Photochemical and chemical properties of metaldehyde and the three NOM surrogates.

	Metaldehyde	Serine	Leucine	Resorcinol
ζ ($M^{-1}.cm^{-1}$)	19.0	0.3	0.5	559.8
Concentration	$5.68x10^{-8}$	$1.89x10^{-5}$	$1.89x10^{-5}$	$1.89x10^{-5}$
$k_{\bullet OH}$ ($M^{-1}.s^{-1}$)	$1.3x10^{9}$ [a]	$3.2x10^{8}$ [b]	$1.7x10^{9}$ [b]	$1.1x10^{10}$ [c]
Log k_{OW}	0.12[d]	-3.07[d]	-1.52[d]	0.80[d]

a: value from Autin et al., 2012; b: values from Xu and Chance, 2005; c: value from Minakata et al., 2009; d: values from Chemspider chemical data base search. Available at: http://www.chemspider.com (accessed April, 2012).

5.3.2 Photoreactor

The system comprised a holding tank and an annular photoreactor. The solution and TiO_2 or H_2O_2 were mixed together in the holding tank and left in contact for 30 min before irradiation. The mixture was then pumped (520U, Watson Marlow) into the reactor in an up flow mode. Air was sparged co-currently in the reactor in order to have a good mixing and to enhance the TiO_2 photocatalytic process by trapping the e^- formed at the surface. The outer wall of the reactor is made of stainless steel with an internal diameter of 0.077 m, and the inner wall consists of a quartz tube (external diameter 0.047 m) mounted at the axial centre of

the reactor (Figure 5-1). The dimensions of the reactor are presented in Table 5-2. The light source was a Trojan 45 W UVC lamp emitting at 253.7 nm which was inserted inside the quartz tube. The photon flux was measured using a microprocessor-controlled radiometer (Cole-Parmer) fitted with a 254 nm UVC sensor, and was found to be 31.3 $W.m^{-2}$.

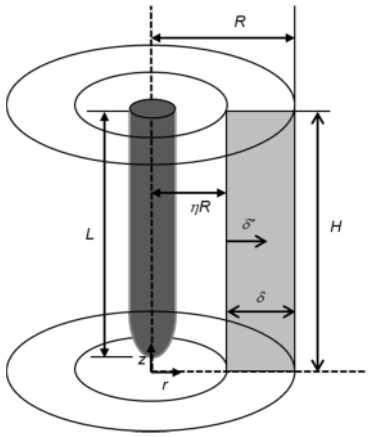

Figure 5-1 - Schematic representation of the geometry of the annular photoreactor.

Table 5-2 - Optical parameters of TiO_2 and H_2O_2 solutions and system parameters.

Model parameter	UV/TiO_2	UV/H_2O_2
Reactor length, *H*	0.38 m	0.38 m
Lamp length, *L*	0.36 m	0.36 m
Gap size, δ	0.015 m	0.015 m
Geometrical parameters	α=1.056, β=15.329	α=1.056, β=15.329
Specific absorption coefficient, κ	2184[a]/188.4[b] $m^2.kg^{-1}$	
Specific scattering coefficient, σ	1456[a]/125.6[b] $m^2.kg^{-1}$	
Scattering albedo, ω	0.4	
Optical thickness, τ	423	
[absorbing species]	100 $mg.L^{-1}$	0.008 M
Decadic molar absorption coefficient, ξ	2255$M^{-1}.cm^{-1}$	19.6 $M^{-1}.cm^{-1}$

[a]: in the absence of alkalinity; [b]: in the presence of alkalinity

The optical properties of TiO_2 were determined for the specific conditions of mixing and particle aggregation of this study. The sum of absorption and scattering coefficients corresponds to the extinction coefficient which can be determined spectrophotometrically (Cabrera et al., 1996). The extinction coefficient was 3640 and 314 $m^2.kg^{-1}$ in the presence and in the absence of alkalinity respectively. Salaices et al. (2002) observed that although an

increase of particle agglomerate sizes leads to smaller extinction coefficients at a given wavelength, it had the same effect on both the scattering and absorption coefficient. In other words, for a given wavelength, the scattering albedo ($\sigma/\sigma+\kappa$) can be assumed constant, and therefore, the ratio of 0.4 determined by Li Puma et al. (2010) for a low pressure lamp irradiating at 253.7 nm was used in this study.

5.3.3 Irradiation procedures

Stock solutions of leucine, serine and resorcinol were prepared in LGW at 500 $mg.L^{-1}$, and metaldehyde at 1 $mg.L^{-1}$. In order to accurately follow the degradation of metaldehyde, an initial concentration of 10 $\mu g.L^{-1}$ ($5.68x10^{-8}$ M) was chosen and a DOC concentration of 3.5 $mg.L^{-1}$ was used so that the molar ratio between metaldehyde and the NOM surrogates was 1:1,000 with equimolar concentrations of serine, leucine and resorcinol. When the influence of alkalinity was tested, $NaHCO_3$ was added so that the alkalinity was 120 $mg.L^{-1}$ as $CaCO_3$. 10 L of solution was freshly prepared before each test by spiking the required volume of each stock solution in LGW. Experiments were carried out at natural pH and at room temperature (20-22˚C). The residence time was controlled by adjusting the flow rate and samples were taken at the outlet of the reactor when the required irradiation time was reached. The concentrations of oxidants were fixed at 100 $mg.L^{-1}$ and 8 mM for TiO_2 and H_2O_2 respectively as found to be optimum concentrations for this application (Autin et al., 2012). Such a high concentration of hydrogen peroxide is unlikely to be used in industrial applications but greatly increased the reaction rate and was used in order to compare the two processes at their optimum potential.

5.3.4 Sample analysis

For UV/TiO_2, samples were filtered through 0.45 μm syringe filters (Millex-HA) to separate the suspended TiO_2 prior to analysis. The analyses were performed using a Waters 2695 LC system coupled with a Waters Quattro Premier Xe MS-MS. The aqueous mobile phase A

consisted of 5 mM ammonium acetate/0.1% formic acid and the organic mobile phase B was acetonitrile/0.1% formic acid. The flow rate was set to 0.2 mL.min^{-1} and the conditions were 50% A and 50% B held for 2 min. The Quattro Premier Xe tandem quadruple mass spectrometer was operated under positive electrospray ionization mode for metaldehyde, leucine and serine and negative electrospray ionization mode for resorcinol. The instrument was operated in multiple reaction monitoring set to monitor ions m/z 194, m/z 131.7, m/z 105.7 and m/z 108.5 for metaldehyde, leucine, serine and resorcinol respectively. Source conditions were as follows: capillary 3.5 kV, source temperature 120 ˚C, desolvation temperature 350 ˚C, and nitrogen drying gas 1000 L.h^{-1}. Calibrated curves were generated prior to each new sequence and the concentrations were determined using Micromass QuantLynx.

The decadic molar absorption coefficient was defined using:

$$A_{254,i} = \xi_i \times l \times C_i \qquad (5\text{-}1)$$

where $A_{254,i}$ is the absorbance of *i* at 254 nm (in cm^{-1}), ξ_i is the decadic molar absorption coefficient of *i* at 254 nm (in M^{-1}.cm^{-1}), *l* is the path length in the spectrophotometer (1 cm) and C_i is the concentration of *i* (in M).

5.3.5 Description of the model used

In AOPs, the quantum yield evaluates the efficiency of a process and is defined as:

$$\Phi = \frac{total\ number\ of\ moles\ of\ pesticide\ transformed}{total\ number\ of\ moles\ of\ photons\ absorbed\ in\ the\ system} = \frac{V(dCi/dt)_{t=0}}{VRPA} \qquad (5\text{-}2)$$

Where $(dC_i / dt)_{t=0}$ is the initial rate of degradation of compound *i* (in M.s^{-1}), *V* is the volume of the reactor (in L) and *VRPA* is the volumetric rate of photon absorption (in e.s^{-1}).

The VRPA, defined as the photon energy absorbed at a specific position in the reaction space (Li Puma et al., 2010) can be estimated by integrating the local volumetric rate of photon absorption (LVRPA) throughout the entire reactor volume, such as:

$$VRPA = \int_{V_r} (LVRPA) dV_r \quad (5\text{-}3)$$

UV/H_2O_2 is a homogeneous system and the photons are absorbed by all the species in solution whilst UV/TiO_2 is a heterogeneous system and the photons are absorbed by both the photocatalyst and the species in solution. For both processes, the concentration of •OH precursor (TiO_2/H_2O_2) is much larger than that of the organic compounds. For UV/TiO_2, more than 99.5% of the photons are absorbed by TiO_2 (absorption coefficient κ_{TiO2}=2.82 cm^{-1} compared to $\kappa_{all\ other\ species}$=0.0106 cm^{-1}) and the contribution from the organic compounds to the LVRPA can be safely neglected. For UV/H_2O_2 due to the low absorption of light at 254 nm by H_2O_2, the fraction of photons absorbed by the •OH precursor represents initially 94.2% of the total photon absorption in multi-component mode. However, as the organics are degraded, the fraction of photon absorbed by H_2O_2 constantly increases and H_2O_2 can also be assumed to be the only absorbing species in the UV/H_2O_2 system in the model.

In homogeneous systems, the LVRPA is a function of position (*r, z*) and time (*t*):

$$LVRPA = LVRPA(r,z,t) \quad (5\text{-}4)$$

Where r and z are the radial and axial coordinates respectively.

As the concentration of H_2O_2 is two orders of magnitude higher than the organics, the concentration of H_2O_2 was assumed to remain constant over the time of irradiation, and therefore the LVRPA becomes independent of time:

$$LVRPA = LVRPA(r,z) \quad (5\text{-}5)$$

Based on the equations described by Zalazar et al. (2008) and the assumption made in this work, the LVRPA spatial distribution can be described using the one-dimensional model as follows:

$$LVRPA(r,z) = \kappa_H \text{ x } I(\eta r,z) \text{ x } exp^{(-\kappa_H x\ \delta^*)} \quad (5\text{-}6)$$

where κ_H is the absorption coefficient of H_2O_2 (in m^{-1}) which is the product of the decadic molar absorption coefficient ζ and the concentration of H_2O_2, $I(\eta r,z)$ is the incident photon flux entering the inner wall of the reactor (in $W.m^{-2}$) and δ^* is the dimensionless reaction space radial coordinate (Figure 5-1).

As H_2O_2 poorly absorbs UV light, a large part of the photons emitted are not absorbed along the reaction space and reach the reactor wall. The reactor is made of stainless steel which is known to absorb UV light (Nicole et al., 1990) and has been previously reported to absorb more than 80% of the light (Bolton, 2000). As no precise values are available in the literature, an arbitrary fraction of light absorbed by the reactor of 85% was chosen and the model was created such that 15% of the photons reaching the reactor wall were reflected into the reaction space. In comparison, if the reactor did not reflect light at all, the VRPA would be 8% larger and if 20% of the photons were reflected in the system (80% absorbed by the reactor wall), no more than 2% difference would be observed in comparison to the case chosen here. Hence, the equation of the LVRPA was reintegrated through the reactor from the reactor wall to the lamp and the total LVRPA was:

$$LVRPA(r,z) = LVRPA(r,z)_{\text{emitted}} + LVRPA(r,z)_{\text{reflected}} \quad (5\text{-}7)$$

In heterogeneous systems the transport of photons is governed by absorption, scattering and emission (Li Puma et al., 2010). The Six-Flux Absorption-Scattering Model (SFM) developed by Brucato et al. (2006) has been successfully applied to annular photoreactors (Li

Puma, 2010) and was used in this study. The main assumptions made in this model are: the TiO_2 particles are uniformly distributed in solution, the optical characteristics are constant independently of space and time, the absorption of energy by the fluid and reactor wall are neglected, the photons with energy greater than TiO_2 band-gap are either absorbed or scattered and scattering follows one of the six directions of the Cartesian coordinates (Li Puma et al., 2010). The LVRPA at a point (r, z) in the reactor space for an infinitely long annular photocatalytic reactor is:

$$LVRPA = \frac{\tau_{app} \times I_{(\eta R),z^*}}{\omega_{corr}(1-\gamma)(1-\eta)R} \times \frac{\eta}{[\eta + (1-\eta)\delta^*} \times [(\omega_{corr} - 1 + \sqrt{1-\omega_{corr}^2}) \exp^{-\tau_{app}\delta^*} + \gamma(\omega_{corr} - 1 - \sqrt{1-\omega_{corr}^2}) \exp^{\tau_{app}\delta^*}] \quad (5\text{-}8)$$

A detailed description of the model can be found in Li Puma et al. (2007) or in supplementary data.

5.3.6 Electrical energy per order

The electrical energy consumption currently represents the main part of the overall operating cost of AOPs and its evaluation is essential in order to evaluate the economic viability of a process. A figure of merit named electrical energy per order (EEo) has been introduced by Bolton et al. (2001) which is defined as the electrical energy (in kWh) required to degrade a given volume of a pollutant, typically 1 m^3, by one order of magnitude, and is expressed in $kWh.m^{-3}$. The EEo is optimally used for low concentration of pollutant when the overall reaction follows first-order and is calculated from the following equation:

$$EEo = \frac{P \times t}{V_T \times \log \frac{Ci}{Cf}} \quad (5\text{-}9)$$

where P is the input power of the lamp (in kW), t is the time of irradiation (in h), V_T is the volume of solution treated (in m^3), C_i and C_f are the initial and final concentrations respectively.

The equation can also be expressed in term of rate constant as described by Bolton and Stefan (2002):

$$EEo = \frac{38.38 \times P}{V_T \times k'} \quad (5\text{-}10)$$

where *k'* is the pseudo-first order rate constant (in min^{-1}).

In addition, the volumetric reaction rate is:

$$r(V) = k' \times C_0 \times V_R \quad (5\text{-}11)$$

where $r(V)$ is the volumetric reaction rate (in $M.s^{-1}.m^3$).

The rearrangement of equation (5-10) and (5-11) enables to express the EEo in function of the reaction rate, such as:

$$EEo = \frac{0.64.10^{-3} \times C_0 \times P}{\frac{V_T}{V_R} \times r(V)} \quad (5\text{-}12)$$

where *EEo* is in $kWh.m^{-3}$, P in kW, C_0 in M and r in $M.s^{-1}.m^3$.

5.4 Results and discussion

Control experiments were carried out to ensure that no direct photolysis or dark adsorption occurred in the systems. The degradation of metaldehyde and the three NOM surrogates in multicomponent mixture achieved no more than 4% removal at a 10 min residence time when neither TiO_2 nor H_2O_2 was added to the system (Figure 5-SI-1). Dark adsorption of the mixture on TiO_2 over a period of two hours indicates that none of the compounds readily

adsorb onto TiO_2 surface (Figure 5-SI-2). Therefore, as direct photolysis and adsorption do not occur in any of the systems, •OH attack is the only route of degradation.

5.4.1 Comparison of metaldehyde degradation by UV/H_2O_2 and UV/TiO_2 in natural and synthetic waters

More than 90% metaldehyde removal was achieved at a 7.5 min residence time in the UV/H_2O_2 system for both natural and synthetic waters in the presence of background organic matter and alkalinity (Figure 5-2). In contrast, less than 50% removal was achieved at a 20 min residence time in the UV/TiO_2 system. These low removals by UV photocatalysis are in accordance with a previous study which showed the inhibitor effect of alkalinity on metaldehyde degradation due to the formation of large TiO_2 aggregates increasing the size from 3.5 μm without alkalinity to 400 μm when carbonate ions were added reducing the surface area of TiO_2 by a factor 150 (Autin et al., 2012). The profiles in natural and synthetic waters with similar characteristics showed no major differences in metaldehyde degradation (Figure 5-2). Such results suggest that the use of synthetic water accurately represents the reactions occurring in natural water and offers the possibility to follow the degradation of all the species in solution which can give important information on the competition between the micropollutant and other water constituents. As alkalinity had a significant impact on metaldehyde removal by UV/TiO_2, simulation are carried out both in the presence and absence of alkalinity to evaluate the extent of this impact and to estimate what could be achieved if a pre-treatment able to break the aggregates was used.

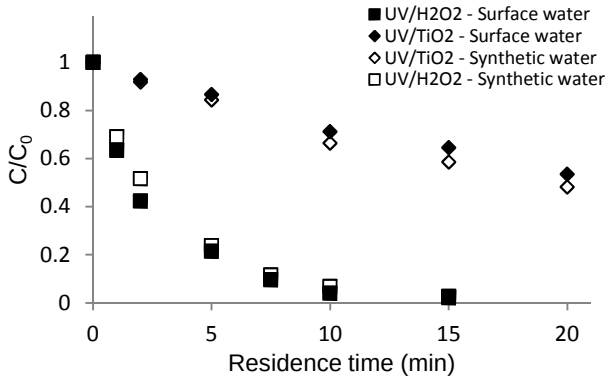

Figure 5-2 - Degradation of metaldehyde in surface water (black) and synthetic water (white) by UV/H_2O_2 (square) and UV/TiO_2 (diamond). [DOC]=3.5 mg.L^{-1}, alkalinity=120 mg.L^{-1} as $CaCO_3$, [H_2O_2]=8 mM, [TiO_2]= 100 mg.L^{-1}, [metaldehyde]=5.68x10^{-8} M= 10 µg.L^{-1}.

5.4.2 Degradation kinetics of metaldehyde in single and multi-component mode

Metaldehyde was well degraded by both processes when no competing species were present in solution (Figure 5-3-A,B). At a 10 min residence time, 95% and 96% of metaldehyde removal were achieved by UV/TiO_2 and UV/H_2O_2 respectively which resulted in first order rate constants of 5.17x10^{-3} and 5.48x10^{-3} s^{-1} in accordance with bench scale tests where the first order rate constants were 4.29x10^{-3} and 4.78x10^{-3} s^{-1} indicating that rate data can be effectively transferred from bench to pilot plant operation. The presence of competitive species reduced the degradation of metaldehyde by both processes (Figure 5-3-A,B). The irradiation of TiO_2 led to the partial degradation of the four compounds with associated pseudo-first order rate kinetics in the order resorcinol > leucine > metaldehyde > serine. For instance, the rate of degradation of resorcinol was k'= 6.73x10^{-3} s^{-1} whilst for serine, the least degraded of the four compounds k'= 2.61x10^{-3} s^{-1}. Despite being at much lower concentration than the three NOM surrogates, metaldehyde was still removed by the UV/TiO_2 process at a degradation rate of k'= 3.93x10^{-3} s^{-1}, compared to k'= 5.17x10^{-3} s^{-1} in single component. The degradation of the multicomponent mixture by UV/H_2O_2 led to faster degradation than by UV/TiO_2 such that the degradation rate for resorcinol was k'= 9.13x10^{-3} s^{-1} and for metaldehyde k'= 4.77x10^{-3} s^{-1} (Figure 5-3-B). The same sequence of rate constants resorcinol > leucine > metaldehyde > serine was observed. The inhibition of the rate constants in multi-

component mode were expected due to the scavenging effect of competing species (Haag and Hoigné, 1985), however the order of degradation does not follow the scavenging rate of each compound ($k'_{\bullet OH,i}$ x [i]) but the reactivity $k'_{\bullet OH,i}$ as metaldehyde which had a scavenging rate two orders of magnitude lower than serine but a reactivity one order of magnitude higher get removed preferentially in comparison to serine.

Whilst alkalinity had no major effect on the UV/H_2O_2 process (Figure 5-3-B), the degradation of metaldehyde and the three NOM surrogates was highly affected in the UV/TiO_2 system (Figure 5-3-A). The presence of alkalinity reduced metaldehyde degradation rate from $k'=3.93x10^{-3}$ s^{-1} in multi-component mode without alkalinity to $k'=3.68x10^{-4}$ s^{-1} in multi-component mode with addition of carbonate ions, 93% slower than in the presence of metaldehyde only.

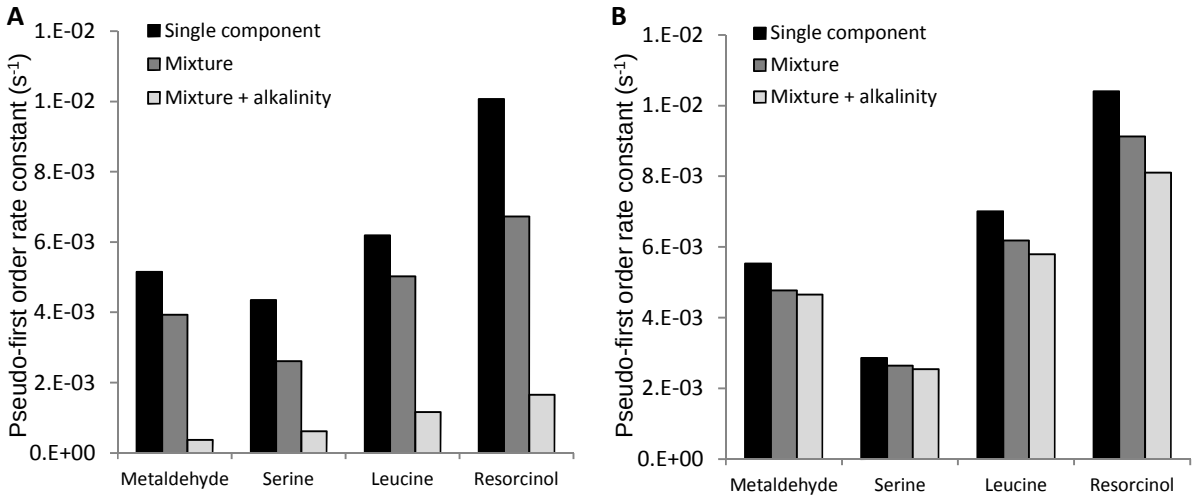

Figure 5-3 - Degradation of metaldehyde, serine, leucine and resorcinol in single component and in multicomponent mixture in the absence and presence of carbonate ions by A) UV/TiO_2 and B) UV/H_2O_2. Alkalinity= 120 mg.L^{-1} as $CaCO_3$. [TiO_2] = 100 mg.L^{-1}, [H_2O_2] = 8 mM UV-C radiation, initial concentrations (µM): [Metaldehyde] = 0.0568; [Leucine] = [Serine] = [Resorcinol] = 18.94.

5.4.2.1 LVRPA radial profiles and VRPA

The LVRPA were different for TiO_2 and H_2O_2 as illustrated by the normalized radial profiles in the middle of the reactor (Figure 5-4-A). The LVRPA at the reactor wall ($\delta^*=0$) was significantly higher for UV/TiO_2 in the absence of alkalinity - well dispersed slurry of TiO_2 -

than for UV/H_2O_2 at 12649 and 837 W.m^{-3} respectively reflecting the difference in absorption coefficients (Table 5-2). In the UV/TiO_2 system, nearly 85% of the photons emitted by the lamp are absorbed within the first 1/3 of reaction space whilst in the UV/H_2O_2 system only 25% of the emitted photons are absorbed within the entire reaction space. As 85% of the photons reaching the wall are absorbed by the reactor, only a small fraction is reflected, and overall, only 36% of the total photons emitted are absorbed by the solution.

The presence of alkalinity greatly reduced the rate of photon absorption in the UV/TiO_2 system with LVRPA=1019 W.m^{-3} at z=0.5 and δ^*=0. As larger aggregates are in solution, the slurry is not as well dispersed and a much larger part of the photons is not absorbed by TiO_2 agglomerates such that only 63% of the photons emitted are absorbed throughout the entire reactor volume (Figure 5-4-A).

The VRPA of the UV/TiO_2 system was 2.5 times larger than in the UV/H_2O_2 system at 1.96 W (Table 5-3). Aggregation of the catalyst particles reduced the VRPA of UV/TiO_2 to 0.62 W such that it became lower than the 0.80 W for the UV/H_2O_2 system. Increasing the catalyst dose enhanced the VRPA in both the presence and absence of alkalinity. In the absence of alkalinity catalyst doses up to 100 mg.L^{-1} significantly increased the VRPA beyond which only minor enhancements were observed. In contrast, aggregation of the catalyst in the presence of alkalinity meant that the VRPA was enhanced up to dose of 600 mg.L^{-1} beyond which the VRPA did not increase (Figure 5-4-B). As alkalinity has no influence on H_2O_2 molecules properties or on the transmissivity of the water, the presence of alkalinity had no impact on the VRPA for the UV/H_2O_2 process which constantly increases with the increase of [H_2O_2] as more photons are absorbed by the solution. At the optimum dose of H_2O_2 (8 mM) the VRPA was 0.80 W which represents a 55% reduction compared to the UV/TiO_2 system even when alkalinity is present. The cost of H_2O_2 plus its own •OH scavenging properties mean that practical economic limits around 27 mg.L^{-1} (0.8 mM) have

been suggested (Hirvonen et al., 1998) and at these levels the VRPA is 0.097 W, 20 times smaller than for UV/TiO_2 demonstrating that the latter is a more effective process at absorbing photons.

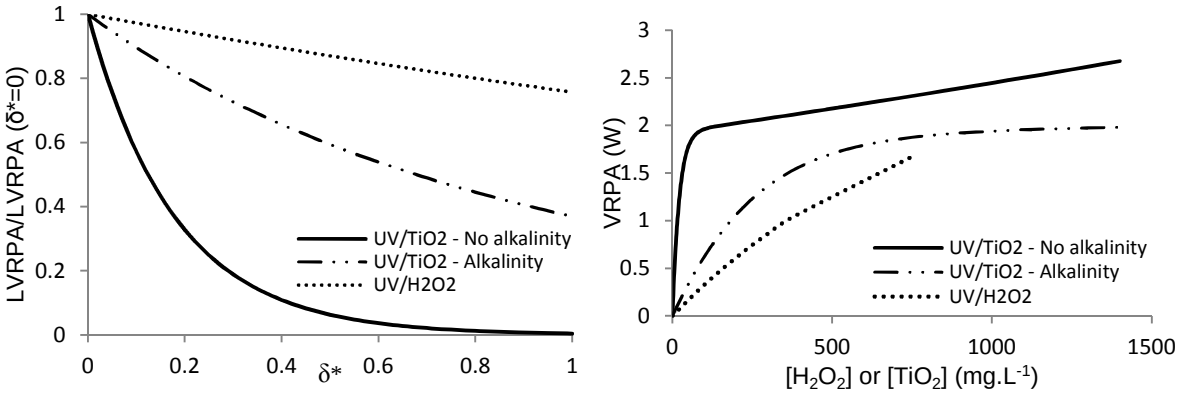

Figure 5-4 - A) Normalized radial profiles of the LVRPA in the middle of the reactor (z*=0.5), as predicted by the radiation models for the conditions in Table 5-1 LVRPA (δ*=0) is 12649, 1019 and 837 W.m^{-3} for UV/TiO_2 without alkalinity, UV/TiO_2 with alkalinity and UV/H_2O_2 systems respectively. B) Volumetric rate of photon absorption as a function of TiO_2 and H_2O_2 concentrations.

Table 5-3 - Volumetric rate of photon absorption, specific quantum yields and overall quantum yield, electrical energy per order and reaction rate constant independent of photon absorption in the different configurations tested.

	UV/TiO_2 No alkalinity	UV/TiO_2 With alkalinity	UV/H_2O_2 No alkalinity	UV/H_2O_2 With alkalinity
VRPA (W)	1.961	0.623	0.800	0.800
VRPA (e.s^{-1})	4.17x10^{-6}	1.32x10^{-6}	1.70x10^{-6}	1.70x10^{-6}
$\Phi_{Metaldehyde/\ Single\ component}$ (mol.e^{-1})	7.97 x 10^{-5}	n.a.	2.10 x 10^{-4}	n.a.
$\Phi_{Metaldehyde/Multi\text{-}compinent}$ (mol.e^{-1})	4.53 x 10^{-5}	2.98 x 10^{-5}	1.81 x 10^{-4}	1.76 x 10^{-4}
$\Phi_{Serine/Multi\text{-}compinent}$ (mol.e^{-1})	7.48 x 10^{-3}	5.89 x 10^{-3}	3.34 x 10^{-2}	3.21 x 10^{-2}
$\Phi_{Leucine/Multi\text{-}compinent}$ (mol.e^{-1})	1.69 x 10^{-2}	1.89 x 10^{-2}	7.81 x 10^{-2}	7.32 x 10^{-2}
$\Phi_{Resorcinol/Multi\text{-}compinent}$ (mol.e^{-1})	2.12 x 10^{-2}	2.67 x 10^{-2}	0.116	0.103
$\Phi_{Overall/Multi\text{-}compinent}$ (mol.e^{-1})	0.0456	0.0516	0.227	0.209
$EEo_{single\ component}$ (kWh.m^{-3})	4.9		4.7	
$EEo_{multi\ component}$ (kWh.m^{-3})	9.0	41.7	5.6	5.7
$k_{T,M}$ (m^3.e^{-1})	0.798	0.526	3.183	3.102

5.4.2.2 Quantum yields

The impact of differences in VRPA on the efficiency of the process, as defined by the quantum yield, was determined by equation (5-1) and the initial rates of degradation observe

in the pilot trials. In single component mode, the quantum yield for metaldehyde was $7.97x10^{-5}$ and $2.10x10^{-4}$ $mol.e^{-1}$ for the UV/TiO_2 and UV/H_2O_2 systems respectively. The efficiency of 0.021% for the UV/H_2O_2 was higher than the 0.008% observed for the UV/TiO_2 system indicating the former was more efficient at using the absorbed photons as the rates of degradation were similar but the VRPA was lower. The presence of NOM reduced the quantum yield of metaldehyde by 47% for UV/TiO_2 and 14% for UV/H_2O_2 but increased overall quantum yield to 4.64% and 22.7% respectively indicating better utilisation of the available photons when more material is available for reaction.

Both the rates of degradation of metaldehyde and NOM surrogates and the VRPA were severely affected by the presence of alkalinity in the UV/TiO_2 process. Interestingly, as the VRPA was more affected than the rates of degradation, the overall quantum yield was slightly greater in the presence of alkalinity. On the other hand, it had no major impact on the quantum efficiency of the UV/H_2O_2 system – 22.7 and 20.9% in the absence and presence of alkalinity respectively.

The quantum yield is proportional to the initial rate of degradation and as metaldehyde is present at concentrations 3 orders of magnitude lower than the background organic matter, the individual quantum yields of metaldehyde are very low for both processes and represent only 0.058% and 0.087% of the overall quantum yields for UV/TiO_2 ad UV/H_2O_2 respectively in the presence of both NOM surrogates and carbonate ions (Table 5-3). The overall quantum yields observed here are in the order of efficiencies previously reported (Zalazar et al., 2008; Li Puma et al., 2010) and the efficiency is 5 times higher for UV/H_2O_2 than for UV/TiO_2.

5.4.2.3 Electrical energy consumption

In single component mode, both processes exhibit similar EEo of 4.9 and 4.7 $kWh.m^{-3}$ for UV/TiO_2 and UV/H_2O_2 respectively (Table 5-3). The presence of background organic matter increased the EEo by 19% for UV/H_2O_2 whilst that of UV/TiO_2 increased more significantly by 84%. More importantly, no difference was observed for UV/H_2O_2 when carbonate ions were added, the same action increased the EEo of the UV/TiO_2 system by 360% with values becoming more than 7 times greater for UV/TiO_2 than for UV/H_2O_2. Crittenden et al. (1999) reported that EEo values of 2.65 $kWh.m^{-3}$ or less were considered favourable. Here, the values reported are slightly higher, however the scale-up from bench scale to full scale is known to decrease the EEo by at least one order of magnitude (Parsons, 2004) and hence, the degradation of metaldehyde by both processes would require less than 1 $kWh.m^{-3}$ and demonstrates the potential to be economically viable.

However, these values have to be balanced as although the electrical energy consumption represents the main cost of AOPs, other parameters also need to be considered especially the cost of chemicals. In this study, optimum concentrations of •OH precursors have been used, e.g. 100 $mg.L^{-1}$ and 8 mM for TiO_2 and H_2O_2 respectively. Such concentration of H_2O_2 appears economically unrealistic for full scale plants, and a reduction of this concentration to 0.8 mM would result in an EEo= 139.1 $kWh.m^{-3}$. Moreover, the high EEo values found for the UV/TiO_2 system are essentially due to the presence of alkalinity which leads to the formation of large TiO_2 aggregates. Breaking these aggregates would lead to greater surface area available and potentially to better rates of degradation, reducing the EEo (theoretically down to values obtained in the presence of NOM surrogates only). However, energy would be required to break the aggregates which adds up to the need of a post-photocatalysis filtration system to separate the treated water from the catalyst which is recirculated in the system.

5.4.2.4 Rate constant independent of photon absorption

The rate constants determined in research studies are often specific to the reactor set-up and geometry as they are not decoupled from the amount of radiation absorbed by the system (Li Puma et al., 2010). As the degradation kinetics of metaldehyde follows pseudo-first order, the reaction rate can be modelled by:

$$-r_M = k_{T,M}(LVRPA)^m C_M \quad (5\text{-}13)$$

where $k_{T,M}$ is the apparent reaction rate constant of metaldehyde degradation independent of photon absorption. In UV/TiO_2 photocatalysis, the rate of reaction is proportional to the radiant flux Φ up to 25 mW.cm^{-2} after which it becomes proportional to $\Phi^{1/2}$ due to the predominance of e^--h^+ recombination over photoreaction (Herrmann, 2005). Here, the light intensity emitted by the lamp is 3.13 mW.cm^{-2} and therefore linear relationship exists between r and LVRPA, resulting in m=1 (always 1 in the case of UV/H_2O_2).

In order to enable the model to be used for continuous and recirculation systems, the rate equations and the material balance were combined and yielded:

$$V_T \frac{dC_M}{dt} = k_{T,M} \times C_M \times \int_{V_R} (LVRPA)^m dV_R \quad (5\text{-}14)$$

Which after integration becomes:

$$\ln\frac{C_M}{C_{0,M}} = -\frac{k_{T,M} \times \int_{V_R} (LVRPA)^m dV_R}{V_T} \times t = k'_M \times t \quad (5\text{-}15)$$

As m=1 in the study:

$$\int_{V_R} (LVRPA)^m dV_R = VRPA \quad (5\text{-}16)$$

And finally:

$$k_{T,M} = \frac{k'_M \times V_T}{VRPA} \quad (5\text{-}17)$$

The rate constants $k_{T,M}$ found here (Table 5-3) can therefore be applied to any reactor configuration with the condition that the radiant flux of the system is <25 mW.cm^{-2} for UV/TiO_2. The values obtained in the presence of both background organic matter and alkalinity should represent the degradation of metaldehyde in surface water containing 3.5 mg.L^{-1} DOC and an alkalinity of 120 mg.L^{-1} as $CaCO_3$.

By combining equations (5-11), (5-12) and (5-17), a relationship between EEo, P, k_T and VRPA is obtained, such that:

$$EEo = \frac{0.64.10^{-3} \times P}{k_T \times VRPA} \quad (5\text{-}18)$$

As already observed above, the alkalinity substantially increases the energy requirement of UV/TiO_2 whilst it does not impact UV/H_2O_2 (Figure 5-5). In fact, the presence of alkalinity reduces the rate of photon absorbed in the system (VRPA) and ultimately results in higher EEo. Consideration of equation (5-18) suggests that the required VRPA to achieve the target EEo of 2.65 kWh.m^{-3} is 1.65 W and 9.75 W for UV/H_2O_2 and UV/TiO_2 systems based on the 45 W lamp used in the current study. Reduction of the lamp power to 15 W reduces the required VRPA to 0.55 and 2.15 respectively. In the set up used in the current work the required EEo was obtained when an optimum concentration was used (0.8mM) but is considerably greater than the 0.097 W obtained at more practical concentrations. Consequently improvements in reactor design that ensure greater utilisation of the transmitted photons are required to ensure economic viability. Such improvement can be achieved by either increasing the reactor channel width to 11.7 cm and/or incorporating new reflecting materials for the inner wall of the reactor such as aluminium (Fu et al., 2006). In contrast,

improvements in the TiO_2 system require that the audit of catalyst is held within the reactive volume and so preferences narrower channel widths of 3 mm associated with longer reactors. Finally, a new source of UV light, UV light emitting diodes (UV-LEDs) have shown great potential in replacing traditional Hg lamps (Vilhunen et al., 2011) and although at this stage of development they exhibit low output power and low wall plug efficiency, they are predicted to become soon competitive with Hg lamps and should outperform them within 6-8 years (Ibrahim, 2012) and hence could result in significant savings in electrical energy consumption.

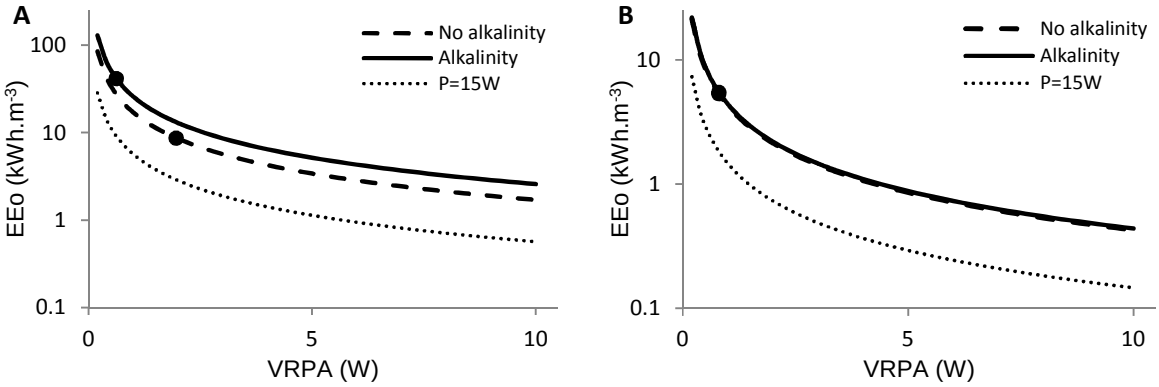

Figure 5-5 - Influence of VRPA, alkalinity and lamp power on the electrical energy requirement for the degradation of metaldehyde by A) UV/TiO_2 and B) UV/H_2O_2. • represent the values obtained in this study. The dash line represents a scenario where a similar VRPA is reached with a 15W lamp instead of the 45W lamp used in the study.

5.5 Conclusion

Both background DOC and alkalinity have an inhibitory effect on the reaction rate of metaldehyde and therefore on EEos, especially for UV/TiO_2 where the alkalinity is a major issue and a chemical or physical process needs to be used to break the TiO_2 aggregates. Moreover, although more photons are absorbed by TiO_2 than H_2O_2, the UV/H_2O_2 process remains more effective in term of quantum yield and energy consumption. The optimisation of reactor design, TiO_2 particles properties, and efficiency of light sources will ultimately reduce the energy consumption and bring AOPs as contenders for new drinking water treatment processes.

5.6 Acknowledgements

The authors would like to express their gratitude for the financial support for this project by Severn Trent Water Ltd.

5.7 References

Autin, O., Hart, J., Jarvis, P., MacAdam, J., Parsons, S.A., Jefferson, B., 2012. Comparison of UV/H_2O_2 and UV/TiO_2 for the degradation of metaldehyde: Kinetics and impact of background organics. Water Res. 46(17), 5655-5662.

Autin, O., Hart, J., Jarvis, P., MacAdam, J., Parsons, S.A., Jefferson, B., 2012. The impact of background organic matter and alkalinity on the degradation of the pesticide metaldehyde by two advanced oxidation processes: UV/H_2O_2 and UV/TiO_2. Water Res. Submitted.

Bolton, J.R., 2000. Calculation of ultraviolet fluence rate distributions in an annular reactor: significance of refraction and reflection. Water Res. 34(13), 3315-3324.

Bolton, J.R., Bircher, K.G., Tumas, W., Tolman, C.A., 2001. Figures-of-merit for the technical development and application of advanced oxidation technologies for both electric- and solar-driven systems – IUPAC Technical Report. Pure Appl. Chem. 73(4), 627-637.

Bolton, J.R., Stefan, M.I., 2002. Fundamental photochemical approach to the concepts of fluence (UV dose) and electrical energy efficiency in photochemical degradation reactions. Res. Chem. Intermediat. 28(7-9), 857-870.

Brucato, A., Cassano, A.E., Grisafi, F., Montante, G., Rizzuti, L., Vella, G., 2006. Estimating radiant fields in flat heterogeneous photoreactors by the six-flux model. AIChE Journal 52(11), 3882-3890.

Cabrera, M.I., Alfano, O.M., Cassano, A.E., 1996. Absorption and scattering of titanium dioxide particulate suspensions in water. J. Phys. Chem. 100(51), 20043-20050.

Chemspider, 2012. Chemical data base search. Available at http://www.chemspider.com (Accessed February 2012).

Crittenden, J.C., Hu, S., Hand, D.W., Green, S.A., 1999. A kinetic model for H_2O_2/UV process in a completely mixed batch reactor. Water Res. 33(10), 2315-2328.

Fu, J., Ji, M., Wang, Z., Jin, L., An, D., 2006. A new submerged membrane photocatalysis reactor (SMPR) for fulvic acid removal using a nano-structured photocatalyst. J. Hazard. Mater. 131(1-3), 238-242.

Haag, W.R., Hoigné, J., 1985. Photo-sensitized oxidation in natural water via •OH radicals. Chemosphere 14(11-12), 1659-1671.

Herrmann, J.-M., 2005. Heterogeneous photocatalysis: state of the art and present applications. Top. Catal. 34(1-4), 49-65.

Hirvonen, A., Tuhkanen, T., Ettala, M., Korhonen, S., Kalliokoski, P., 1998. Evaluation of a field-scale UV/H_2O_2-oxidation system for the purification of groundwater contaminated with PCE. Environ. Technol. 19(8), 821-828.

Ibrahim, M.A.S., 2012. Commercial evaluation of UV-LED in water treatment applications. MSc thesis, Cranfield University, UK, 2012.

Katsoyiannis, I.A., Canonica, S., von Gunten, U., 2011. Efficiency and energy requirements for the transformation of organic micropollutants by ozone, O_3/H_2O_2 and UV/H_2O_2. Water Res. 45(13), 3811-3822.

Li Puma, G., Puddu, V., Tsang, H.K., Gora, A., Toepfer, B., 2010. Photocatalytic oxidation of multicomponent mixtures of estrogens (estrone (E1), 17β-estradiol (E2), 17α-ethynylestradiol (EE2) and estriol (E3)) under UVA and UVC radiation: Photon absorption, quantum yields and rate constants independent of photon absorption. Appl. Catal. B: Environ 99(3-4), 388-397.

Li Puma, G., Toepfer, B., Gora, A., 2007. Photocatalytic oxidation of multicomponent systems of herbicides: Scale-up of laboratory kinetics rate data to plant scale. Catal. Today 124(3-4), 124-132.

Li Puma, G., Yue, P.L., 1999. Photocatalytic oxidation of chlorophenols in single-component and multicomponent systems. Ind. Eng. Chem. Res. 38(9), 3238-3245.

Minakata, D., Li, K., Westerhoff, P., Crittenden, J., 2009. Development of a group contribution method to predict aqueous phase hydroxyl radical (HO•) reaction rate constants. Environ. Sci. Technol. 43, 6220-6227.

Nicole, I., De Laat, J., Dore, M., Duguet, J.P., Bonnel, C., 1990. Use of UV radiation in water treatment: measurement of photonic flux by hydrogen peroxide actinometry. Water Res., 24(2), 157-168.

Parsons, S.A., 2004. Advanced Oxidation Processes for Water and Wastewater Treatment, IWA, UK.

Pereira, V.J., Weinberg, H.S., Linden, K.G., Singer, P.C., 2007. UV degradation kinetics and modeling of pharmaceutical compounds in laboratory grade and surface water via direct and indirect photolysis at 254 nm. Environ. Sci. Technol. 41(5), 1682-1688.

Rosenfeldt, E.J., Linden, K.G., 2007. The $R_{OH,UV}$ concept to characterize and the model UV/H_2O_2 process in natural waters. Environ. Sci. Technol. 41(7), 2548-2553.

Salaices, M., Serrano, B., de Lasa, H.I., 2002. Experimental evaluation of photon absorption in an aqueous TiO_2 slurry reactor. Chem. Eng. J. 90(3), 219-229.

Satuf, M.L., Brandi, J., Cassano, A.E., Alfano, O.M., 2007. Scaling-up of slurry reactors for the photocatalytic degradation of 4-chlorophenol. Catal. Today 129(1-2), 110-117.

Song, W., Ravindran, V., Pirbarazi, M., 2008. Process optimization using a kinetic model for the ultraviolet radiation-hydrogen peroxide decomposition of natural and synthetic organic compounds in groundwater. Chem. Eng. Sci. 63(12), 3249-3270.

Vilhunen, S., Puton, J., Virkutyte, J., Sillanpää, M., 2011. Efficiency of hydroxyl radical formation and phenol decomposition by using UV light emitting diodes and H_2O_2. Environ. Technol. 32(8), 865-872.

Xu, G., Chance, M.R., 2005. Radiolytic modification and reactivity of amino acid residues serving as structural probes for protein footprinting. Anal. Chem. 77(14), 4549-4555.

Zalazar, C.S., Satuf, M.L., Alfano, O.M., Cassano, A.E., 2008. Comparison of H_2O_2/UV and heterogeneous photocatalytic processes for the degradation of dichloroacetic acid in water. Environ. Sci. Technol. 42(16), 6198-6204.

5.8 Supporting Information.

5.8.1 Description of the equations used for the determination of the LVRPA for heterogeneous photocatalysis.

The six-flux absorption-scattering model used in this study to determine the volumetric rate of photon absorption and ultimately the quantum yields in a photocatalytic reactor has first been introduced by Brucato et al. (2006) et was further developed by Li Puma et al. (2010). The different equations needed to model the light absorption in the photocatalytic reactor are developed below. The LVRPA at a point (r, z) in the reactor space for an infinitely long annular photocatalytic reactor is:

$$\mathrm{LVRPA}=\frac{\tau_{app}\times I_{(\eta R),z^*}}{\omega_{corr}(1-\gamma)(1-\eta)R}\times\frac{\eta}{[\eta+(1-\eta)\delta*}\times[(\omega_{corr}-1+\sqrt{1-\omega_{corr}^2})\exp^{-\tau_{app}\delta^*} + \gamma(\omega_{corr}-1-\sqrt{1-\omega_{corr}^2})\exp^{\tau_{app}\delta^*}] \quad (5\text{-}19)$$

where δ^* is the dimensionless radial coordinate in the reaction space δ, η is the ratio between the radius of the inner and outer wall of the annulus, τ_{app} is the apparent optical thickness such as:

$$\tau_{\mathrm{app}}=a\tau\sqrt{1-\omega_{corr}^2} \quad (5\text{-}20)$$

where τ is the optical thickness, with:

$$\tau=(\sigma+\kappa)c_{cat}\delta \quad (5\text{-}21)$$

and a, b, ω_{corr} and γ are model parameters with:

$$a=1-\omega\ p_f-\frac{4\omega^2 {p_s}^2}{1-\omega\ p_f-\omega\ p_b-2\omega\ p_s} \quad (5\text{-}22)$$

$$b = \omega\ p_b + \frac{4\omega^2 {p_s}^2}{1-\omega\ p_f - \omega\ p_b - 2\omega\ p_s} \tag{5-23}$$

where p_b, p_f and p_s are the probability of backward, forward and side scattering and are equal to 0.71, 0.11 and 0.045 respectively (Brucato et al., 2006).

$$\omega_{corr} = \frac{b}{a} \tag{5-24}$$

$$\gamma = \frac{1-\sqrt{1-\omega_{corr}^2}}{1+\sqrt{1-\omega_{corr}^2}} \exp^{-2\tau_{app}} \tag{5-25}$$

ω is the scattering albedo defined as:

$$\omega = \frac{\sigma}{\sigma + \kappa} \tag{5-26}$$

where σ and κ are the specific mass scattering and absorption coefficients respectively.

Finally, the radiant flux at the inner wall of the annulus $I_{(\eta R),z^*}$, which varies along the axial direction was modelled as a line source as described elsewhere (Li Puma et al., 2010) and can be represented by:

$$I_{(\eta R),z^*} = \frac{S_l}{4\pi\eta R}\left\{\arctan\left(\frac{\beta}{2}(2\alpha z^* - \alpha + 1)\right) - \arctan\left(\frac{\beta}{2}(2\alpha z^* - \alpha - 1)\right)\right\} \tag{5-27}$$

where S_l is the radiation emission of the lamp per unit time and unit length of the lamp:

$$S_l = 2\pi r_l I_w \tag{5-28}$$

α and β are the geometrical design parameters of an annular photoreactor:

$$\alpha = \frac{H}{L} \tag{5-29}$$

$$\beta = \frac{L}{\eta R} \tag{5-30}$$

And z* is the dimensionless axial coordinate:

$$z^* = \frac{z}{H} \tag{5-31}$$

5.8.2 Degradation of metaldehyde, serine, leucine and resorcinol by direct photolysis

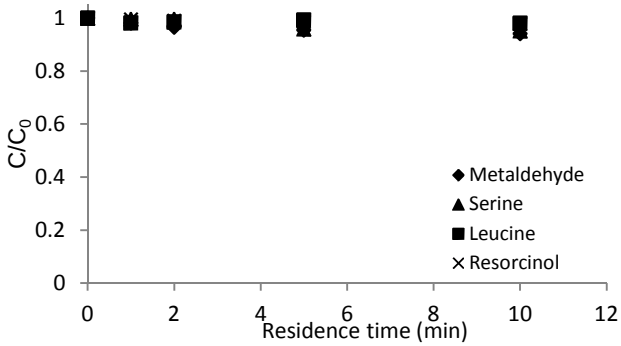

Figure 5-SI-1 - Direct photolysis of metaldehyde and the three model compounds. [Metaldehyde]=5.68x10^{-8} M; [Model compounds]= 5.68x10^{-5} M.

5.8.3 Dark adsorption of metaldehyde, serine, leucine and resorcinol onto TiO_2

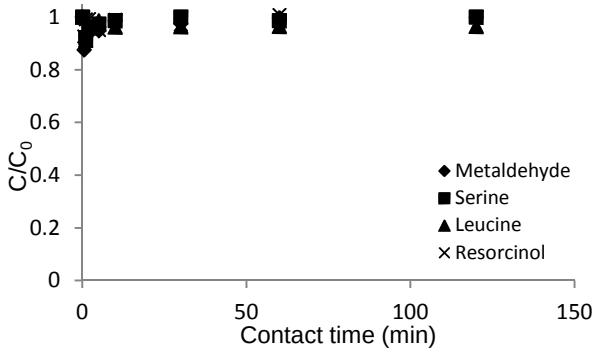

Figure 5-SI-2 - Dark adsorption of metaldehyde and 3 model compounds onto TiO_2. [Metaldehyde]=5.68x10^{-8} M; [Model compounds]= 5.68x10^{-5} M, [TiO_2]=100 mg.L^{-1}.

CHAPTER 6 EVALUATION OF A UV-LIGHT EMITTING DIODES UNIT FOR THE REMOVAL OF MICROPOLLUTANTS IN WATER FOR LOW ENERGY ADVANCED OXIDATION PROCESSES

CHAPTER 6: EVALUATION OF A UV-LIGHT EMITTING DIODES UNIT FOR THE REMOVAL OF MICROPOLLUTANTS IN WATER FOR LOW ENERGY ADVANCED OXIDATION PROCESSES

Olivier Autin [a], *Christophe Romelot*[b], *Lena Rust*[c], *Julie Hart* [d], *Peter Jarvis* [a], *Jitka MacAdam* [a], *Simon A. Parsons* [a], *Bruce Jefferson* [a]

[a] Cranfield Water Science Institute, Department of Environmental Science and Technology, Cranfield University, Bedfordshire, MK43 0AL, UK.

[b] Université de Poitiers, Laboratoire de Chimie et Microbiologie de l'Eau, 40 Avenue du Recteur Pineau, 86000, Poitiers, France.

[c] Technical University of Berlin, Department of Water Quality Control

[d] Severn Trent Water LTD., Severn Trent Centre, PO Box 5309, Coventry, West Midlands, CV3 9FH, UK.

6.1 Abstract

There is growing interest in using light emitting diodes (LEDs) as alternative to traditional mercury lamps for the removal of micropollutants by advanced oxidation processes due to their low energy consumption and potential for high efficiency and long lifetime. This study investigates the penetration and coverage of the light emitted by LEDs in order to build an optimised LED collimated beam apparatus. From the experimental data cost analysis was conducted in order to identify when LEDs will become economically viable. It was observed that if their development follows the predictions, LEDs should be a viable alternative to traditional lamps within seven years for both UV/H_2O_2 and UV/TiO_2 processes. However, parameters such as wall plug efficiency and input power need to improve for LEDs to become competitive.

Keywords: UV light emitting diodes, advanced oxidation processes, metaldehyde, cost analysis, titanium dioxide, hydrogen peroxide.

6.2 Introduction

Advanced oxidation processes (AOPs) utilising UV light have been suggested as an alternative to traditional technologies for the removal of micropollutants in drinking water treatment (Pereira et al., 2007; Chelme-Ayala et al., 2010; Sanches et al., 2010). AOPs are based on the formation of the highly reactive hydroxyl radicals •OH provided by UV irradiance of H_2O_2 or TiO_2 and are based on traditional low pressure (LP) or medium pressure (MP) mercury lamps. Uptake of the technology has been relatively limited due to a high energy requirement associated to the high input power and low light efficiency of the current UV lamp technology (Würtele et al., 2011). In addition, several drawbacks are associated with the traditional mercury lamps used in AOPs including long-term exposure instability due to overheating, low photonic efficiency resulting in high energy consumption, a short lifetime and problems related to end of life disposal as mercury is specified as hazardous air pollutant by USEPA (Table 6-1) (Tayade et al., 2009; Würtele et al., 2011).

Table 6-1 - UV lamps properties. Adapted from Ibrahim (2012).

	Low pressure lamp	Medium pressure lamp	Light emitting diode (Prediction 2020)
Typical wavelength (nm)	Monochromatic 254	Polychromatic 200-500	Any from 240
Wall plug efficiency (%)	35-38	10-20	75
Lifetime (h)	8 000-10 000	4 000-8 000	100 000
Electrical input (W)	8-100	100-60 000	1
Operating temperature (ºC)	40	600-900	20

Light emitting diodes (LEDs) have been commercialized for decades with recent developments of the technology permitting LEDs to emit UV light down to very low

wavelengths (240 nm). LEDs offer potential advantages over traditional UV lamps such as a better efficiency in converting electricity into light (high quantum yields), lower power requirements, compactness and robustness, no warm-up time, no disposal problems, and potential for long lifetimes (Table 6-1) (Chen et al., 2007; Würtele et al., 2011). However, due to the very high cost and low output power at this stage of development, UV LEDs have mostly been tested for water disinfection (Bak et al.; 2010; Würtele et al., 2011) and for photocatalysis using UV-A light ($\lambda > 365$ nm) (Shie et al., 2008; Tayade et al., 2009; Chen et al., 2007) and to date only one attempt has been made to use wavelengths shorter than 360 nm for AOP purposes where the study looked at the influence of H_2O_2 and phenol concentrations as well as the irradiation wavelength on phenol decomposition (Vilhunen et al., 2010).

Rapid change in bulb properties can be expected over the next few years as development work enhances the attributes. Comparison is most readily made to red light LEDs which were first invented in 1968 and are now widely used. Historical data shows that for every decade of development the output per bulb has increased by a factor of 20 and the cost fallen by a factor of 10, a relationship known as Haitz's law which is analogous to the equivalent profile in the microelectronics sectors as described by Moore's law (Steele, 2007). Development of more recent high brightness LEDs for lighting indicates an even more rapid development path with costs reducing by a factor of 7 within 5 years although in part this is driven by the size of the potential market for domestic lighting. Numerous examples now exist where this trade-off is effective in the case of visible light LEDs. For instance, in 2006 a factory in the USA switched to LED lighting incurring an increased capital cost of 3 times which was repaid within less than 5 years through the reduction in the annual electricity costs (LEDs magazine, 2012).

The aim of this work was primarily to characterize the fundamental properties of the UV-LED/TiO_2 system. Initially, the penetration and coverage of UV-LED light were characterized in order to design and develop a UV-LED quasi-collimated beam apparatus which could enable the comparison of LEDs and LP lamps for the removal of micropollutants by AOPs in term of UV fluence applied to the water sample. Two AOPs were chosen in this study, UV/TiO_2 due to its potential for chemical free water treatment (no chemical addition during reaction) which was compared to UV/H_2O_2 the most widely used AOP (Parsons, 2004). UV/TiO_2 is a complex technology and hence, the study investigated the influence of operational parameters such as TiO_2 concentration, light intensity and irradiation wavelength on the reaction kinetics of degradation of the dye methylene blue which was chosen due to its wide use for research purposes in UV photocatalysis (Mills and McFarlane, 2007).

Finally, the work uses models previously developed in several research studies (Chatterley and Linden, 2010; Ibrahim, 2012) and predictions given by LED suppliers coupled with experimental data determined in this study to evaluate the critical parameters which need to be improved for UV-LED based AOPs to be economically competitive compared to traditional UV lamps.

6.3 Material and methods

6.3.1 Chemicals and reagents

Nitric acid (HNO_3), sodium hydroxide (NaOH), ethanol (C_2H_5OH), hydrochloric acid (HCl), metaldehyde, serine, leucine, hydrogen peroxide (35% w/w) and $NaHCO_3$ were all laboratory grade and purchased from Fisher Scientific (Loughborough, UK). The glass slides used were standard microscope slides (26 x 76 mm, 1mm thick) and also purchased from Fisher Scientific (Loughborough, UK). Resorcinol, methylene blue, potassium oxalate, 1,10-phenanthroline, iron (III) chloride and sodium acetate from Sigma-Aldrich (Poole, UK)

at analytical purity or above. Titanium isopropoxide ($Ti(O\text{-}i\text{-}C_3H_7)_4$) (98+%) was purchased from Acros Organics (Poole, UK) and sulphuric acid from BDH Chemicals (Poole, UK). Commercial Aeroxide® P25 Degussa titanium dioxide, anatase to rutile ratio of 80:20 was purchased from Lawrence Industries (Tamworth, UK).

6.3.2 Preparation of TiO_2 sol-gel coatings

For the characterization of penetration and coverage of UV light emitted by LEDs, TiO_2 was immobilized onto a glass slide using an adaptation of the method described by Alam and Cameron (2002). The glass slide was washed in 0.1 M HNO_3 for 60 min, followed by overnight soaking in 0.1 M NaOH, then rinsed with ultrapure water and dried at 120˚C for 30 min. The sol-gel solution was prepared by mixing 100 mL of 0.1 M $Ti(O\text{-}i\text{-}C_3H_7)_4$ in C_2H_5OH (cooled with an ice bath and stirred using a magnetic stirrer), with 100 mL of 0.15 M C_2H_5OH and 0.005 M HCl. The sol-gel solution was kept in the dark in an airtight container and replaced every week. The glass slide was then dipped into the sol-gel solution, removed at a rate of 6 $mm.s^{-1}$ and heated at 260˚C for 10 min. The dipping and heating was repeated 10 times in order to obtain thick layers of TiO_2. The glass slide was finally dipped in a 5 $mg.L^{-1}$ methylene blue solution in order to obtain a complex methylene blue-TiO_2 on the top layer of the glass slide.

6.3.3 Experimental set-ups

AlInGaN-based UV-LEDs with emission wavelengths of 255 nm, 310 nm and 365 nm were used as the light source and purchased from Sensor Electronic Technology Inc. (Columbia, South Carolina). LED chips are encapsulated and hermetically sealed in metal-glass TO-39 and SMD packages with UV-transparent optical and flat windows.

The determination of the penetration and coverage of the UV light was carried out using a module containing only one LED irradiating at 255 nm which was connected in series with a

150 Ω resistor in order to obtain a current of 20 mA when powered by a 9 V battery. The methylene blue/TiO_2 coated glass slide was put in water and irradiated at different distances between the slide and the LED.

From this initial work, two modules containing 21 LEDs were built, the first one was made of three strings of 7 LEDs emitting at 255 nm, 310 nm and 365 nm and the second one with 21 LEDs emitting at 255 nm. Each module was connected following the same design: three strings of 7 LEDs and the appropriate resistor mounted in series and the three strings connected in parallel and controlled by a switch, allowing the system to work with 7, 14 or 21 LEDs. The modules were attached to an E3612A d.c. power supply (0-60 V, 0-0.5A) manufactured by Agilent Technologies, and set in order to have a current of 20 mA through each string of the modules. The LEDs were positioned in three concentric circles. Low pressure (LP) tests were carried out in a Wedeco AG bench scale collimated beam apparatus (Herford, Germany) fitted with four 30 W monochromatic LP Hg lamps emitting at 254 nm. The lamps were allowed to warm up for 30 min to ensure consistent light output before irradiating the test solutions.

6.3.4 Irradiance determination

UV irradiance for LP and LED light sources was determined by potassium ferrioxalate actinometry chosen for its efficiency and constancy over the range 250-400 nm (quantum yield Φ=1.25) as described by Hatchard and Parker (1955). The irradiance was found to be 2.33 $mW.cm^{-2}$ for the LP setting, whilst it was 0.031, 0.065, and 0.099 $mW.cm^{-2}$ for 7, 14 and 21 LEDs emitting at 255 nm respectively. Finally, the irradiance was 0.080 $mW.cm^{-2}$ for the 310 nm LED system and 0.151 $mW.cm^{-2}$ for the 365 nm LED system.

6.3.5 Irradiation procedure

The UV exposure was expressed in UV fluence as described by Bolton and Stefan (2002) in order to compare the two systems. Irradiation time was controlled by a shutter and by turning on and off the LEDs with a switch for LP and LEDs tests respectively. For LEDs and LP tests, 50 mL and 250 mL of test solution containing 10 $mg.L^{-1}$ of methylene blue (or 10 $\mu g.L^{-1}$ of metaldehyde) was respectively placed in a Petri dish at 7 mm and 22 cm from the light source and stirred with a magnetic stirrer. For UV/TiO_2 experiments, the appropriate amount of TiO_2 was added to the solution and a contact time of 15 min was allowed for adsorption before the irradiation started, whilst in the case of UV/H_2O_2 the experiment started directly after addition of H_2O_2. All experiments were duplicated and averaged values are reported.

6.3.6 Synthetic and natural waters

The surface water was collected post-GAC from a drinking water treatment works in the Severn Trent Water region, UK and had a DOC of 3.5 $mg.L^{-1}$ and an alkalinity of 120 $mg.L^{-1}$ as $CaCO_3$. The water was stored in the dark at 4˚C until used for experiments. For experiments in synthetic water, a DOC of 3.5 $mg.L^{-1}$ was obtained by mixing equimolar concentrations of serine, leucine and resorcinol.

6.3.7 Analysis

For the characterization of light coverage and penetration, pictures were taken with a FinePix S5600 camera (Fujifilm) without flash in macro mode at a constant distance of 22.5 cm between the camera and the glass slide for homogeneity of the results. The software Image Pro plus was used to determine the diameter and the colour removal of the oxidised zone. For methylene blue experiments, a 2 mL aliquot of methylene blue was withdrawn from the Petri dish after irradiation and centrifuged at 4000 rpm for 10 min with a MSE Micro Centaur centrifuge (Sanyo) in order to separate the solution from the TiO_2 particles. For UV/H_2O_2,

H_2O_2 had no impact on the absorbance and the samples were analysed directly after withdrawal. The surfactant was then withdrawn and the absorbance at 663 nm was measured with a UV-Vis Spectrophotometer (Jenway, UK).

For metaldehyde, 1 mL aliquots were withdrawn and the analyses were performed by LC-MS-MS using a Waters 2695 LC system coupled with a Waters Quattro Premier Xe MS-MS. 50% of aqueous mobile phase A consisting of 5 mM ammonium acetate/0.1% formic acid and 50% of organic mobile phase B consisting of acetonitrile/0.1% formic acid were used at a flow rate of 0.2 $mL.min^{-1}$ and held for 2 min. The Quattro Premier Xe tandem quadruple mass spectrometer was operated under positive electrospray ionization mode and the instrument was operated in multiple reaction monitoring set to monitor the ion m/z 194. Source conditions were as follows: capillary 3.5 kV, source temperature 120˚C, desolvation temperature 350˚C, and nitrogen drying gas 1000 $L.h^{-1}$. Calibrated curves were generated prior to each new sequence and the concentrations were determined using Micromass QuantLynx.

6.4 Results and discussion

6.4.1 Penetration and coverage of UV light emitting by LEDs

The irradiation of the methylene blue/TiO_2 complex at a distance of 1 mm from the LED resulted in initial signs of methylene blue decolouration within 5 min (Figure 6-1). Further irradiation led to a larger decolourized zone of 8.4 mm diameter and 73% colour removal after 120 min. Increasing the distance between the LED and the complex required longer irradiation times to observe signs of decolouration, and whilst the degree of colour removal was lower than at 1 mm, a greater zone of irradiation was oxidized and at a distance of 7 mm, a diameter of 17 mm was oxidized after 120 min (Figure 6-1). Increasing the distance from 3 to 7 mm only reduced the colour removal from 54 to 52% whilst the diameter of the

oxidation zone increased from 11.6 mm to 17.0 mm respectively. At 8 mm from the complex, the zone of irradiation was similar to that at 7 mm, but the colour removal was only 34% whilst at a distance of 10 mm no detectable decolouration was achieved after 120 min (Figure 6-2). From these initial tests, a distance of 7 mm between the LED and the irradiation zone appears as a good compromise between spreading and intensity of irradiation and at this distance the LED is able to irradiate a circular zone of 17 mm in diameter. These values were utilised in the design of a 21 LEDs module where each LED was separated by around 17 mm from each other and the modules were then positioned 7 mm above the solution during the experimental work.

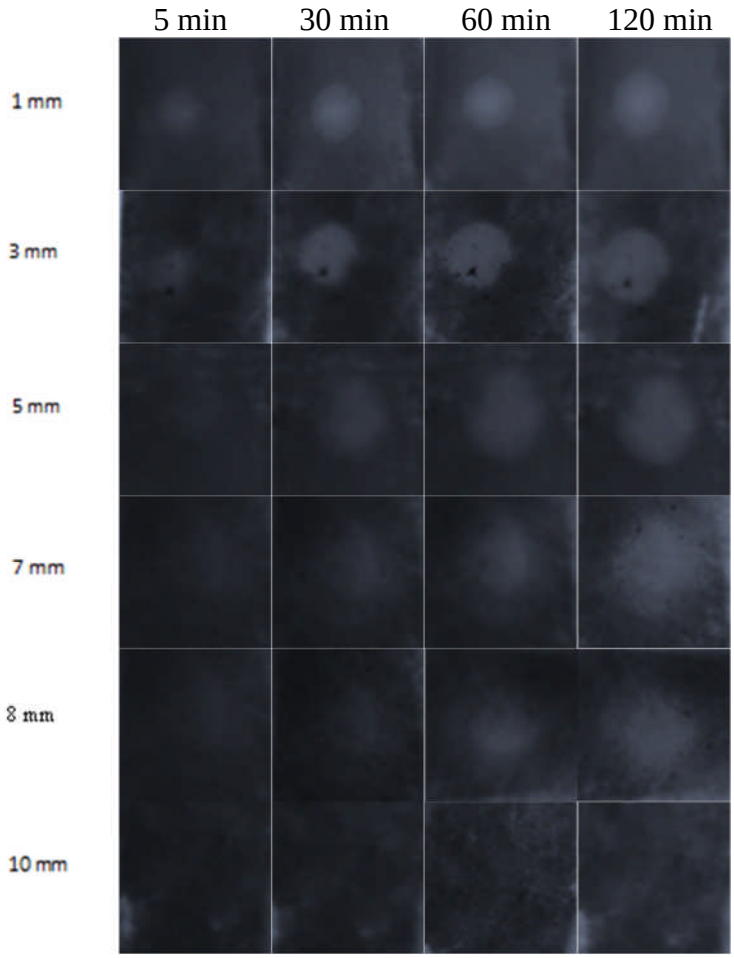

Figure 6-1 - Pictures of oxidation zone at different distances between complex and LED and different irradiation times. The complex consists of methylene blue adsorbed onto TiO_2 coated on microscope glass slides. λ=255 nm.

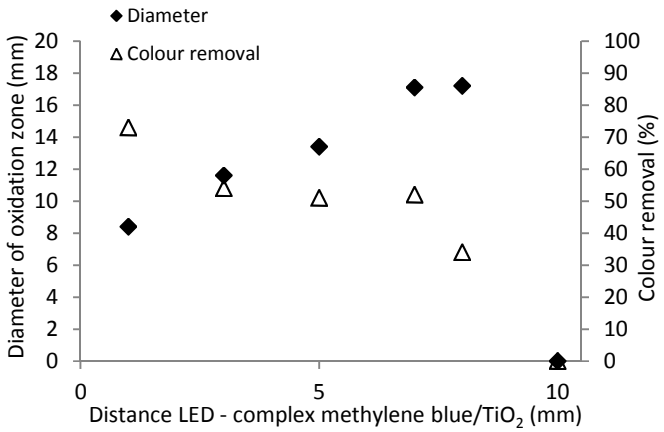

Figure 6-2 - Evolution of diameter of oxidation zone and colour removal as a function of the distance between the LED and the complex.

6.4.2 Effect of operational parameters on reaction kinetics

When no TiO_2 was added to the solution, no more than 8% of methylene blue was removed as a consequence of irradiating the sample with a UV dose of 1250 $mJ.cm^{-2}$, suggesting that direct photolysis alone is not effective, which can be explained by the poor absorbance of methylene blue at 254 nm (Tayade et al., 2009). The degradation of methylene blue by LEDs was compared to that by low pressure Hg lamps and the results show that similar degradations are obtained for similar fluences. For example at 1500 $mJ.cm^{-2}$ 83 and 84% of methylene blue was degraded for LEDs and LP lamps resulting in rate constants of $1.01x10^{-3}$ and $1.08x10^{-3}$ $cm^2.mJ^{-1}$ respectively (Figure 6-3-A). The TiO_2 concentration was varied from 0 to 1500 $mg.L^{-1}$ whilst the concentration of methylene blue was kept constant at 10 $mg.L^{-1}$ for all the experiments (Figure 6-3). The addition of TiO_2 led to significant enhancement of methylene blue removal up to 500 $mg.L^{-1}$ where the pseudo-first order rate constant reached $1.01x10^{-3}$ $cm^2.mJ^{-1}$. Increasing the catalyst dose further did not enhance the degradation rate even generating slight reduction in the rate constant (Figure 6-3-B). Similar behaviour has been widely reported and attributed to light scattering and screening effects at higher TiO_2 concentrations (Tayade et al., 2009; Ahmed et al., 2011; Bouanimba et al., 2011) and shows that the choice of optimal catalyst concentration is critical.

The degradation with three different light intensities of 0.031, 0.065 and 0.099 $mJ.cm^{-2}$ corresponding to the use of 7, 14 or 21 LEDs at 255 nm respectively showed similar fluence-based degradations regardless of the number of LEDs. In fact, the fluence-based pseudo-first order rate constants were $0.99x10^{-3}$, $1.03\ x10^{-3}$ and $1.01\ x10^{-3}$ $cm^2.mJ^{-1}$ for 7, 14 and 21 LEDs respectively (Figure 6-3-C) which corresponds to a linear increase of the time-based rate constants with light intensity which is in accordance with previous studies (Chen et al., 2007; Wang et al., 2011; Wang et al., 2006). Such findings are supported by theory which indicates that at low light intensity, the rate of reaction is proportional to the intensity (I) and becomes proportional to the square root of the intensity ($I^{1/2}$) at higher intensity, typically over 25 $mW.cm^{-2}$ due to the enhancement of e^-/h^+ recombination which becomes predominant over the oxidation process at high intensities (Hermann, 2005; Wang et al., 2011). It is worth noting that the output power for the next generation of UV/LEDs is predicted to reach up to 675 mW (Ibrahim, 2012) which represents a 5000-fold increase in comparison with the current bulbs on the market, but this figure remains significantly lower than LP lamps at 8-100W with typical intensities in the range 1-10 $mW.cm^{-2}$ (Li Puma et al., 2007; Katsoyiannis et al., 2011; Autin et al., 2012a). Hence, it is very likely that LED-based AOPs will work under linear light intensity dependency regimes.

The influence of the wavelength on the photocatalytic degradation of methylene blue shows that the three ranges of UV (A, B and C) are able to remove the dye (Figure 6-3-D), although the efficacy of methylene blue removal followed the order 310 nm> 255 nm> 365 nm. In fact, after exposure to UV irradiation doses of 1500 $mJ.cm^{-2}$, 90%, 74% and 60% removal were observed at 310, 255 and 365 nm resulting in first order rate constants of $1.41x10^{-3}$, $0.99x10^{-3}$ and $0.61x10^{-3}$ $cm^2.mJ^{-1}$ respectively. When a catalyst is irradiated with photons having energy equal or greater than its band gap energy, there is creation of e^-/h^+ pairs (Hermann, 2005). In the case of TiO_2, the band gap energy is equal to 3.2 eV which

corresponds to every wavelength shorter than 400 nm (Agrios and Pichat, 2005; Herrmann, 2005), however for a similar UV fluence applied to the sample, large variations were observed between the different wavelengths and here UV-B appears as the most suitable for UV photocatalysis.

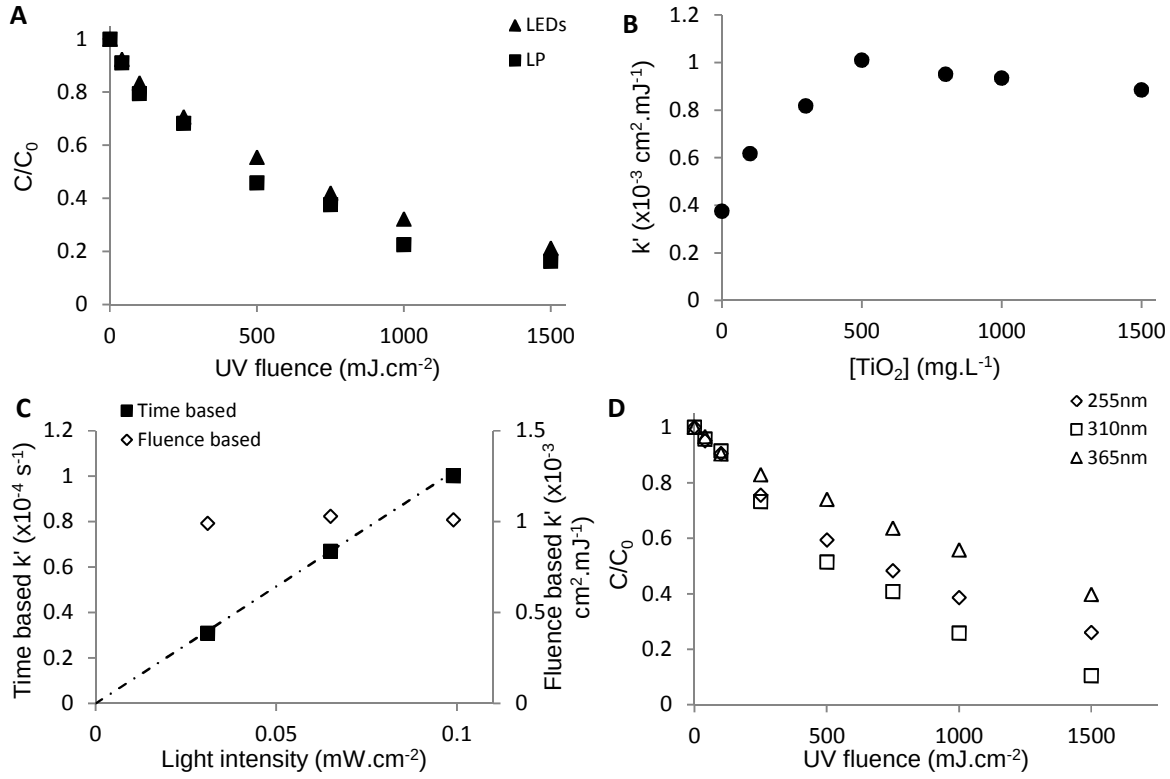

Figure 6-3 - Effect of A) Type of light source, B) TiO_2 concentration, C) Light intensity and D) Irradiation wavelength on MB degradation. $[MB]_0$=10 mg.L^{-1}, irradiation with UV LEDs (except for A), TiO_2= 500 mg.L^{-1} (Except for B), I=0.099 mJ.cm^{-2} (except for C) and λ=255 nm (except for D).

6.4.3 Cost analysis

The cost analysis is based on a case study of using an AOP for the removal of the micropollutant metaldehyde from a lowland water source from an initial concentration of 0.25 µg.L^{-1} down to 0.1 µg.L^{-1} (Table 6-2). Two cases are analysed based on existing case study cost data for LP lamps. The first is a small scale system treating 460 m3.d^{-1} to represent a decentralised unit (Ibrahim, 2012) and the other a larger works treating a flow of 71 ML.d^{-1} (Martin, 2012). In both cases the validated design for the LP system was taken from the

reference and the equivalent economic analysis undertaken so that the conditions under which LED become economically favourable could be determined. In both case studies the whole life cost was used based on a 10 and 15 year lifetime for the large and small works respectively.

Table 6-2 - prediction of the evolution of LED characteristics (adapted from Ibrahim, 2012).

Year	Efficiency (%)	Input power (mW)	Ageing factor (%)	Output power (mW)	Lifetime (h)	Price/bulb (£)
2007	1	30	60	0.18	200	210*
2010	2	30	60	0.36	1500	12
2012	8	125	70	7	10000	3.2
2015	16	500	80	64	30000	3.2
2020	75	1000	90	675	100000	0.05

* In 2007, mass production was not available and only individual pricing was available (and remains currently expensive).

The design of the AOPs are based on experimentally determined rate constants (supplementary information) of $1.48x10^{-3}$ $cm^2.mJ^{-1}$ for UV/TiO_2 and $1.20x10^{-3}$ $cm^2.mJ^{-1}$ for UV/H_2O_2 corresponding to UV fluences of 620 and 765 $mJ.cm^{-2}$ required to reach the target 60% removal using the operational parameters provided in Table 6-2 The comparison of LED versus LP lamps for the small works was based on a 15 years WLC. To enhance the sensitivity of the comparison between traditional and LED the capital cost was calculated with respect to the lamps only assuming all other components would be consistent. In that way the trade-off between lamp cost and electricity use can be examined directly. Electricity costs were assumed fixed over the 15 years at £0.09 per KWh and hydrogen peroxide fixed at $£270.m^{-3}$.

The development of LED was based on collated historical data and future predictions found in the literature (Table 6-2). Analysis of the data revealed that the development path of LEDs follows the predicted trend up to 2012 and is consistent with Haitz's law where the price of

light generated by LEDs drops by a factor of 10 and the output power per bulb increases by 20 every decade (Steele, 2007). Historical data shows that the wall plug efficiency has increased from 1% in 2007 to 8% in 2012 increasing the bulb life from 200 h to 10,000 h, the latter already exceeds standard LP lamps. If predictions hold then the wall plug efficiency of LED will double standard bulb levels by 2020 enabling operation at a temperature of 20°C and an expected bulb life of close to 100,000 h (11 years). This compares to typical operating temperatures of 40°C and operational life of around 1 year for standard LP bulbs.

The 15 year whole life cost for the LED systems over the period 2007 to 2012 decreased by five orders of magnitude as result of improvements in input power, wall plug efficiency and bulb price reflecting the early stages of development. However, based on the current state of development the WLC of the LED system would be 150 times greater than the traditional LP system. In comparison once the bulbs reach the predicted levels of 2020 the LED system will be 40% of the WLC of the standard LP version. Analysis of the time development profile indicates that the cost neutral point will occur in 6 to 7 years (Figure 6-4). Comparison of the different AOPs indicates that based on 2020 data the TiO_2 system will be 64% of the WLC of the H_2O_2 based system. The savings are derived mainly from the ability to operate without the need for chemicals (23% of the total saving) coupled to a slight improvement in the required fluence. This represent a best case scenario as problems associated with alkalinity derived aggregation of the catalyst have been excluded (Autin et al., 2012b). Ultimately implementation of the technology will require this to be resolved by utilising additional energy for aggregate breakup reducing the difference between the systems and this represents a key area for further development.

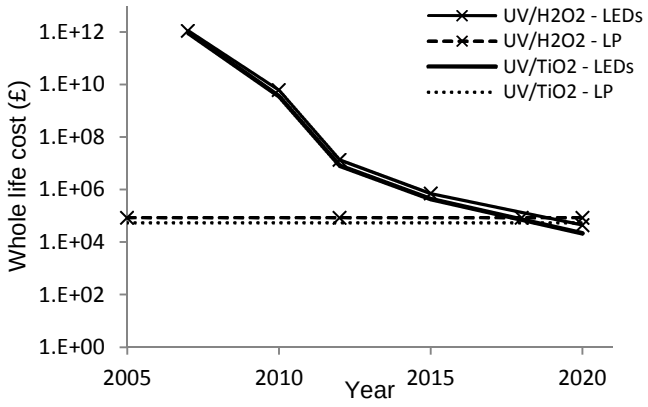

Figure 6-4 - Whole life cost development for UV/H_2O_2 and UV/TiO_2 systems. Comparison between traditional low pressure lamps and UV-LEDs according to the predictions provided in Table 6-2.

More detailed analysis of the impact of the different aspects of LED bulb enhancement (Table 6-2) was assessed to identify the critical characteristics required for the LED to become cost neutral over the 15 WLC assessment (Figure 6-5). Under current limits of input power (125 mW) and lifetime (10,000 h) the required output power exceeds what is possible and so further development is required before the LED system will be cost viable in comparison. As both input power and bulb life increase the conditions required to match LP lamps becomes less stringent such that at 1,000 mW and 100,000 h (Figure 6-5, bottom right) a bulb price of £1.5 and an output power of 330 mW is required. This represents a reduction to 50% of current bulb prices and an increase in wall plug efficiency from the current level of 8% to 37% which is within the range of predicted development over the next 8 years.

The relative significance of bulb price and efficiency depends on the input power of the bulbs (Figure 6-6). At low input powers, the price per bulb is the dominant factor on the WLC but as input power increases efficiency has a much greater impact. To illustrate, at an input power of 125 mW an increase in efficiency from 20 to 60% increases the available cost per bulb for neutrality to increase from £0.11 to £0.93. Whereas, at an input power of 750 mW the same change in efficiency generates an available price difference per bulb of £4.94. Equivalent analysis for the larger scale system reveals similar results consistent with the fact

that UV systems are modular in nature and consequently have an economy of scale factor approaching one (Figure 6-6-B). This is the same as other modular technologies like membranes were economic comparison of appropriate technologies disfavours modular systems at larger scales. Here the comparison is between lamps and any difference can be attributed to an improvement in UV delivery at larger scale which should in principle apply to both systems.

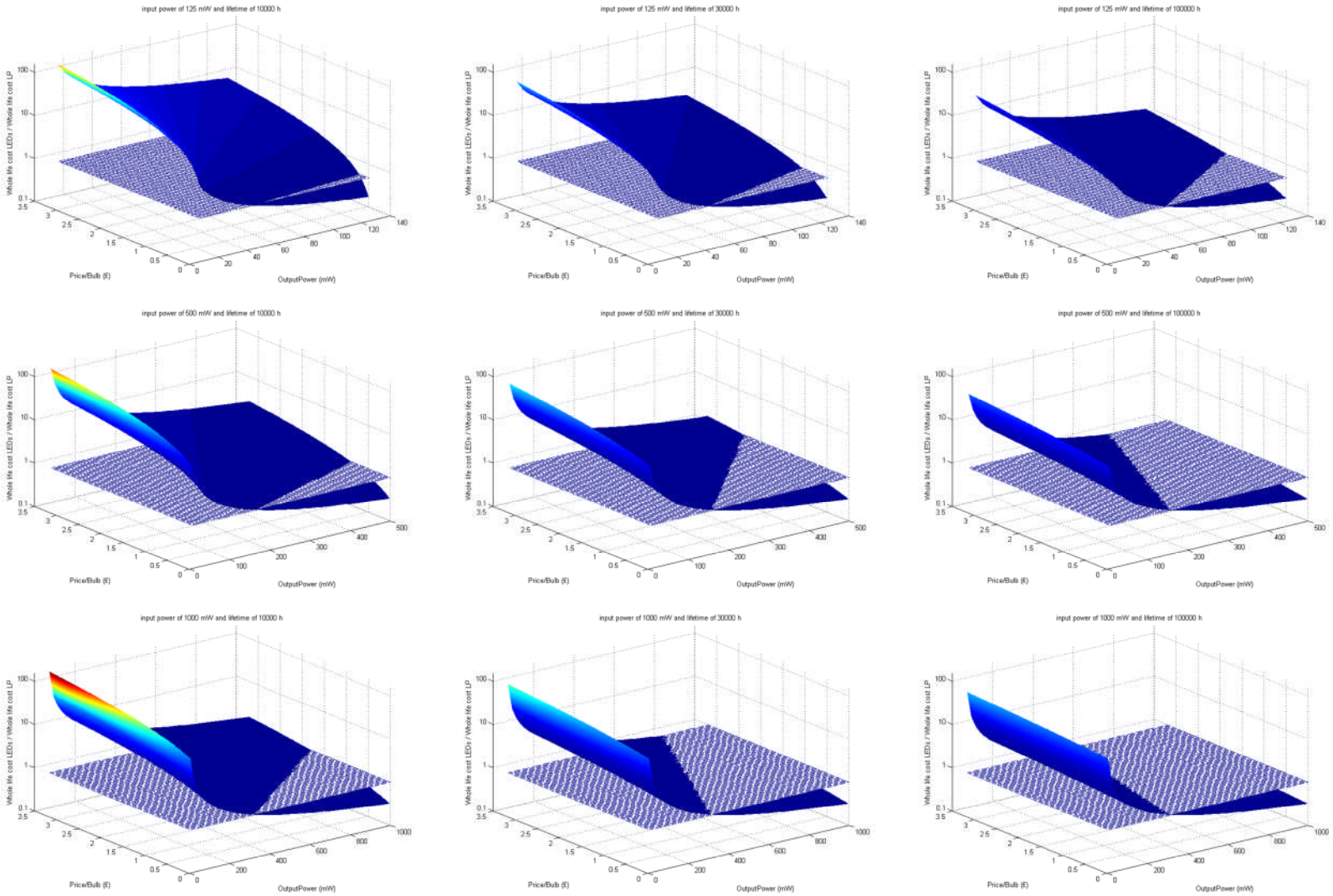

Figure 6-5 - Influence of Price/bulb and output power of LEDs on the relative cost of the UV/TiO_2 system for 60% metaldehyde removal. Plain= whole life cost LEDs/whole life cost LP, and grid = cost neutrality between LEDs and LP lamp systems.

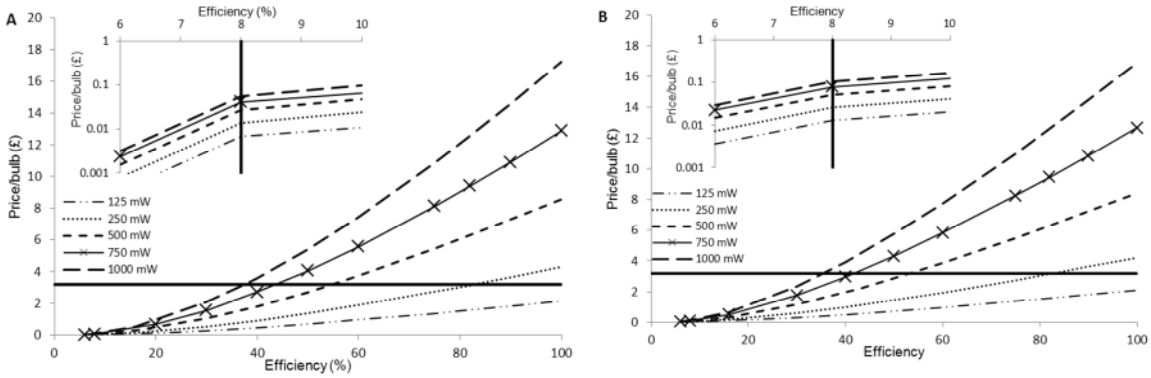

Figure 6-6 - Influence of input power on the efficiency and price/bulb required to reach the cost neutral point between LED and LP lamps. The ageing factor was fixed at 80% for all scenarios. A) 460 $m^3.d^{-1}$ and B) 71 $ML.d^{-1}$.

6.5 Conclusion

The efficacy of UV-LED bulbs providing appropriate irradiance for use in AOPs has been demonstrated. Economic assessment based on whole life cost over a fifteen year period suggests that, assuming development continues as predicted, LED will be an economically viable alternative to standard UV bulbs in seven to eight years. Additional benefits can be expected as the small bulb size enables more optimised reactor design to be developed that should reduce dose requirements further extending the opportunity that LED bulbs provide. Looking further into the future the continued development will drive down the energy associated with the use of AOP making the overall technology a more viable alternative especially in places where current systems are struggling to meet treatment needs such as the removal recalcitrant micro-pollutants such as metaldehyde. However, for these predictions to happen, several parameters need to improve especially the efficiency (resulting in longer lifetimes as well) and the input power in order to give UV/TiO_2 AOPs a chance of implementation at larger scale.

6.6 Acknowledgements

The authors would like to express their gratitude for the financial support for this project by Severn Trent Water Ltd.

6.7 References

Agrios, A.G., Pichat, P., 2005. State of the art and perspectives on material and applications of photocatalysis over TiO_2. J. Appl. Electrochem. 35(7-8), 655-663.

Ahmed, S., Rasul, M.G., Brown, R., Hashib, M.A., 2011. Influence of parameters on the heterogeneous photocatalytic degradation of pesticides and phenolic contaminants in wastewater: A short review. J. Environ. Manage. 92(3), 311-330.

Alam, M.J., Cameron, D.C., 2002. Preparation and characterization of TiO_2 thin films by sol-gel method. J. Sol-Gel Sci. Technol. 25(2), 137-145.

Autin, O., Hart, J., Jarvis, P., MacAdam, J., Parsons, S.A., Jefferson, B., 2012a. Comparison of UV/H_2O_2 and UV/TiO_2 for the degradation of metaldehyde: Kinetics and the impact of background organics. Water Res. 46(17), 5655-5662.

Autin, O., Hart, J., Jarvis, P., MacAdam, J., Parsons, S.A., Jefferson, B., 2012b. The impact of background organic matter and alkalinity on the degradation of the pesticide metaldehyde by two advanced oxidation processes: UV/H_2O_2 and UV/TiO_2. Water Res. Submitted.

Bak, J., Ladefoged, S.D., Tvede, M., Begovic,T., Gregersen, A., 2010. Disinfection of pseudomonas aeruginosa biofilm contaminated tube lumens with ultraviolet C light emitting diodes. Biofouling 26(1), 31-38.

Bolton, J.R., Stefan, M.I., 2002. Fundamental photochemical approach to the concepts of fluence (UV dose) and electrical energy efficiency in photochemical degradation reactions. Res. Chem. Intermediat. 28(7-9), 857-870.

Bouanimba, N., Zouaghi, R., Laid, N., Sehili, T., 2011. Factors influencing the photocatalytic decolourization of bromophenol blue in aqueous solution with different types of TiO_2 as photocatalyst. Desalination 275(1-3), 224-230.

Chatterley, C., Linden, K.G., 2010. Demonstration and evaluation of germicidal UV-LEDs for point-of-use water disinfection. J. Water Health 8(3), 479-486.

Chelme-Ayala, P., El-Din, M.G., Smith, D.W., 2010. Degradation of bromoxynil and trifluralin in natural water by direct photolysis and UV plus H_2O_2 advanced oxidation process. Water Res. 44(7), 2221-2228.

Chen, H.-W., Ku, Y., Wu, C.-Y., 2007. Effect of LED optical characteristics of temporal behaviour of o-cresol decomposition by UV/TiO_2 process. J. Chem. Technol. Biotechnol. 82(7), 626-635.

Hatchard, C.G., Parker, C.A., 1956. A new sensitive chemical actinometer. II. Potassium ferrioxalate as a standard chemical actinometer. Proc. R. Soc. Lond. A 235(1203), 518-536.

Hermann, J.M., 2005. Heterogeneous photocatalysis: State of the art and present applications. Top. Catal. 34(1-4), 49-65.

Ibrahim, M.A.S., 2012. Commercial evaluation of UV-LED in water treatment applications. MSc thesis, Cranfield University, UK, 2012.

Katsoyiannis, I.A., Canonica, S., von Gunten, U., 2011. Efficiency and energy requirements for the transformation of organic micropollutants by ozone, O_3/H_2O_2 and UV/H_2O_2. Water Res. 45(13), 3811-3822.

LEDs magazine. GE LED lighting upgrade saves $120000 annually at Marriott headquarters. Available at http://ledsmagazine.com/news/9/4/9 (Accessed September, 2012).

Li Puma, G., Puddu, V., Tsang, H.K., Gora, A., Toepfer, B., 2010. Photocatalytic oxidation of multicomponent mixtures of estrogens (estrone (E1), 17β-estradiol (E2), 17α-ethynylestradiol (EE2) and estriol (E3)) under UVA and UVC radiation: Photon absorption, quantum yields and rate constants independent of photon absorption. Appl. Catal. B: Environ 99(3-4), 388-397.

Martin, B., 2012. A comparison of peroxone and UV hydrogen peroxide advanced oxidation processes on the degradation of selected pesticides at a treatment work in the South West of England. MSc thesis, Cranfield University, UK, 2012.

Mills, A., McFarlane, M., 2007. Current and possible future methods of assessing the activities of photocatalyst films. Catal. Today 129(1-2), 22-28.

Parsons, S.A., 2004. Advanced Oxidation Processes for Water and Wastewater Treatment, IWA, UK.

Pereira, V.J., Weinberg, H.S., Linden, K.G., Singer, P.C., 2007. UV degradation kinetics and modeling of pharmaceutical compounds in laboratory grade and surface water via direct and indirect photolysis at 254 nm. Environ. Sci. Technol. 41(5), 1682-1688.

Sanches, S., Barreto Crespo, M.T., Pereira, V.J., 2010. Drinking water treatment of priority pesticides using low pressure UV photolysis and advanced oxidation processes. Water Res. 44(6), 1809-1818.

Shie, J.-L., Lee, C.-H., Chiou, C.-S., Chang, C.-T., Chang, C.-C., Chang, C.-Y., 2008. Photodegradation kinetics of formaldehyde using light sources of UVA, UVC and UVLED in the presence of composed silver titanium oxide photocatalyst. J. Hazard. Mater. 155(1-2), 164-172.

Steele, R.V., 2007. The story of a new light source. Nature Photon. 1(1), 25-26.

Tayade, R.J., Natarajan, T.S., Bajaj, H.C., 2009. Photocatalytic degradation of methylene blue dye using ultraviolet light emitting diodes. Ind. Eng. Chem. Res. 48(23), 10262-10267.

Vilhunen, S., Puton, J., Virkutyte, J., Sillanpää, M., 2011. Efficiency of hydroxyl radical formation and phenol decomposition by using UV light emitting diodes and H_2O_2. Environ. Technol. 32(8), 865-872.

Wang, W.-Y., Ku, Y., 2006. Photocatalytic degradation of reactive red 22 in aqueous solution by UV-LED radiation. Water Res. 40(12), 2249-2258.

Wang, Z., Liu, J., Dai, Y., Dong, W., Zhang, S., Chen, J., 2011. Dimethyl sulphide photocatalytic degradation in a light-emitting-diode continuous reactor: kinetic and mechanistic study. Ind. Eng. Chem. Res. 50(13), 7977-7984.

Würtele, M.A., Kolbe, T., Lipsz, M., Külberg, A., Weyers, M., Kneissl, M., Jekel, M., 2011. Application of GaN-based ultraviolet-C light emitting diodes – UV LEDs – for water disinfection. Water Res. 45(3), 1481-1489.

6.8 Supporting Information

6.8.1 Degradation of metaldehyde in surface and synthetic waters by UV/TiO_2 and UV/H_2O_2.

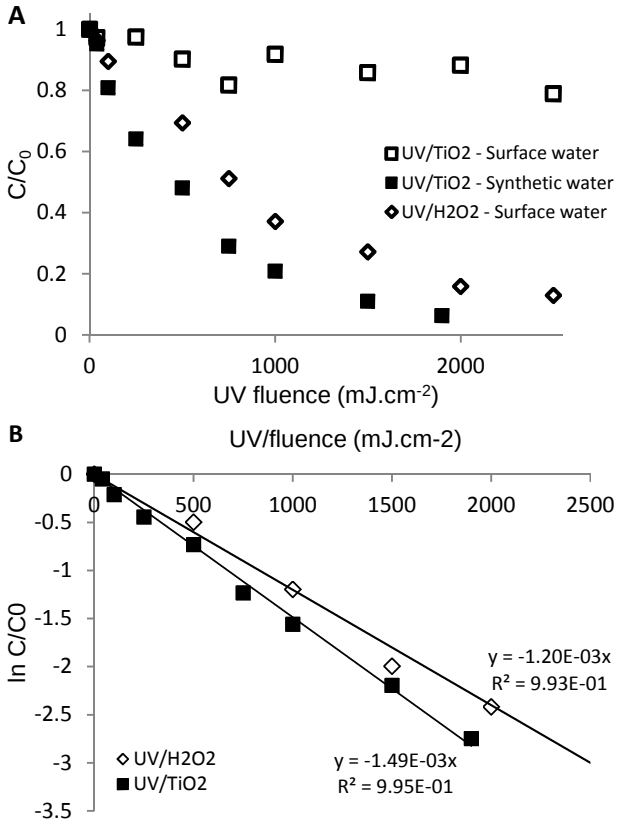

Figure 6-SI-1 - A) Metaldehyde degradation by UV/TiO_2 and UV/H_2O_2 in surface and synthetic waters and B) corresponding kinetics for the determination of the pseudo-first order rate constants.

6.8.2 Cost model used for the calculation of whole life cost

Whole life cost = Capital cost + (Annual energy cost + Annual replacement cost) x 15

With:

Capital cost = Number of lamps x Price/lamp

Annual energy cost = Number of lamps x Input power (in kW) x Electric cost x 24 x 365

Annual replacement cost = 24 x 365 / Lifetime x Number of lamp x Price/lamp

Where:

Number of lamps = Power required / Output power

Energy consumed = Number of lamps x Input power

CHAPTER 7 IMPLICATIONS OF THE WORK

CHAPTER 7: IMPLICATIONS OF THE WORK

7.1 Are AOPs able to remove micropollutants?

The evaluation of the potential of AOPs is essentially based on the reactivity of micropollutants towards •OH, the main oxidising species formed in AOPs. It is well documented that second order rate constants of micropollutants towards •OH, $k_{\bullet OH}$, are in the range 10^8-10^{10} $M^{-1}.s^{-1}$ (Haag and Yao, 1992). These are several orders of magnitude faster than their reaction with ozone, one of the current processes of choice for micropollutant removal in drinking water, where k_{O3} are in the range 10^{-2}-10^4 $M^{-1}.s^{-1}$ (Hoigné and Bader, 1983; Yao and Haag, 1991). This highlights the great potential of AOPs to compete with existing technologies. The study of the relationships between micropollutant properties and reactivity towards •OH has shown that whilst there is no clear correlation between physico-chemical properties and reactivity, the structure of micropollutants is the crucial factor influencing their treatability. The presence of N-C=O moieties, a large number of C-H bonds and the presence of sulphur or nitrogen atoms in the pesticide molecule favours •OH attacks and are generally associated with high reactivity. Saturated aromatic rings and carboxylic acid moieties prevent •OH attacks often resulting in lower reactivity and therefore one can evaluate the likelihood of micropollutant removal by a simple look at the structure of the molecule.

However, the experimental evaluation of AOPs potential is essential to confirm the veracity of the initial estimation given by the second order rate constant. One of the key findings of this work was that UV/TiO_2 and UV/H_2O_2 were equally effective at removing metaldehyde in pure systems under optimised conditions (Chapter 3). However, background organic matter and alkalinity, constituents unavoidably present in

natural water sources, are associated with •OH scavenging due to their high concentrations (Haag and Hoigné, 1985). Whilst the effect on the UV/H_2O_2 process can be easily tackled with a slightly longer UV exposure, the presence of alkalinity in the UV/TiO_2 process totally inhibits the degradation of micropollutants due to the aggregation of TiO_2 particles. Therefore, AOPs appear as a viable approach for micropollutant removal but the presence of other water constituents currently prevents the development of the technology due to the high energy cost related to the long exposures required. As a consequence, a better understanding of the impact of the different water constituents on micropollutants removal is critical.

7.2 What is the impact of water constituents on AOPs?

One of the key findings of this work was that the use of model compounds as NOM surrogates and $NaHCO_3$ for alkalinity adjustment spiked in laboratory grade water was able to closely simulate real surface waters (Chapter 4, 5). As a result, the direct competition for •OH between background organic matter and micropollutants can be monitored during UV irradiation. Model compounds with high reactivity such as resorcinol are degraded preferentially in mixtures of compounds due to their greater scavenging rates, and hence one can expect a micropollutant to be hardly removed in the presence of highly reactive organic matter such as humic substances (Westerhoff et al., 1999). However, the scavenging rate of the micropollutant is several orders of magnitude lower than that of background organic matter due to the large difference in concentration between the $\mu g.L^{-1}$ and lower concentrations of micropollutants and the $mg.L^{-1}$ and higher concentrations of background organic matter. Therefore a change in reactivity of background organic matter does not greatly influence the fraction of •OH scavenged by the micropollutant. The main consequence is that fairly similar rates of

micropollutant degradation are obtained regardless of the character of the organic matter. Another important message of this work was that background organic matter acts more as a scavenger of •OH than as a competitor with the micropollutant. The findings show that for a given ratio between a micropollutant and the background organic matter, the greater the background organic matter concentration, the greater the inhibition effect on the micropollutant degradation. In other words, whilst a change in micropollutant concentration does not impact its rate of degradation, an increase of background organic matter concentration greatly inhibits micropollutant removal. Therefore, spiking relatively high concentrations of micropollutants in a water matrix in research studies should not greatly affect the observed findings. This enables findings from laboratory work to be translated into the performance in the field with a high degree of confidence.

The implication to drinking water treatment is that different approaches need to be taken depending on the quality of the water. For NOM-rich waters, a pre-treatment is essential to remove the bulk of NOM and the AOP should be placed just before the disinfection stage in the flow sheet and used as a micropollutant barrier only. In such case, the nature of NOM does not influence the removal of micropollutants and this configuration can be used for all types of water. For waters with low concentrations of NOM, the AOP can be used as both a micropollutant and NOM removal system and has the potential to replace the current GAC or ozone system. This will, especially be the case for hydrophobic waters, characterised by highly reactive precursors towards •OH. However, for hydrophilic-NOM rich waters, longer UV fluences will be required and the use of a pre-treatment may be necessary.

The other main source of inhibition of micropollutant degradation is the alkalinity, including the carbonate and bicarbonate ions HCO_3^- and CO_3^{2-}. This inhibition has for a long time been attributed to the •OH scavenging effect of the ions (Haag and Hoigné, 1985; Schmelling et al., 1997) which have reactivity towards •OH of $k_{•OH,HCO3^-} = 8.5x10^6\ M^{-1}.s^{-1}$ and $k_{•OH,CO3^{2-}} = 3.9x10^8\ M^{-1}.s^{-1}$ (Buxton et al., 1988) and a similar effect has been found here for the UV/H_2O_2 process, with a reduction of degradation rates in the range 2-11% depending on the compounds and configurations (Chapter 4, 5). However, the aggregation of TiO_2 particles due to alkalinity in the UV/TiO_2 system results in a decrease of the total surface area available by a factor 150 (Chapter 4) and can lead to the inhibition of metaldehyde degradation rates as high as 91% in the presence of 120 $mg.L^{-1}$ as $CaCO_3$ of alkalinity (Chapter 5). As a consequence, the UV fluence required to degrade a certain level of micropollutant would increase by a factor of 10 in comparison to an alkalinity-free water. It has also been observed that the simple presence of alkalinity, even at low concentrations, led to a high inhibition of micropollutant degradation (Bhagianathan, 2012). Such findings suggest that whilst alkalinity is not a major issue for UV/H_2O_2 systems, in the current form of the technology the UV/TiO_2 system becomes totally unviable from an economic point of view. Only a simple solution, such as chemically changing the pH or physically elevating the shear rate in the reactor to break up the aggregates, will enable UV/TiO_2 photocatalysis to become a competitive alternative.

7.3 When will AOPs be economically viable?

This has been illustrated in terms of the comparative operating costs of current technology options compared to AOPs. The assessment includes the cost of lamp replacement, energy and chemicals over a 10 year period and so provides an appropriate

comparison of operating costs. Consequently, adoption of AOPs appears to provide an economically feasible alternative offering nearly a 50% reduction in opex compared to the next lowest option (Table 7-1). The picture is further enhanced when future developments in UV-LED technology are considered. Estimates based on current predictions for 2020 (Chapter 6) would reduce opex to between £6.8-12.ML^{-1} based on H_2O_2. However, the lowest cost option is UV/TiO_2, where estimates are £7.1.ML^{-1} based on traditional lamps and £2.3.ML^{-1} based on LED bulbs, although these estimates do not consider the cost related to separation which will slightly increase this figure.

Realisation of the UV/TiO_2 process requires the issues around alkalinity derived aggregation to be addressed and this should represent the key focus of further research and development.

Table 7-1 - Cost of treatment for metaldehyde removal based on a DWTWs treating 23 $ML.d^{-1}$.

	Current granular activated carbon plant	Powdered activated carbon	Catchment management	UV/H_2O_2		UV/TiO_2	
				Low pressure	LEDs	Low pressure	LEDs
£.ML^{-1}	1124	45.5	33.3	18.9	6.8	7.1	2.3

7.4 References

Bhagianathan, G.K., 2012. Comparison of UV-TiO_2 and UV-H_2O_2 processes for TOC removal. MSc thesis, Cranfield University, UK.

Buxton, G.V., Greenstock, C.L., Helman, W.P., Ross, A.B., 1988. Critical review of rate constants for reactions of hydrated electrons, hydrogen atoms and hydroxyl radicals (•OH/•O^-) in aqueous solution. J. Phys. Chen. Ref. Data 17(2), 513-886.

Haag, W.R., Hoigné, J., 1985. Photo-sensitized oxidation in natural water via •OH radicals. Chemosphere 14(11-12), 1659-1671.

Haag, W.R., David Yao, C.C., 1992. Rate constants for reaction of hydroxyl radicals with several drinking water contaminants. Environ. Sci. Technol. 26(5), 1005-1013.

Hoigné, J., Bader, H., 1983. Rate constants of reactions of ozone with organic and inorganic compounds in water. I. Non-dissociating organic compounds. Water Res. 17(2), 173-183.

Schmelling, D.C., Gray, K.A., Kamat, P.V., 1997. The influence of solution matrix on the photocatalytic degradation of TNT in TiO_2 slurries. Water Res. 31(6), 1439-1447.

Westerhoff, P., Aiken, G., Amy, G., Debroux, J., 1999. Relationships between structure of natural organic matter and its reactivity towards molecular ozone and hydroxyl radicals. Water Res. 33(10), 2265-2276.

Yao, C.C.D., Haag, W.R., 1991. Rate constants for direct reactions of ozone with several drinking water contaminants. Water Res. 25(7), 761-773.

CHAPTER 8 CONCLUSIONS AND FUTURE WORK

CHAPTER 8: CONCLUSIONS AND FUTURE WORK

8.1 Conclusions

- AOPs provide an economic alternative to current treatment options for metaldehyde removal.
- Highly reactive micropollutants are linked with the presence of N-C=O moieties, a large number of C-H bonds and the presence of sulphur or nitrogen atoms in their structure which favours •OH attacks whilst saturated aromatic rings and carboxylic acid moieties prevent •OH attacks often resulting in low reactivity.
- Micropollutants can be spiked into water for treatability tests however, the SR from the background water constituents must represent more than 85% of the total SR for the findings to be valid.
- Despite its relatively low reactivity towards •OH in comparison to other pesticides, metaldehyde is well removed by UV/TiO_2 and UV/H_2O_2 at similar reaction rates in pure systems under optimised concentrations of TiO_2 of 100 mg.L^{-1} and H_2O_2 of 8 mM.
- The presence of background constituents significantly reduces the rate of metaldehyde degradation, which is attributed to:
    (1) •OH scavenging in the case of UV/H_2O_2
    (2) Catalyst aggregation in the case of UV/TiO_2.
- The degradation of micropollutants by AOPs is controlled by the background scavenging rate rather than by the concentration of micropollutant. Therefore, a variation in organic matter concentration will have a much greater impact than a variation of micropollutants concentration on the required UV dose.

- Although the concentration of organic matter is the key regulator, its character has also an impact and hydrophobic materials are more likely to inhibit micropollutants removal than hydrophilic materials due to their relatively higher SR per unit mass.
- UV light emitting diodes appear as a promising alternative to current low pressure and medium pressure mercury lamps and their predicted development will make them economically viable within the next 7-8 years.

8.2 Future work

- The break-up of TiO_2 aggregates due to alkalinity should represent the key focus of further development as the chemical free potential of UV/TiO_2 offers an ideal alternative to current treatment technologies. The future work should look at the influence of elevated shear into the reactor space on the breakage of the aggregates and could be carried out using a static mixer. The work would investigate the influence of different shear rates on the breakage of the TiO_2 aggregates and the relationship between shear rate and removal efficiency should be determined.
- In relation to the previous point, the effect of pH on the aggregation of TiO_2 particles /adsorption onto TiO_2 particles should be investigated. Although the initial tests tend to conclude that alkalinity species rather than pH affect the TiO_2 aggregation, further work needs to be carried out to confirm this statement. The work should look at the effect of each of the different species involved in alkalinity (i.e. H_2CO_3, HCO_3^- and CO_3^{2-}) on the inhibition of micropollutant degradation. This can be achieved by adjusting the pH of the water as H_2CO_3 will present in acidic conditions and as the pH of the water increases alkalinity will become present under HCO_3^- form and ultimately CO_3^{2-} at pH above 10.3.

- The development of a new analytical method able to determine the intermediates formed during irradiation would be of great interest in order to investigate the reaction mechanism and better understand the trade-off between the loss of identity of the parent compounds and their complete removal (mineralisation). It would also enable to estimate the potential toxicity of the formed by-products and their associated risks for the environment.
- On-site trials at full scale would enable to confirm the findings determined at bench scale and pilot scale which will inform on water treatment works performances. This work would first look at the optimum UV dose required by generating a UV dose response curve for the two processes and then the pilot plant would be run at a fixed UV dose for a relatively long period to establish the consistency of performance.
- Further investigations on UV-LEDs are critical in order to optimise reactor designs to ultimately bring AOPs economically competitive for various applications in water treatment. Two designs of UV-LED reactors could be developed, an annular photoreactor which could be directly compared to the data obtained with the low pressure lamp annular photoreactor and a thin film slurry reactor where the LEDs would be placed on two parallel plates, which seems more adapted to this technology. The present work showed that in the current state of the technology, the plates should be separated by no more than 1.5 cm for optimum effectiveness due to the low light intensity emitted by the LEDs. However, the future development of LEDs is expected to lead to a 100-fold improvement of the light intensity which will therefore enable the LED reactor to use a wider reactor channel, indicating that the reactor design will be LED characteristic specific and will constantly evolve until 2020.

Appendix A: Description of experimental set-ups

Three different systems have been used for this thesis. The work undertaken in chapter 3 "Comparison of UV/H_2O_2 and UV/TiO_2 for the degradation of metaldehyde: Kinetics and the impact of background organics" and chapter 4 "The impact of background organic matter and alkalinity on the degradation of the pesticide metaldehyde by two advanced oxidation processes: UV/H_2O_2 and UV/TiO_2" was carried out in a quasi-collimated beam apparatus as described in Figure A-1. 250 mL of solution was placed in a 20 cm diameter petri-dish representing a depth of 1.2 cm irradiated, 22 cm away from the lamps.

Figure A-1 – Quasi-collimated beam apparatus used for bench scale experiments. The system includes 4 UV-C lamps irradiating at 254 nm and irradiate the solution placed in the petri-dish.

In chapter 6 "Evaluation of a UV-LEDs unit for the removal of micropollutants in water for low energy advanced oxidation processes", a similar approach of quasi-collimated beam was used in order to build the unit (Figure A-2, 3, 4). The LEDs were positioned

in three concentric circles and placed 0.7 cm above the solution. In this case, a smaller volume of 50 mL of solution was placed in a 9 cm diameter petri-dish so that a similar solution depth was used in comparison to low pressure lamps.

Figure A-2 – A) UV LED unit comprising a power supply and a 21 UV-LEDs array, B) Magnetic stirrer and 9 cm petri-dish used during experiments and C) Overall set-up with LED array positioned on top of the petri-dish.

Finally, in chapter 5 "Comparison of UV/TiO_2 and UV/H_2O_2 processes in an annular photoreactor: influence of water quality on micropollutant removal, quantum yields and energy consumption" the work was carried out in an annular photoreactor (Figure A-3). The UV lamp was mounted at the centre of the reactor and the solution was circulated in an up flow mode. The reactor was made of stainless steel and the inner wall consists of a quartz tube. Air was sparged co-currently in the system in order to avoid electron-hole recombination in the UV/TiO_2 system. The reactor is 38 cm long and the gap between

the lamp and the reactor wall, which corresponds to the channel path, is 1.5 cm corresponding to a reactor volume of 1.15 L.

Figure A-3 – Annular photoreactor used in pilot scale experiments.

Appendix B: Reactions between •OH and organic compounds in aqueous solution

Three main mechanisms are believed to occur in competitive ways in aqueous solution between hydroxyl radicals and organic compounds: electron transfer, hydrogen abstraction and electrophilic addition (Oppenländer, 2003).

The hydrogen abstraction step is believed to be the dominant pathway (Masschelein, 2002) and reacts as follows:

$$\bullet OH + ... + RH_2 = ..., RH\bullet + H_2O$$

The C-H bond is the active bond and the likelihood of reaction is related to the type of C-H bond (i.e. primary, secondary and tertiary) where the reactivity increases with the C-atom saturation due to the greater stability of the primary carbon-centered radical (Minakata et al., 2009). The hydrogen abstraction reaction generates organic radicals which by addition of molecular oxygen yield peroxyl radicals (Legrini et al., 1993):

$$RH\bullet + O_2 = RHO_2^{\bullet}$$

The organic peroxyl radicals $RHO_2^{\bullet}$ can further initiate thermally-controlled oxidations by:

- Decomposition and hydrolysis $RHO_2^{\bullet} = RH^+ + (O_2^{-\bullet} + H_2O) = RH^+ + H_2O_2$
- Homolysis ($RHO_2^{\bullet} + ..., RH_2 = RHO_2H + RH\bullet$)
- Deactivation by hydrolysis of $O_2^{-\bullet}$ into H_2O_2.

Another possibility is the direct electrophilic addition to organic π-bond systems such as carbon-carbon double bond systems (i.e. alkenes or aromatic compounds). For alkenes,

the probability of addition to either of the carbon is controlled by the functional groups bonded to the unsaturated carbons whilst the addition to the aromatic ring is highly regioselective due to the electrophilic character of •OH. The electron-withdrawing and -donating functional groups will significantly influence the ratio of ortho-, meta-, para- and ipso- positions as well as the reaction rates as described in chapter 2 and by Minakata et al. (2009). Electrophilic addition is of particular interest for the rapid dechlorination of chlorinated phenol yielding chloride ions (Masschelein,, 2002).

The electron transfer reactions can be represented by:

$$\bullet OH + RX = OH^- + RX^{+\bullet}$$

This reaction corresponds to the reduction of •OH to hydroxide anions by an organic substrate. It generally occurs when hydrogen abstraction and electrophilic addition reactions are disfavoured, which has been found particularly important in the case of multiple halogen-substituted compounds (Legrini et al., 1993).

However, hydroxyl radicals do not react necessarily with organic compounds and can react together if too high concentrations of •OH are produced to form hydrogen peroxide such as:

$$\bullet OH + \bullet OH = H_2O_2$$

References

Legrini, O., Oliveros, E., Braun, A.M., 1993. Photochemical processes for water treatment. Chem. Rev. 93, 671-698.

Masschelein, W.J. edited for English by Rice, R.G., 2002. Ultraviolet light in water and wastewater sanitation, Lewis Publishers, London.

Minakata, D., Li, K., Westerhoff, P., Crittenden, J., 2009. Development of a group contribution method to predict aqueous phase hydroxyl radical (HO•) reaction rate constants. Environ. Sci. Technol. 43, 6220-6227.

Oppenländer, T., 2003. Photochemical purification of water and air - Advanced oxidation processes (AOPs): Principles, reaction mechanisms, reactor concepts, Wiley-VCH Verlag, Germany.